



Ca' Foscari  
University  
of Venice

Master's Degree programme  
in  
Sustainable Chemistry  
and Technologies  
"LM54"

Final Thesis

**Synthesis of luminescent coordination compounds  
with bidentate [N,P]-donor ligands containing the  
iminophosphorane functional group**

**Supervisor**

Ch. Prof. Marco Bortoluzzi

**Graduand**

Fabio Trigatti

Matriculation Number 894986

**Academic Year**

2023 / 2024



## Index

Abstract	1
1. Introduction	2
1.1. General aspects of photoluminescence	2
1.2. Luminescence in <i>d</i> -block elements	4
1.3. Copper and its luminescence	7
1.4. Zinc and its luminescence	13
1.5. Iminophosphoranes	17
2. Aim of the thesis	22
3. Experimental section	23
3.1. Materials and methods	23
3.2. Characterizations	25
3.3. Computational data	26
3.4. Synthesis of 1-((diphenylphosphaneyl)methyl)- <i>N</i> ,1,1-triphenyl- phosphanimine, $\text{NPh}=\text{PPh}_2\text{CH}_2\text{PPh}_2$ (dppmNPh)	27
3.5. Synthesis of Cu complexes	27
3.6. Synthesis of Zn complexes	30
4. Result and discussion	33
4.1. Staudinger reactions between diphosphines and organoazides	33
4.2. Copper(I) complexes with dppm <sup>NPh</sup>	40
4.3. Zinc(II) complexes with dppm <sup>NPh</sup>	55
5. Conclusions	66
6. Appendix	68
7. Bibliography	71

## Abstract

The aim of this thesis is the application of bidentate [N,P]-donor ligands for the preparation of luminescent metal complexes with centres having  $d^{10}$  electronic configuration belonging to the first row of the d-block.

The Staudinger reaction between a stoichiometric ratio of bis(diphenylphosphino)methane (dppm) and phenylazide ( $\text{PhN}_3$ ) afforded a stable asymmetric iminophosphorane that was employed to coordinate  $d^{10}$  metal centres. The ligand 1-((diphenylphosphaneyl)methyl)-*N*,1,1-triphenyl-phosphanimine ( $\text{dppm}^{\text{NPh}}$ ) shows a greenish fluorescence at the solid state.

The reaction of  $\text{dppm}^{\text{NPh}}$  with suitable Cu(I) and Zn(II) precursors allowed to obtain air-sensitive homoleptic and halide complexes. The luminescence of homoleptic complexes is centred in the green region and involves excited states composed by ligands and metals orbitals. The luminescence of Zn(II) derivative is noticeably greater.

Cu(I) halide complexes are most likely coordination polymers characterized by greenish luminescence, enhanced by traces of organic solvent. Experimental data suggest that the interaction with the solvent molecules increases the radiative decay rate.

Zn(II) halide complexes are poorly soluble in organic solvents. Lifetime measurements on the chloro- and bromo-complexes at room temperature clearly indicate that the emission is a fluorescence from the coordinated ligands, while the presence of iodide in coordination sphere favours a non-radiative decay, probably anticipated by intersystem crossing.

# 1. Introduction

## 1.1. General aspects of photoluminescence

Luminescence is the spontaneous emission of light after the absorption of energy by matter. When an electromagnetic radiation is used for excitation the phenomenon is indicated as photoluminescence. Photons of suitable energy can excite specific sites in molecules, and the gain of energy allows the molecule to reach an excited state. The energy excess can be lost through a radiative pathway, with emission of a photon, or through a vibrational decay related to the structure of the compound. The second process is non-radiative and, according to the Frank-Condon rules, it is favoured in the presence of high-energy oscillators and small energy gaps. If photoluminescence mechanisms such as up-conversion are neglected, the emitted photons are less energetic than the absorbed ones. This difference is called Stokes shift<sup>1</sup>.

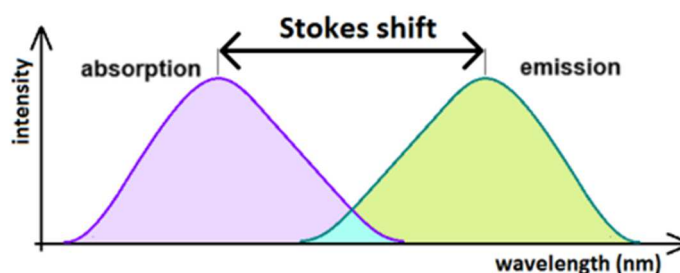


**Figure 1.** Stokes shift between adsorption and emission.

The two best known types of photoluminescence in the field of organic chromophores are fluorescence and phosphorescence, experimentally discriminated on the basis of the radiative decay time. The former mechanism is faster, with a decay time in the  $10^{-9}$  s range. The electronic transition associated is between two different levels with the same multiplicity. The second mechanism is instead much slower (microseconds or more), since it implies the forbidden transition of the electron between states with different multiplicity, for instance from triplet to singlet states.

The process where electrons change spin state is called intersystem crossing (ISC). It is very rare that the direct absorption of radiation leading to a multiplicity change could be observed, in particular if only light atoms are present, given the spin selection rule. The same rule also affects the decay time, making the phosphorescence decay long. The population of the phosphorescent emitting state requires that, after the spin-allowed

excitation, a non-radiative pathway associated to spin change populates an excited state energetically close to the singlet excited state. The ISC is promoted by strong spin-orbit coupling, with the magnetic momenta associated with spin and orbit of the electron that interact in quantized mode. High nuclear charges magnify the effect. The amount of interaction is generally represented by the coupling constant  $\lambda_{SO}$ , typically ranging from 0.02 – 0.07 eV, 0.1 – 0.2 eV and 0.3 – 0.5 eV respectively for 3d, 4d and 5d elements<sup>2</sup>.

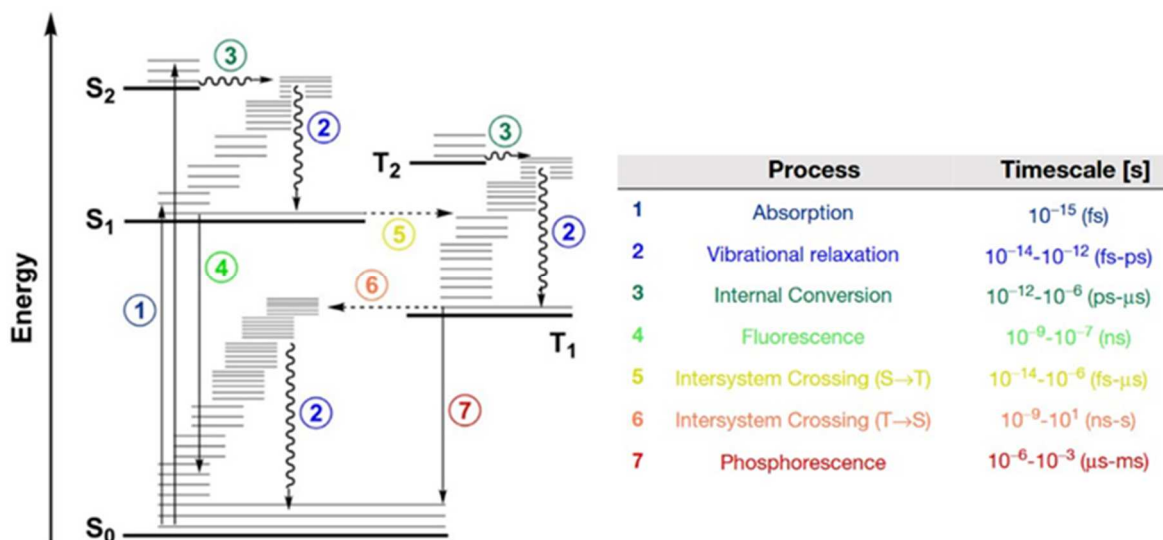


**Figure 2.** Jablonski energy diagrams comparing different radiative decay processes.

Another radiative decay in between fluorescence and phosphorescence is the thermally activated delayed fluorescence (TADF)<sup>3</sup>, that can occur when the lowest excited states with different multiplicity are very close in energy, a condition that is reached when the exchange energy between the unpaired electrons at the excited triplet state is low. The population of the excited triplet state is due to an intersystem crossing, but the opposite process (reverse intersystem crossing, RISC) can also occur thanks to the low energy gap. The relative population of the two states depends upon the temperature according to the Boltzmann distribution. The emission from the singlet state is favoured because of the different time scales of the fluorescent and phosphorescent radiative decays, despite the singlet excited state is energetically higher than the triplet one. The whole process makes the TADF last longer than the common fluorescence.

It is worth noting that the correct determination of the nature of the emitting states can be a very complicated task from an experimental point of view<sup>4</sup>. For this reason, the studies

concerning the luminescent features of materials are often supported by computational investigations<sup>5</sup>.

## 1.2 Luminescence in *d*-block elements

Some metal complexes of *d*-block elements can give photoluminescence thanks to metal-centred transitions in the partially filled *d*-shell. Transitions of this type are influenced by different aspects, such as the nature of the ligands and the geometry of the complex. The description of the orbital structure can be modelled according to both the crystal field and the molecular orbitals theories. The first approach considers the ligands as negative point charges surrounding the metal and the interactions are electrostatic. The loss of degeneration and the occupation of *d*-orbitals determine a stabilizing contribution, the crystal field stabilization energy. The molecular orbital theory instead describes the interactions as superpositions of metal and ligand orbitals, these last grouped in symmetry-adapted linear combinations (SALCs). The interactions can be potentially built starting from any of valence metal orbital, but only those having adapted energy and symmetry interact with the appropriate SALC to form a bond with the ligand. Molecular orbitals can be bonding, non-bonding or antibonding and their occupations stabilize or destabilize the complex. Non-bonding orbitals do not form bonds, but can be involved in electronic transitions<sup>6</sup>. The localization of the molecular orbitals can be evaluated from the coefficients of the linear combinations. The molecular orbital theory offers more possibilities to describe the different electronic transitions on the basis of the orbitals involved<sup>7</sup>.

Elements belonging to the *d*-block can form luminescent complexes, categorized on the basis of the origin of the emitted photon. The first category is composed by complexes where the emissions come from multielectronic wavefunctions deriving from *d*-orbitals. The orbitals of the ligands are implicated in the population of the emitting levels, in the determination of the excited state energies and in the definition of the coordination sphere, thus influencing spectroscopic properties such as wavelength maximum, bandwidth, excitation range and lifetime<sup>8</sup>.

A second category of luminescent complexes is characterized by the direct participation of ligand orbitals in the emission process because of the charge transfer between ligands and metal. When the electron moves from a metal-centred *d*-orbital to an antibonding  $\pi$ -

acceptor orbital a MLCT (metal to ligand charge transfer) occurs. The mechanism working in the opposite direction, for instance from a  $\pi$ -donor ligand to an empty metal orbital, is called LMCT (ligand to metal charge transfer). A less common transition involves only orbitals of the coordinating ligands and it is called LLCT (ligand to ligand charge transfer)<sup>9</sup>. When there is no participation of metal orbitals and only one ligand is involved the transition is LC (ligand-centred), while the opposite situation is the MC (metal-centred) transition that happens when the ligand orbitals are negligibly involved.

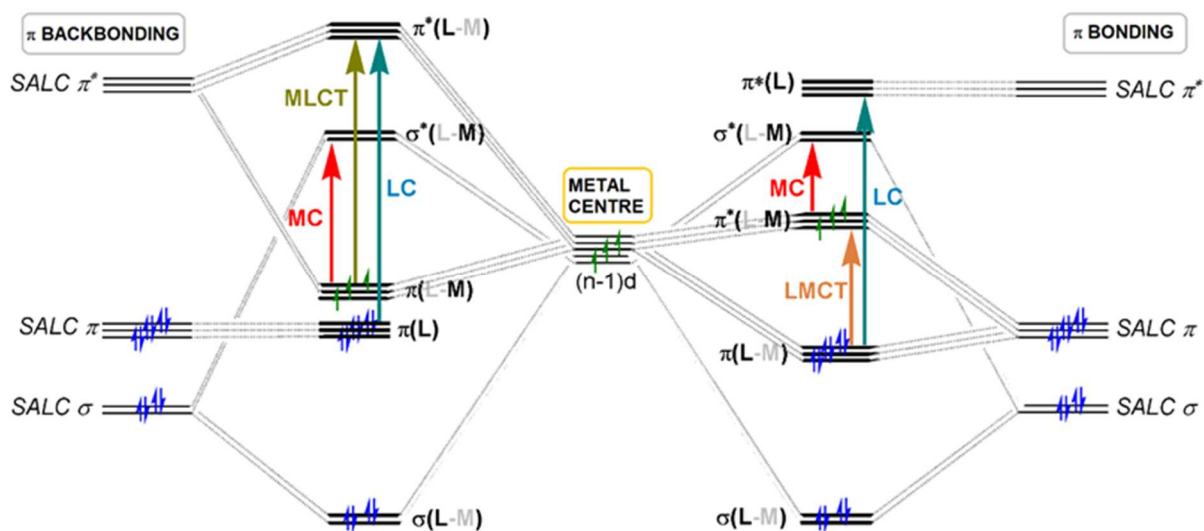


**Figure 3.** Molecular orbitals diagrams for a regular octahedral complex with  $\sigma$  and  $\pi$  metal-ligand interactions. Metal-centred (MC), ligand-centred (LC), metal-to-ligand charge transfer (MLCT) and ligand to-metal charge transfer (LMCT).

The diagram in Figure 3 does not consider LLCT and mechanisms involving intersystem crossing are not depicted.

The studies on luminescent compounds have been focused for a long time on the use of complexes of metals belonging to the second and third transition series. Compounds of this type show good properties for technological applications, such as chemical stability, high quantum yield, large Stokes shifts and efficient harvesting of singlets and triplets excitons. Selected applications involve OLEDs (organic light-emitting diodes) and LECs (light-emitting electrochemical cells)<sup>10</sup>.

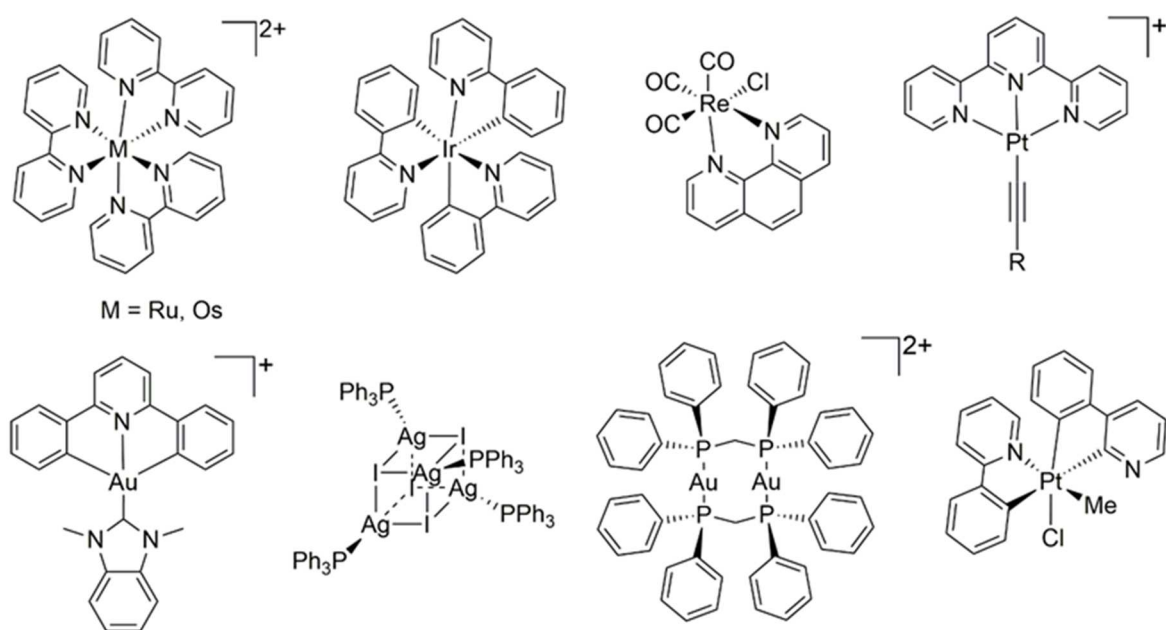


**Figure 4.** Examples of luminescent complexes with elements of the second and third transition series.

Complexes based on heavy metal centres present problems related to high cost, toxicity and supply chain issues, so the interest is shifting to more sustainable, cheaper and environmentally friendly elements, as those included in the first row of *d*-block<sup>11</sup>. The research based on light elements has to deal with more issues respect to the use of heavier metals because of a generally lower stability, a favoured non-radiative decay associated to the lower separation of *d*-orbitals and the reduced probability of ISC. Despite these problems, highly luminescent complexes have been already synthesized with metal centres such as chromium(III), iron(III) and copper(I), stabilized by different types of ligands<sup>12</sup>.

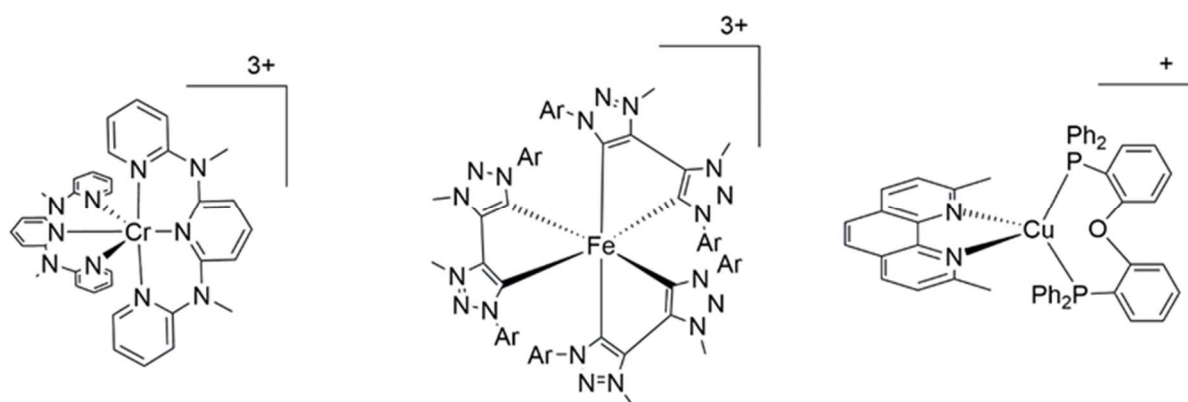


**Figure 5.** Examples of luminescent complexes based on first row *d*-metals.

### 1.3 Copper and its luminescence

Copper is a first-row transition element having  $Z=29$  and it belongs to group 11, the coinage metals group, with silver and gold. Its electronic configuration is  $[\text{Ar}]4s^13d^{10}$  and the two main oxidation states are  $\text{Cu}^{\text{I}}$  ( $d^{10}$ ) and  $\text{Cu}^{\text{II}}$  ( $d^9$ ). It has two stable isotopes,  $^{63}\text{Cu}$  and  $^{65}\text{Cu}$ , whose abundances are respectively 69% and 31%. Copper can be found in nature as sulfide, oxide or carbonate. Common minerals for its extraction are chalcopyrite  $\text{CuFeS}_2$ , chalcocite  $\text{Cu}_2\text{S}$ , cuprite  $\text{Cu}_2\text{O}$  and malachite  $[\text{Cu}_2\text{CO}_3(\text{OH})_2]$ <sup>13</sup>. The coordination chemistry of copper at the elemental state is possible only at extremely low temperatures, while the known complexes of  $\text{Cu}^{\text{III}}$  generally behave as strong oxidants. The common oxidation states of copper are  $\text{Cu}^{\text{I}}$  and  $\text{Cu}^{\text{II}}$ . The standard reduction potential in aqueous solution at 25°C are 0.15 V for  $\text{Cu}^{2+} + e^- \rightarrow \text{Cu}^+$  and 0.52 V for  $\text{Cu}^+ + e^- \rightarrow \text{Cu}^0$ .  $\text{Cu}^{\text{I}}$  is thus unstable in water and tends to disproportionate. This behaviour is to be ascribed to the higher charge/area ratio of the divalent ion, whose interactions with water overcome the second ionization energy<sup>14</sup>. Despite that, poorly soluble salts resist to disproportionation and the introduction of suitable ligands increases the stability of copper(I) in solution. Copper(I) organometallic complexes are generally soluble in organic solvents, depending upon the nature of the ligands in the coordination sphere. The coordination numbers of copper(I) are 2, 3 or 4, and the coordination geometries are primarily determined by the minimization of the steric repulsions. The electronic distribution of the metal centre is symmetric because of the completely filled  $d^{10}$  configuration, and  $d-d$  metal centres transition are not possible. Copper(I) complexes are thus typically colourless in the absence of coordinated chromophores. The luminescent behaviour is usually associated, in particular in mononuclear complexes, to MLCT mechanisms thanks to the coordination of appropriated ligands. Upon excitation the metal centre is formally oxidized to copper(II), while the ligands are reduced, thus  $\pi$ -conjugated systems play a pivotal role. Minerals do not exhibit luminescent properties since copper is normally present in the divalent, air-stable oxidation state. Copper(II) derivatives are usually blue-green coloured thanks to absorption in the visible and NIR region partially related to  $d-d$  transitions, but the luminescence is quenched by fast vibrational decays between non-degenerate  $d$ -orbitals.

Copper(I) derivatives are of interest from a technological point of view as they can exhibit peculiar emission features deeply influenced by the coordinated ligands, such as temperature-dependent lifetimes. Small changes in the coordination sphere can lead to

the alteration of the frontier molecular orbitals and therefore of the emission bands<sup>15</sup>. Studies about luminescent copper(I) complexes must deal with the sometimes difficult population of the triplet excited states. Moreover, the achievement of high quantum yields is complicated by the non-radiative decay, favoured by the Jahn-Teller flattening distortion after the MLCT excitation and the instability of the complexes at the excited state. The formal copper(II) oxidation state obtained after the irradiation prefers a tetragonally distorted geometry, and the strong geometry difference between ground and excited state favours the vibrational coupling. A proper choice of the coordination sphere allows to strongly reduce the vibrational decays. In addition, at the excited state the metal centre can coordinate a new ligand, counterions or solvent molecules, forming a pentacoordinated excited complex (exciplex) that can follow a non-radiative decay route<sup>15</sup>. Because of these reasons, the emissions in solution are generally weak since non-radiative decays are favoured. The quenching phenomena are magnified in the presence of molecules that can give oxidative quenching or species with low energy triplet states, such as anthracene<sup>16</sup>.

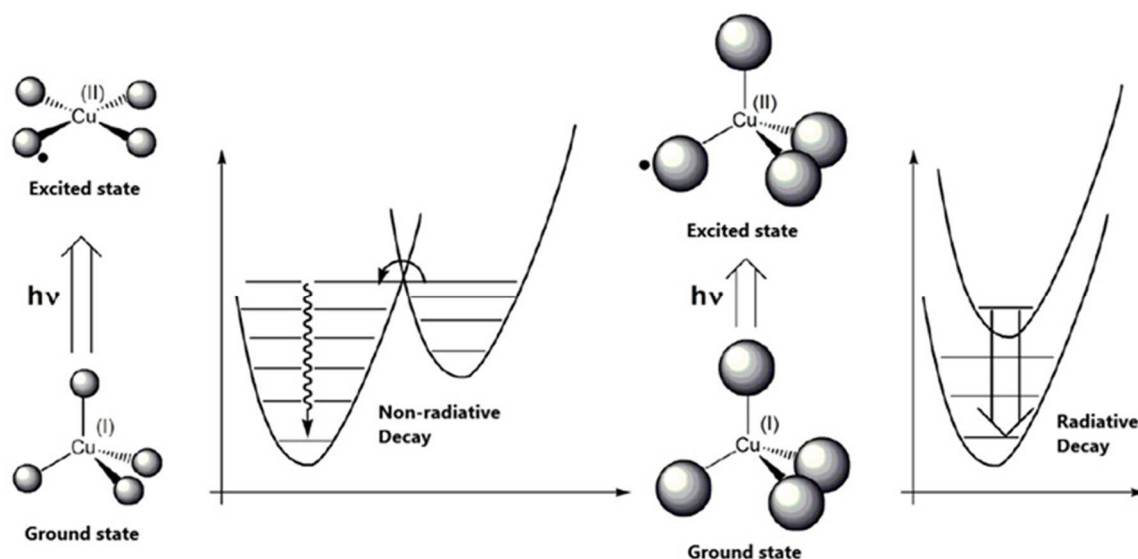


**Figure 6.** Non-radiative and radiative decay paths in tetrahedral copper(I) complexes.

Copper(I) derivatives can be divided depending on the charge: anionic complexes do not usually present luminescent properties, whereas neutral and cationic ones with N- and P-donor ligands are widely studied. For instance, the different luminescence of  $[\text{Cu}(\text{phen})_2]^+$  (phen = 1,10-phenanthroline) and  $[\text{Cu}(\text{dmp})_2]^+$  (dmp=2,9-dimethyl-1,10-phenanthroline) is related to the stabilization of the tetrahedral geometry due to the steric bulk of the

substituents, combined with the greater energy gap between excited and ground state in the second species.

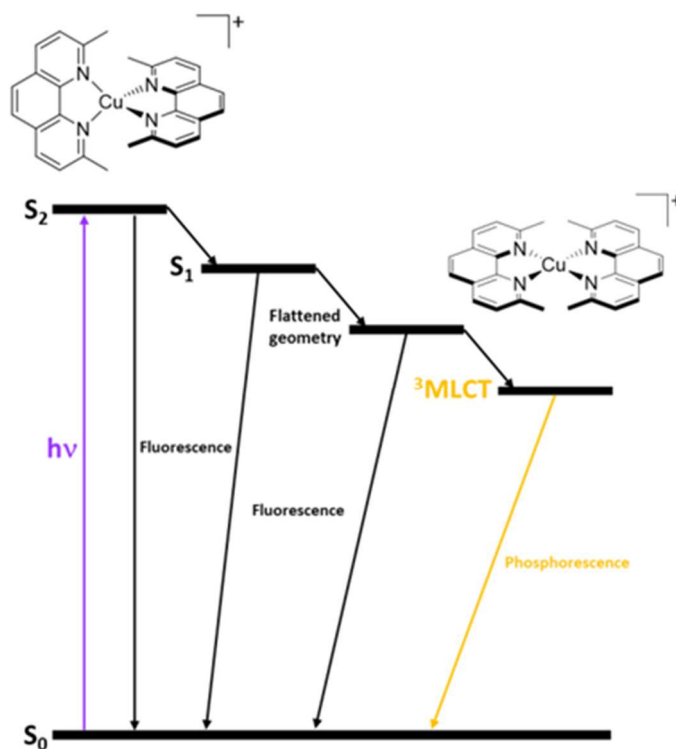


**Figure 7.** Emission of [Cu(dmp)<sub>2</sub>]<sup>+</sup>.

Heteroleptic complexes with [N,N]- and [P,P]-donor chelate ligands are widely studied thanks to their high luminescence at the solid state with long excited state lifetimes. Computational calculations show that the HOMO usually involves the lone pairs of the P-donor moieties and the copper(I) *d*-orbitals, while the LUMO is mainly composed of the antibonding overlap among [N,N] *p*-orbitals. Enhancement of the luminescent properties is observed with the use of bidentate phosphines probably because of their chelation and the improvement of charge transfer with wide P-Cu-P angles<sup>17</sup>.

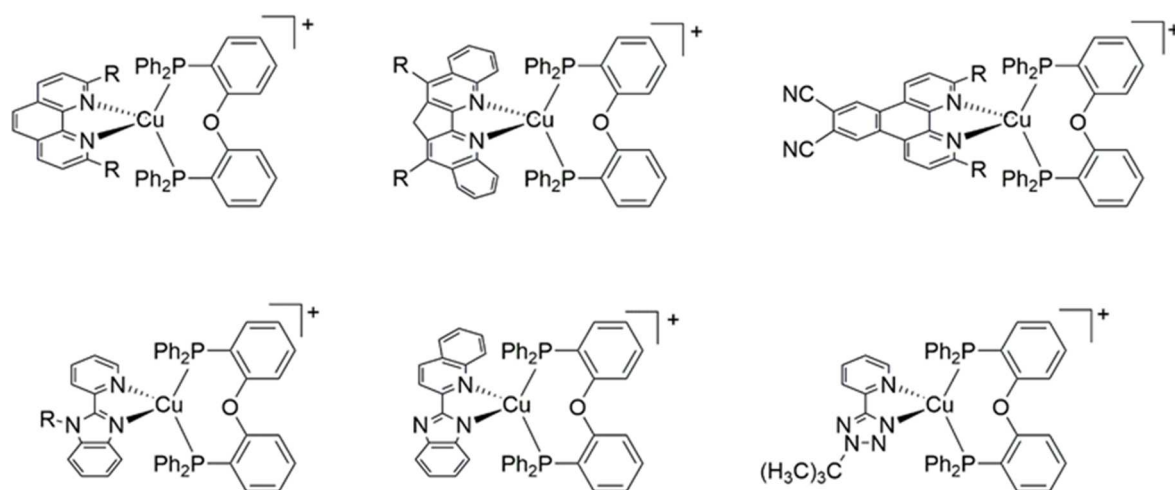


**Figure 8.** Examples of heteroleptic [N,N][P,P] donor copper(I) complexes.

In order to tune the luminescent emission, the addition of an alkyl group to the N-donor moiety generally lead to hypsochromic shift of the absorption maxima, while the increment of  $\pi$ -conjugation with suitable groups leads to a bathochromic shift to longer wavelengths<sup>17b,e</sup>.

The luminescence of copper(I) derivatives can be also tuned with external *stimuli*, and reports on cluster complexes with thermochromic, rigidochromic and mechanochromic properties can be found in the literature. In the first case the variation of temperature shifts the emission maxima thanks to changes in the relative energies of the levels involved. The second approach depends upon the nature of the substituents on the ligands, designed to avoid structural rearrangements. Mechanochromism is instead related to the disruption of Cu---Cu and  $\pi$ - $\pi$  stacking interactions thanks to the change of molecular conformation. Thermal treatments or recrystallization are generally required to restore the original emission<sup>18</sup>.

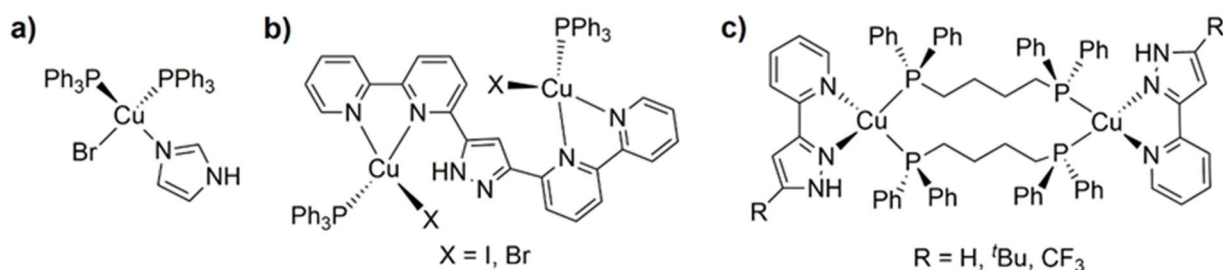


**Figure 9.** Examples of Cu complexes with thermochromic, rigidochromic and mechanochromic luminescent features.

An intriguing way to modify the luminescence features is vapochromism, *i.e.* the reversible rearrangement induced by solvent vapours or interstitial solvation. Vapochromism is commonly used to highlight the presence of VOCs (volatile organic solvents), that react with the complexes forming metal-solvent bonds, with consequent alteration of the luminescence<sup>19</sup>.

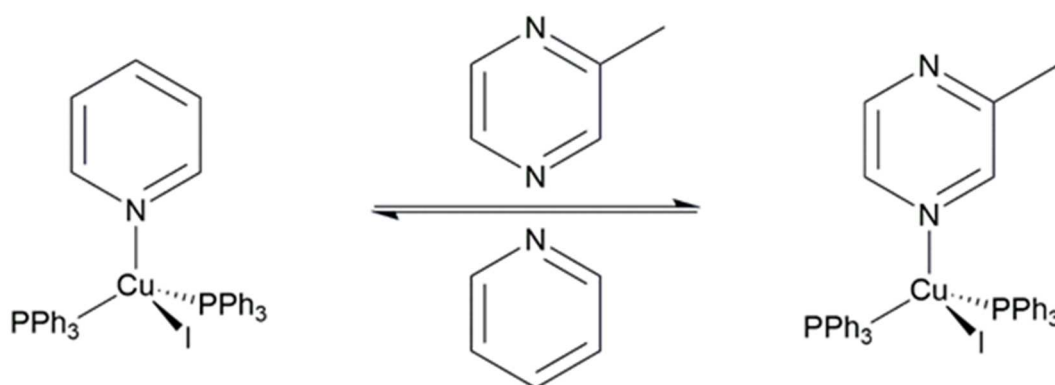


**Figure 10.** Vapochromic exchange mechanism for [CuI(py)(PPh<sub>3</sub>)<sub>2</sub>].

Copper(I) complexes with suitable ligands, such as halides, can form coordination polymers with unique electronic properties. These polymers can be useful to build sensors based on metal-organic frameworks (MOFs), that allow to detect the presence of specific analytes thanks to the change of the luminescent features. Van der Waals and cuprophilic interactions are important together with  $\pi$ - $\pi$  stackings for the tuning of the luminescence<sup>20</sup>.

The luminescent properties of polynuclear species are influenced by the nature of the halides. For instance, the emission maxima blue-shifts on increasing the atomic number of the halide in dinuclear and tetranuclear complexes, such as that sketched in Figure 11. This effect can be justified on considering that the population of the (M+X)LCT excited states requires the formal oxidation of Cu(I), more difficult when softer halides are coordinated<sup>21</sup>.

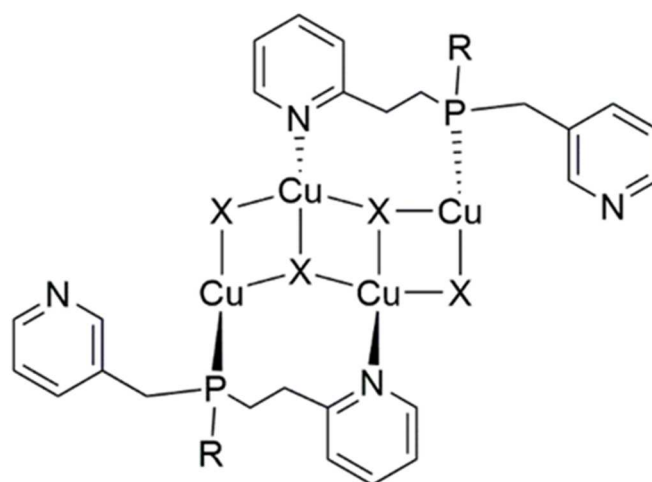


**Figure 11.** Complexes having general formula  $[Cu_4X_4L_2]_n$  ( $X = Cl, Br, I$ ;  $L =$  pyridin-phosphine ligand).

Cationic and neutral copper(I) heteroleptic complexes with N- and P-donors in the coordination sphere are widely studied for their luminescence, sometimes related to TADF. The first synthesized compound belonging to this family is  $[Cu(phen)(PPh_3)_2]^+$ . A wide range of complexes is reported in the literature, and bidentate mixed [N,P]-donor ligands play a role of growing importance. For instance, copper(I) complexes of 2-(diphenylphosphino)-6-methylpyridine showed intense emissions with high quantum yields<sup>22</sup>.

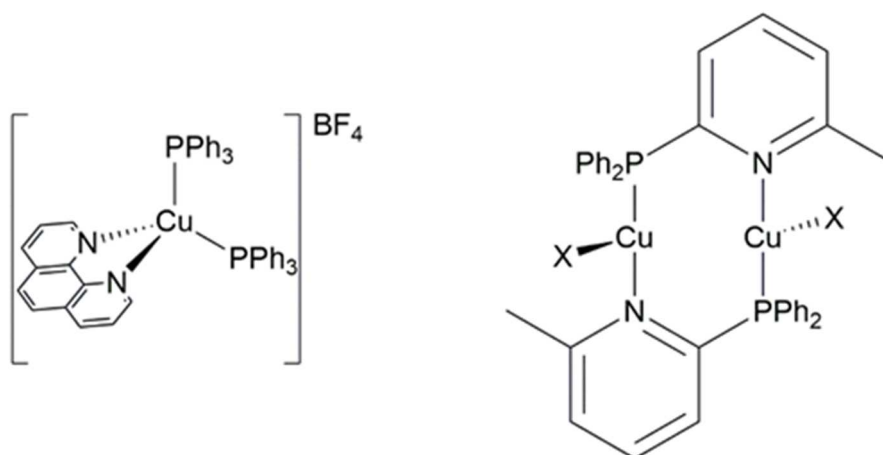


**Figure 12.** Early examples of TADF Cu complexes.

The emission from TADF materials is characterized by two components: a shorter  $S_1 \rightarrow S_0$  fluorescence and a longer  $T_1 \rightarrow S_0$  phosphorescence<sup>23</sup>. On changing ligands in the coordination sphere it is possible to modulate the luminescence features. Several families

of TADF complexes typically present pyridine and imidazole derivatives as ligands. In presence of halides in the coordination sphere  $^1(M+X)LCT$  and  $^3(M+X)LCT$  transitions acquire relevance and the relative contributions of TADF and phosphorescence depend on the coordinated halide<sup>24</sup>.

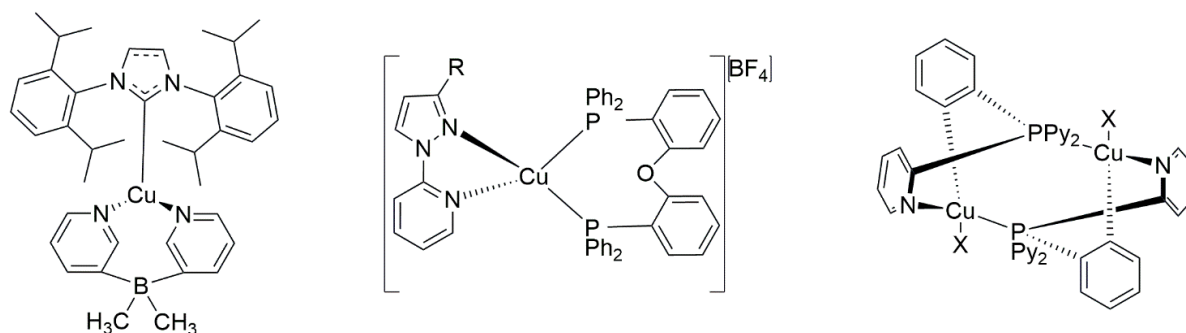


**Figure 13.** Different Cu(I) TADF-emitting complexes.

These TADF complexes are of current interest to build third generation OLEDs, less energy demanding and more stable than the previous generations. Moreover, the excited states involved in the luminescence are suitable for the development of photocatalytic systems<sup>24d, 25</sup>.

TADF properties are revealed by recording steady-state and time-resolved emission spectra at different temperatures. In particular, lowering the temperature leads to a change of the decay curves because of the increasing contribution of the triplet excited states.

#### 1.4 Zinc and its luminescence

Zinc is another abundant element of interest for luminescent materials. It has  $Z=30$  and belongs to group 12. There are five different isotopes and the most common in nature is  $^{64}\text{Zn}$  (49% of total). The electronic configuration is  $[\text{Ar}]4s^23d^{10}$  and the main oxidation state is  $\text{Zn}^{\text{II}}$ , with completed  $d$ -shell. In nature zinc is commonly found in minerals together with sulphur (sphalerite and wurtzite) and other heavy chalcogens. More rarely, zinc can be found in carbonates, silicates and oxides together with iron. ZnS doped with silver, copper or manganese shows luminescent features used in the production of X-ray screens, cathode ray tubes and glow-in-the-dark products. The luminescence features can be tuned on changing the doping elements<sup>26</sup>. ZnS is also employed for the realization

of luminescent quantum dots, *i.e.* nanoparticles of semiconductors exhibiting photoluminescence. The maximum of emission depends upon the size of the nanoparticle, normally in the 1 - 10 nm range. On decreasing the size, the band gap between valence band and conduction band increases, with consequent blue shift. The luminescence of quantum dots is governed by quantummechanical effects associated to quantum confinement.

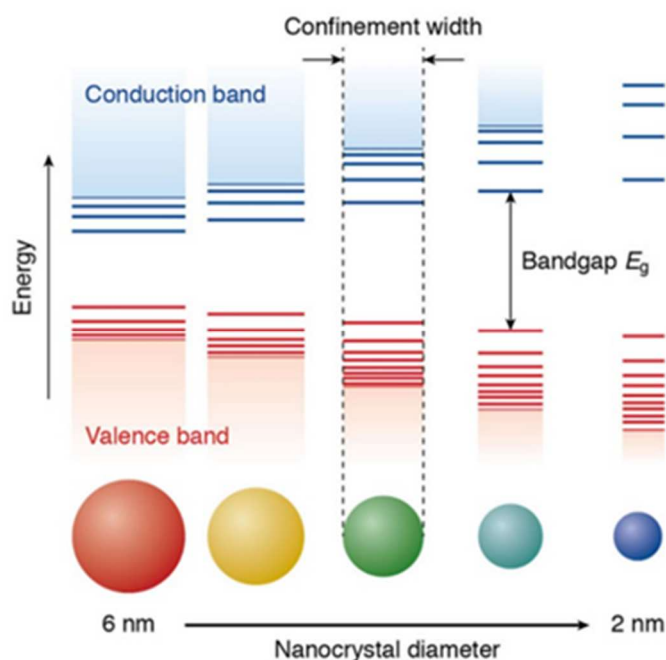


**Figure 14.** Size and emission of quantum dots.

Furthermore, zinc is essential for living beings<sup>27</sup>, where it is the second most abundant element belonging to the *d*-block. Its main role is as Lewis acid and it can be found in a wide variety of enzymes involved in acid-base reactions<sup>27a</sup>. Divalent zinc is in fact characterized by a high charge over radius ratio, therefore it is a quite strong Lewis acid. Zinc commonly forms complexes with coordination numbers between four and six, mainly with N-, O- and S- donor ligands, cyanide and halides. Possible geometries are tetrahedral, trigonal bipyramidal, square-based pyramidal and octahedral depending upon the features of the ligands in the coordination sphere, with the first geometry satisfying the 18-electrons rule.

Since the 3*d* shell is completely filled, zinc(II) is diamagnetic and *d-d* transition are not possible. Therefore, luminescence is commonly related to  $\pi^* \rightarrow \pi$  LC and LLCT

mechanisms enhanced by the coordination to the metal centre, while MLCT transitions are not favoured because the absence of higher oxidation states of the metal centre<sup>28</sup>.

The effect of the coordination on LC transitions in zinc(II) complexes is usually related to the increase of rigidity, disfavoring radiative decay routes. Moreover, the energies of the ligand orbitals are altered because of the partial delocalization of the electron density on the metal centre. In some cases the excited states can have almost partial LMCT/LLCT nature, if the antibonding  $\sigma^*$  molecular orbitals with  $d$ -component from  $\text{Zn}^{\text{II}}$  have suitable energy<sup>29</sup>.

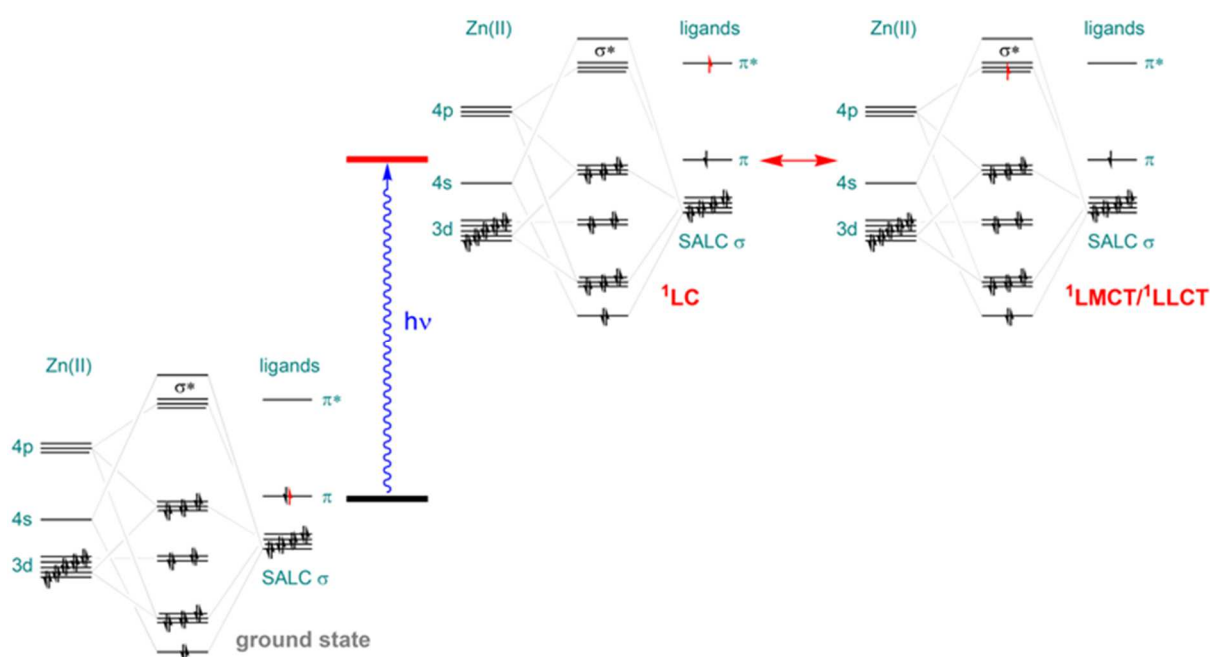


**Figure 15.** Possible mixed character of the excited states in zinc(II) complexes (tetrahedral geometry taken as example).

Luminescence from zinc complexes is therefore mainly associated to fluorescence, primary involving ligand-centred excited states<sup>28,30</sup>. Phosphorescence, even if not common, is possible when the ISC probability is sufficient and TADF decay has been also observed<sup>31</sup>. Phosphorescent molecular and polymeric zinc(II) complexes showed ms-long lifetimes<sup>29,32</sup>.

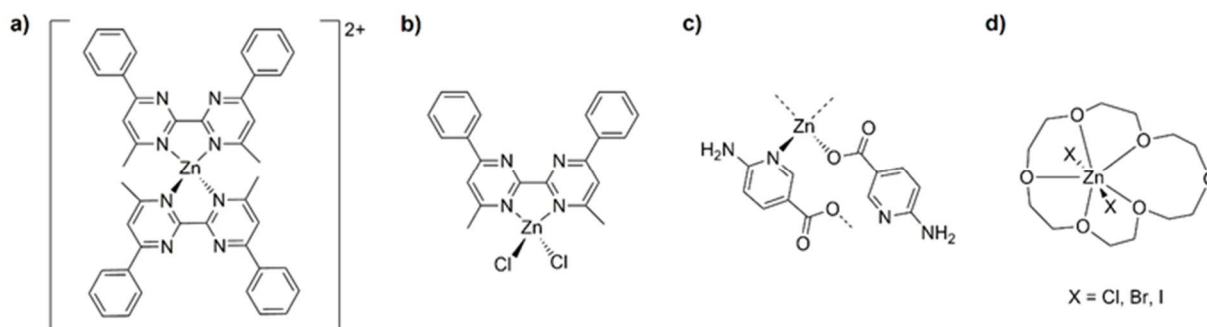


**Figure 16.** Phosphorescent zinc(II) complexes.

Phosphorescent complexes are influenced by the presence of heavy atoms in the molecule. For example, the emission of  $[\text{Zn}_3(\text{HPO}_3)_2(\text{tib})_2]\text{X}_2$  [ $\text{X} = \text{Cl}, \text{Br}, \text{I}$ ;  $\text{tib} = 1,3,5$ -tris(1-imidazolyl)-benzene] varies from fluorescence to phosphorescence on increasing the atomic number of the halide<sup>33</sup>. Zn(II) halide complexes having general formula  $[\text{ZnX}_2\{\text{O}=\text{P}(\text{NMe}_2)_2\text{Ind}\}_2]$  ( $\text{O}=\text{P}(\text{NMe}_2)_2\text{Ind} = N,N,N',N'$ -tetramethyl-*P*-indol-1-ylphosphonic diamide) exhibited milliseconds-long LC phosphorescence only when  $\text{X} = \text{Br}$  or  $\text{X} = \text{I}$ .

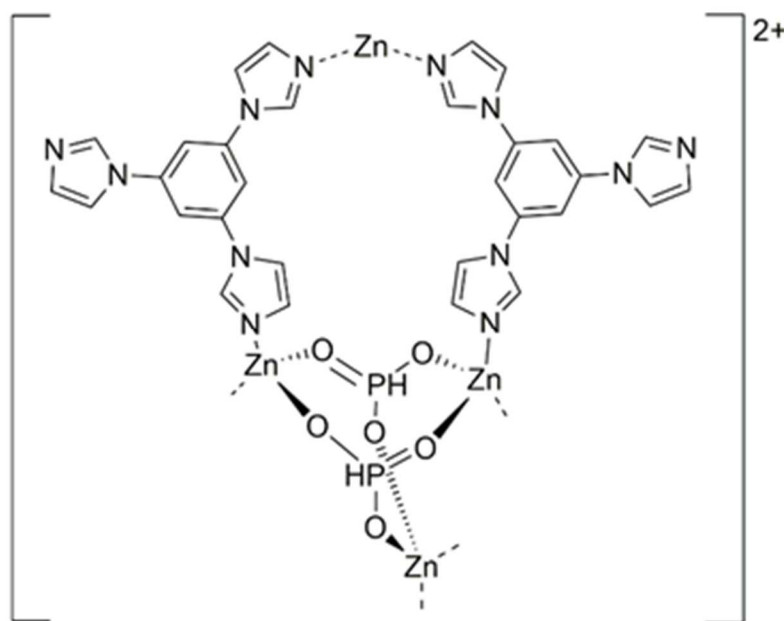


**Figure 17.**  $[\text{Zn}_3(\text{HPO}_3)_2(\text{tib})_2]^{2+}$  ( $\text{tib} = 1,3,5$ -tris(1-imidazolyl)-benzene).

Typical ligands for luminescent zinc(II) complexes are combinations of N-donor heterocycles and O-donors derived from the phenate moiety<sup>34</sup>.

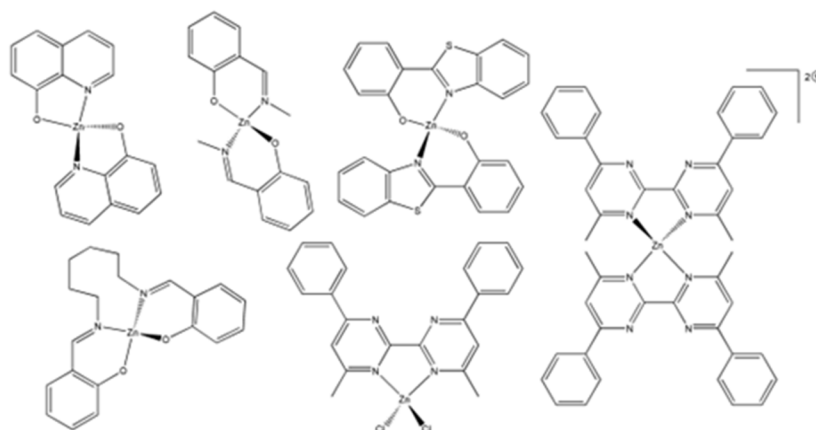


**Figure 18.** Examples of luminescent Zn(II) complexes.

Zinc(II) complexes are considered for OLEDs since 2000s, with the synthesis of suitable  $[Zn(N^{\wedge}O)_2]$  and  $[Zn(O^{\wedge}N^{\wedge}NO)]$  complexes ( $N^{\wedge}O$  = 8-hydroxyquinolate, conjugate base of N-methyl salicylimine, 2-(2-benzothiazolyl)phenate;  $O^{\wedge}N^{\wedge}O$  = conjugate base of N,N'-disalicylidenehexane-1,6-diamine)<sup>35</sup>. It is possible to obtain blue emitters such as the complex reported by Wang and co-workers with diphenyl-6,6'-dimethyl-2,2'-bipyrimidine and more recently with the polydentate ethylenediamine Schiff base shown in Figure 19<sup>32a,36</sup>.

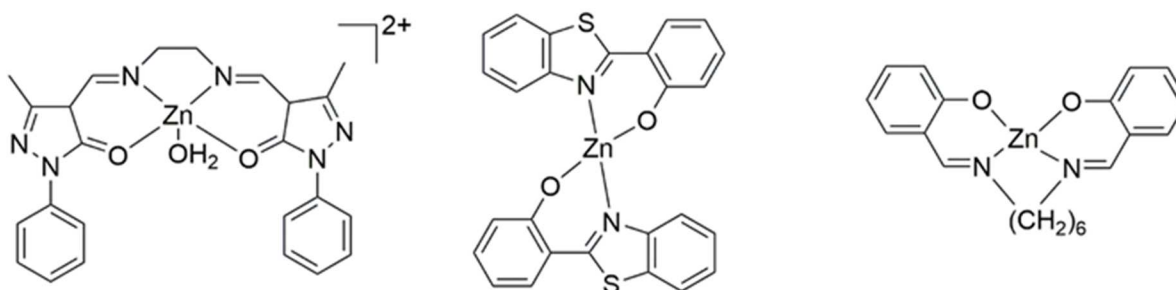


**Figure 19.** Zn(II) luminescent complexes used in OLEDs.

## 1.5 Iminophosphoranes

Iminophosphoranes represent a class of ligands having general formula  $NR^{\prime}=PR_3$ . These species are known under different names: iminophosphoranes, phosphinimines or phosphazenes. The first synthesis was reported by Staudinger in a work concerning the oxidation of phosphines with organoazides<sup>37</sup>. Those molecules are extensively utilized as catalysts for different organic reactions<sup>38</sup>.

As ligands, they are strong  $\sigma$  and  $\pi$  donors because of the noticeable electron density present on the N atom, highlighted by the ylidic form described in Figure 20. Changing the substituents on both N- and P- atoms alters the electron donating properties. No evidence of  $\pi$ -acidity is reported.

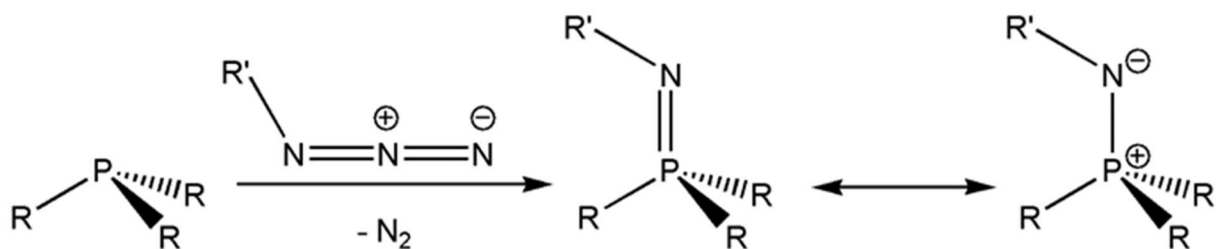


**Figure 20.** Staudinger reaction and resonance forms of iminophosphoranes.

Iminophosphoranes easily interact with electron-deficient metals, while they act as labile ligands for electron-rich metal centres, therefore they are considered hard donors<sup>39</sup>. When the iminophosphorane moiety is part of multidentate ligands with softer donors, coordination compounds with a wider range of metals are possible. In literature, numerous applications of iminophosphorane complexes have been documented. These organometallic compounds serve as effective catalysts for various types of reactions. For instance, mixed ligands featuring both phosphine and iminophosphorane donor groups have been employed in the last years for the development of catalytic systems based on late-transition metals, mainly of Groups 7 e 11, applied in relevant transformations in synthetic organic chemistry such as hydrogenations, C-C couplings, rearrangements or heteroannulation reactions<sup>40</sup>.

Detailed studies on luminescent complexes with iminophosphoranes are scarce. Complexes of noble metals with the N-aminoquinoline substituted iminophosphorane ligand shown in Figure 21 exhibited <sup>3</sup>LC or <sup>3</sup>MLCT emissions. These compounds also showed anti-cancer activity<sup>41</sup>.

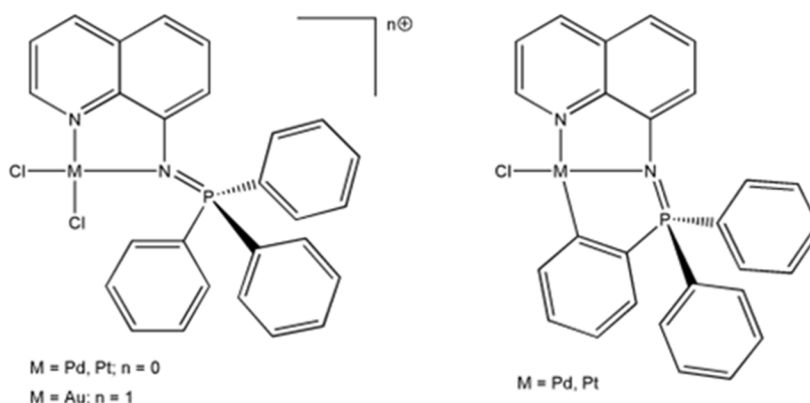


**Figure 21.** Luminescent noble metal complexes with iminophosphorane based ligand in the coordination sphere.

Complexes of copper(I) with iminophosphorane ligands have been studied for their application in the Copper-Catalyzed Azide-Alkyne Cycloaddition (CuAAC), but no study on the luminescence of the species was reported<sup>42</sup>.

Widely studied iminophosphorane ligands derive from the reaction of bis(diphenylphosphino)methane with two equivalents of azide, to obtain symmetric molecules that form upon coordination six-member metallacyclic rings, as depicted in Figure 22. Several metal centres belonging to the first transition series were investigated, such as Mn(II), Co(II), Ni(II) and Zn(II)<sup>43</sup>. As an example, Figure 23 shows the single-crystal X-ray structure of the tetrahedral complex  $[\text{CoCl}_2\{\text{CH}_2(\text{PPh}_2=\text{NPh})_2\}]$ <sup>44</sup>. It is however worth noting that most of the coordination chemistry studies concern bis(iminophosphoranyl)methanides, *i.e.* the conjugate bases obtained from the deprotonation of the methylene bridge between the phosphorus atoms<sup>45</sup>. The structure of the square-planar complex  $[\text{NiBr}\{\text{CH}(\text{PPh}_2=\text{NAr})_2\}]$  (Ar = 2,6-*i*-PrC<sub>6</sub>H<sub>3</sub>) obtained from single-crystal X-ray diffraction is provided as an example in Figure 23. The degree of delocalization on the metallacycle depends upon the metal-centred orbitals involved.



**Figure 22.** Typical reaction affording the formation of complexes with the conjugate bases of methylene-bridged bis-iminophosphoranes.  $MR_2$  = divalent metal alkyl complex.

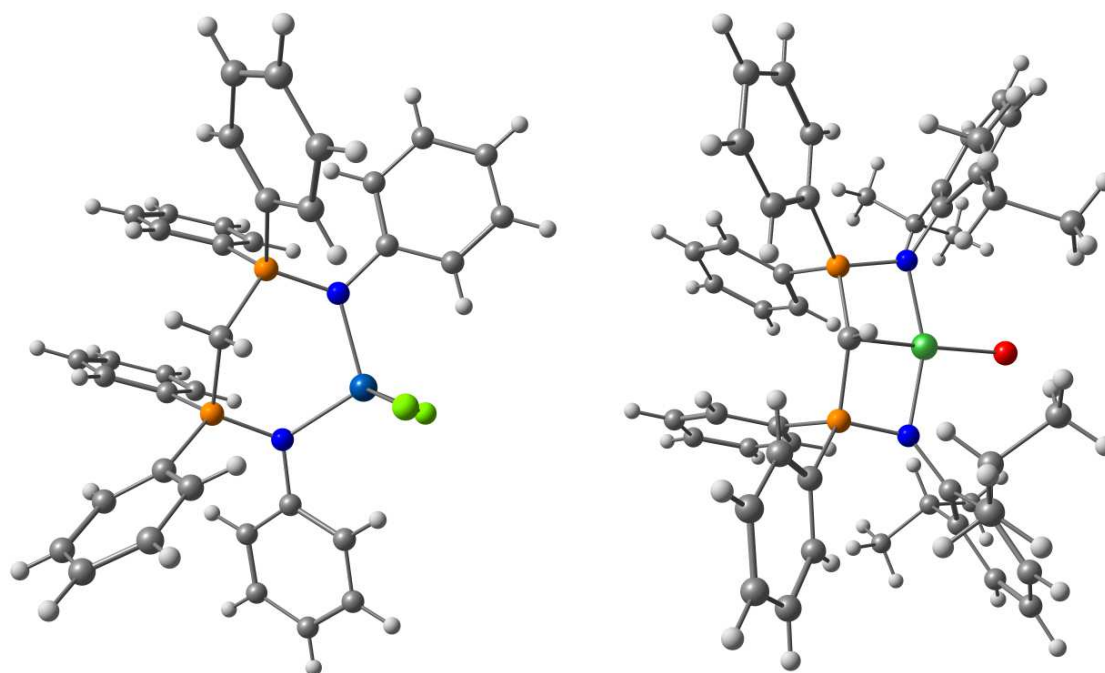


**Figure 23.** X-ray structures of  $[CoCl_2\{CH_2(PPh_2=NPh)_2\}]$  (left) and  $[NiBr\{CH(PPh_2=NAr)_2\}]$  (right). Co, turquoise; Ni, dark green; Cl, green; Br, red; P, orange; N, blue; C, grey; H, white.

For what concerns asymmetrical [N,P]-iminophosphoranes, some compounds have been synthesized, without isolation, as intermediates in the preparation of [N,O]- and [N,S]-ligands as depicted in Figure 24<sup>46</sup>. The phosphine-iminophosphorane  $Me_3SiN=PPh_2CH_2PPh_2$ , obtained by reacting  $Me_3SiN_3$  and  $dppm$ , represents a rare example of structurally characterized compound of this type. The single-crystal X-ray structure is shown in Figure 25<sup>47</sup>.

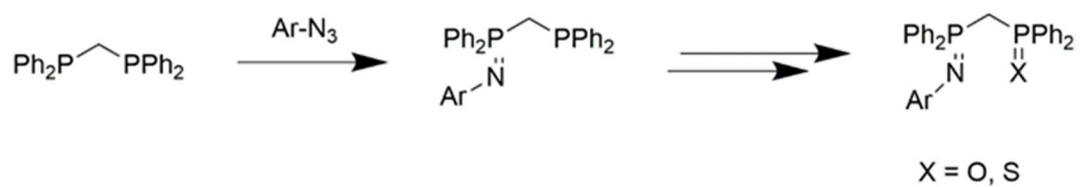


**Figure 24.** Formation of asymmetric [N,O]- [N,S]- ligand through asymmetric [N,P]- iminophosphorane intermediate.

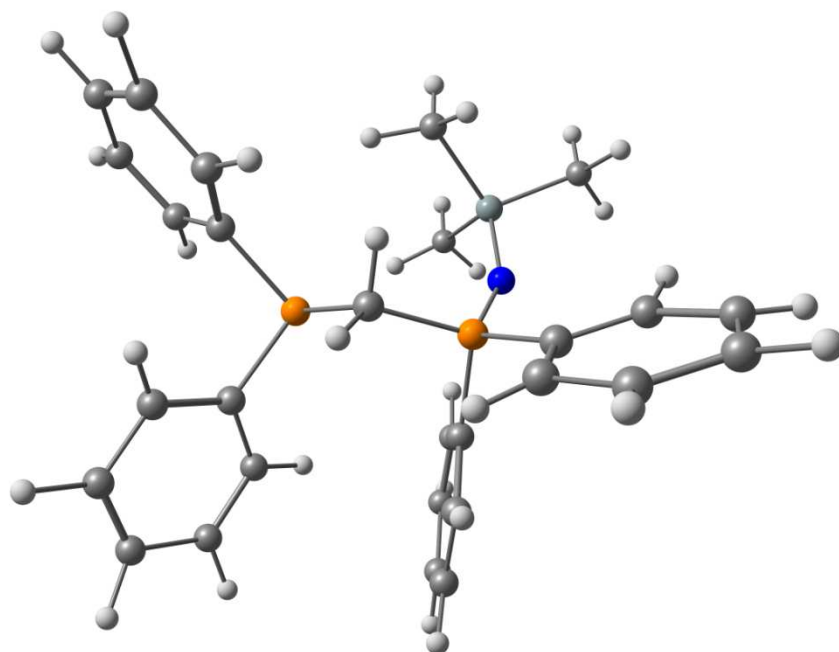


**Figure 25.** X-ray structure of  $\text{Me}_3\text{SiN}=\text{PPh}_2\text{CH}_2\text{PPh}_2$ . P, orange; N, blue; C, grey; H, white.

## 2. Aim of the thesis

The lack of information concerning the luminescence features of iminophosphorane complexes prompted to start a study concerning selected coordination compounds. In particular, the copper(I) and zinc(II) metal centres, both characterized by  $d^{10}$  electronic configuration but with different luminescence mechanisms, were chosen. Given the increased stability associated to the use of multidentate ligands and the generally good luminescence exhibited by copper(I) complexes with mixed [N,P] coordination sphere, the investigation was focused on bidentate [N,P]-ligands containing one iminophosphorane moiety. The first objective of the thesis is thus the isolation and characterization of phosphine-iminophosphorane ligands, derived from the Staudinger reaction between organoazides and bidentate phosphines. Aliphatic and aromatic azides will be used, while bis(diphenylphosphino)methane and 1,2-bis(diphenylphosphino)ethane will be considered as precursors. Once obtained stable ligands, their reaction with suitable metal precursors will be studied with the aim to isolate and characterize new homoleptic and halide metal complexes. The last objective of the thesis is the investigation of the luminescence features, whose rationalization will be supported by electrochemical studies and DFT calculations.

### 3. Experimental section

#### 3.1. Materials and methods

The commercial inorganic and organic reagents were purchased from Merck and used without further purification. The solvents were dried and purified following reported procedures and stored under inert atmosphere<sup>48</sup>. Deuterated solvents for NMR spectroscopy were Euriso-Top products, used as received.

CuX (X = Cl, Br) anhydrous precursors were synthesized in almost quantitative yield by reducing copper(II) salts with sodium sulfite in the presence of the proper halide<sup>49</sup>. A solution of 3.8 g (30 mmol) of Na<sub>2</sub>SO<sub>3</sub> in 25 ml of water is added dropwise under stirring to a solution containing 30 mmol of hydrated CuX<sub>2</sub> (X = Cl, Br) in 5 ml of H<sub>2</sub>O. The mixture changes colour and white CuX slowly separates. The precipitate and the supernatant liquid are subsequently poured into a solution containing 500 mL of water, 0.5 g of Na<sub>2</sub>SO<sub>3</sub> and 1 ml of concentrated HX (X = Cl, Br). The mixture is then stirred and after sedimentation the supernatant liquid is decanted. The solid is washed with diluted H<sub>2</sub>SO<sub>4</sub> and it must always be covered by a layer of this acid solution to prevent its oxidation. Copper(I) halide is then washed four times with 10 ml of glacial acetic acid, three times with 15 ml of dry ethanol and finally six times with 8 ml of anhydrous ether. Due to its air instability, the products are stored inside the glove box. Quantitative yield. CuI was purchased from Aldrich and used as received.

Cu( $\kappa^2$ -BH<sub>4</sub>)(PPh<sub>3</sub>)<sub>2</sub> was synthesized in quantitative yield by reducing copper(II) sulfate with NaBH<sub>4</sub> in the presence of triphenylphosphine<sup>50</sup>. In typical preparation, 0.5 g (2.0 mmol) of copper(II) sulfate pentahydrate and 2.5 g (9.2 mmol) of triphenylphosphine are placed in a flask along with 40 ml of methanol. The resulting suspension is heated until the solids are completely dissolved. After cooling the solution at room temperature, small aliquots of 0.5 g of NaBH<sub>4</sub> are slowly added. The formation of H<sub>2</sub> is observed. The crude product that separates is filtered and dried under reduced pressure. The compound is dissolved in 20 ml of dichloromethane and the solution is filtered on paper filter. After that 25 ml of methanol are added to the solution. Dichloromethane is then removed under reduced pressure until the precipitation of the complex. The product is collected by filtration and dried *in vacuo*. Quantitative yield.

[Cu(NCCH<sub>3</sub>)<sub>4</sub>][BF<sub>4</sub>] was obtained following a procedure reported in literature<sup>51</sup>. The synthesis was performed inside the glove box. To a stirred solution of 0.500 g of copper(I) oxide (3.5 mmol) in 20 mL of acetonitrile, HBF<sub>4</sub>·Et<sub>2</sub>O (1.0 mL) is added. The evolution of

the reaction is indicated by the dissolution of the red solid  $\text{Cu}_2\text{O}$ . After the disappearance of the solid, the solvent is evaporated under reduced pressure to give a brownish solid, that is purified. The precipitate is firstly dissolved in dichloromethane and then the solid impurities are eliminated by centrifugation. This procedure is repeated two times, and all the organic fractions are filtered on cotton and collected together. The solvent is concentrated under reduced pressure, then the complex is precipitated with diethyl ether, filtered and stored inside the glove box. Yield: 60%.

The zinc precursors  $\text{ZnX}_2$  (anhydrous,  $\text{X} = \text{Cl}, \text{Br}, \text{I}$ ),  $\text{Zn}(\text{ClO}_4)_2 \cdot 6\text{H}_2\text{O}$  and  $\text{Zn}_{(\text{s})}$  were purchased from Alfa-Aesar and used as received.

The organic azides were prepared under a fume hood following reported methods. In particular, aliphatic azides were obtained through substitution of bromide by the azide ion, while aromatic azides were synthesized by nitrosation of the corresponding organic hydrazines<sup>52</sup>. Safety note: organic azides are potentially explosive compounds. All the manipulations were carried out using limited quantities of reactants, with careful control of the temperature during all the synthetic steps. Once prepared, the organic azides were stored at  $-25^\circ\text{C}$ . The detailed synthesis of phenylazide,  $\text{PhN}_3$ , is the following: In a flask, phenylhydrazine hydrochloride (4.44 g, 30 mmol) is dissolved in 30 ml of water containing 3 ml of concentrated HCl under stirring. The solution is then cooled in an ice-salt bath. Subsequently, a solution of 2.50 g (30 mmol) of  $\text{NaNO}_2$  is added dropwise, causing the solution to turn orange. After 2 hours, the product is extracted with diethyl ether and dried over anhydrous  $\text{Na}_2\text{SO}_4$ . The solvent is removed under reduced pressure. The product is purified by chromatography on silica column using pentane as the eluent. The solvent is again removed under reduced pressure, yielding a yellow oil with an approximate yield of 55%. To prepare *p*-methylbenzyl azide, *p*-methylbenzylbromide (4.08 g, 22 mmol) is added to a DMSO solution (40 mL) containing 1.62 g of sodium azide. The reaction mixture is stirred overnight at room temperature. Water is added to the reaction mixture and the product is extracted using diethyl ether. The organic solution is dried over anhydrous  $\text{Na}_2\text{SO}_4$  and the solvent is removed under reduced pressure. The organic azide is obtained in nearby quantitative yield.

Unless otherwise stated, the other preparations were carried out in a pressure-controlled glove box (MBraun Labstar) filled with  $\text{N}_2$ . A gas circulation pump connected with a reservoir of activated zeolites allowed to remove traces of water and solvents. The glove box was equipped for organic and inorganic syntheses.

### 3.2. Characterizations

Conductivity measurements were carried out on  $10^{-3}$  M solutions using a Radiometer Copenhagen CDM83 instrument. The temperature was kept at 298 K with a thermostatic bath. The results were interpreted on the basis of literature data<sup>53</sup>.

Melting points were determined using a FALC 360 D instrument equipped with a video recording device.

Infrared spectra in the  $4000 - 450 \text{ cm}^{-1}$  range were recorded with a Perkin-Elmer Spectrum One FT-IR instrument. The samples were dispersed in KBr under  $\text{N}_2$  atmosphere. ATR spectra (diamond crystal) were collected with a Perkin Elmer Spectrum Two spectrometer.

NMR spectra were collected using Bruker Avance 300 and Avance 400 instruments operating respectively at 300.13 MHz and 400.13 MHz of  $^1\text{H}$  resonance.  $^1\text{H}$  NMR and  $^{13}\text{C}$  NMR spectra were referred to the partially non-deuterated fraction of the solvent, itself referred to tetramethylsilane.  $^{31}\text{P}\{^1\text{H}\}$  NMR resonances were referred to 85%  $\text{H}_3\text{PO}_4$  in water.

The absorption spectra of dichloromethane solutions of ligands and complexes were recorded at room temperature with a Yoke 6000Plus double-beam spectrophotometer.

Emission (PL) and excitation (PLE) spectra as well as time-resolved photoluminescence measurements were recorded at room temperature on solid samples with a Horiba Jobin Yvon Fluorolog-3 spectrofluorometer. Air-tight quartz tubes were used and filled under inert atmosphere to prevent the interaction of oxygen- and moisture-sensitive compounds with air. The source was a continuous wave xenon arc lamp, and the wavelength of excitation was selected with a double Czerny-Turner monochromator. Suitable long-pass filters were placed in front of the acquisition systems to avoid second-order effects. The detector was composed by a Hamamatsu R928 photomultiplier tube and a iHR320 monochromator. Photoluminescence decay curves were collected in Multi-Channel Scaling mode (MCS) or Time-correlated Single Photon Counting mode (TCSPC) employing Horiba SpectraLED and NanoLED pulsed sources.

The room-temperature photoluminescence quantum yields ( $\Phi$ ) at the solid state were measured by means of an OceanOptics HR4000CG UV-VIS-NIR detector, fiber-coupled to an integrating sphere connected to OceanOptics UV LED continuous sources ( $\lambda_{\text{excitation max}} = 310 \text{ nm}$ ). Values are reported as average of three measurements.

Cyclic voltammetry measurements were performed at variable scan rate on acetone solutions using an eDAQ ET014-199 potentiostat. Lithium perchlorate was introduced as

supporting electrolyte. The working electrode was a platinum disk (1 mm diameter), while the auxiliary electrode was a 1.6 mm diameter Pt-coated titanium rod. All the electrodes were provided by eDAQ. Ferrocene was added as internal standard and a Pt wire was used as pseudo-reference electrode. All the measurements were carried out at room temperature under argon atmosphere.

XRF spectra were recorded with a Thermo Scientific Niton XL3t instrument. Weighted amounts of solid samples were dispersed in silica gel and stored in polypropylene holders.

The single-crystal X-ray structure determinations were carried out at CACTI (Universidade de Vigo) at 100 K using a Bruker D8 Venture Photon II CMOS detector and Mo-K $\alpha$  radiation ( $\lambda = 0.71073 \text{ \AA}$ ).

### 3.3. Computational details

Computational geometry optimizations, IR simulations and time-dependent DFT (TDDFT) calculations<sup>54</sup> were performed with the PBEh-3c method, which is a reparametrized version of the hybrid-GGA PBE0 functional (with 42% HF exchange) that uses a split-valence double-zeta basis set (def2-mSVP) and adds three corrections considering dispersion, basis set superposition and other basis set incompleteness effects<sup>55</sup>. Further calculations were carried out with the r<sup>2</sup>SCAN method, based on the *meta*-GGA r<sup>2</sup>SCAN functional combined with a tailor-made triple- $\zeta$  Gaussian atomic orbital basis set with refitted D4 and geometrical counter-poise corrections for London-dispersion and basis set superposition error<sup>56</sup>. Another functional, used in particular for TD-DFT calculations<sup>57</sup>, is the hybrid *meta*-GGA TPSS0 (25% Hartree-Fock exchange)<sup>58</sup>, combined with Ahlrich's polarized triple- $\zeta$  def2-TZVP basis set<sup>59</sup>. In selected cases the C-PCM solvation model was added to the calculations<sup>60</sup>.

The software used was ORCA version 5.0.3<sup>61</sup>, running on Intel x86-64- based workstations. The output was elaborated using MultiWFN, version 3.8<sup>62</sup>.

### 3.4. Synthesis of 1-((diphenylphosphaneyl)methyl)-N,1,1-triphenyl-phosphanimine, $\text{NPh}=\text{PPh}_2\text{CH}_2\text{PPh}_2$ ( $\text{dppm}^{\text{NPh}}$ )

In a typical preparation, bis(diphenylphosphino)methane ( $\text{dppm}$ , 1.117 g, 2.9 mmol) was dissolved in 30 mL of toluene, then 0.415 g (3.5 mmol) of phenylazide were slowly added under stirring. The reaction mixture was left under stirring under  $\text{N}_2$  atmosphere for 2 hours at room temperature. The solvent was then removed under reduced pressure. Addition of diethyl ether caused the separation of a light-yellow solid exhibiting greenish luminescence by irradiation with Wood lamp. The product was collected by filtration, washed two times with diethyl ether and dried under vacuum. Yield 40%. Note: large quantities of bis(diphenylphosphino)methane monoxide ( $\text{dppm}^{\text{O}}$ ) are formed if traces of water are present in the phenylazide.

*Characterization of  $\text{dppm}^{\text{NPh}}$ .* M.p. 68 °C (dec.). IR (KBr,  $\text{cm}^{-1}$ ): 3012-2941 ( $\nu_{\text{CH}}$ ), 1590-1436 ( $\nu_{\text{CC}}$  aromatic), 1333 ( $\nu_{\text{NC}}$ ), 1106 ( $\nu_{\text{PN}}+\delta_{\text{CH}}$ ).  $^1\text{H}$  NMR ( $\text{CDCl}_3$ , 300 K):  $\delta$  7.85-7.15 (m, 20H, P-Ph); 7.10-6.55 (m, 5H, N-Ph); 3.27 (d, 2H,  $J_{\text{PH}} = 12.9$  Hz,  $\text{PCH}_2\text{P}$ ).  $^{31}\text{P}\{^1\text{H}\}$  NMR ( $\text{CDCl}_3$ , 300 K): AB spin system,  $\delta_{\text{A}} = 4.03$  ppm ( $\text{PPh}_2=\text{NPh}$ ),  $\delta_{\text{B}} = -27.9$  ppm ( $\text{PPh}_2$ ),  $J_{\text{PP}} = 53.8$  Hz.  $^{13}\text{C}\{^1\text{H}\}$  NMR ( $\text{CDCl}_3$ , 300 K):  $\delta$  133.0-117.0 (aromatic CH), 29.7 ( $^1J_{\text{PC}} = 30.2$  Hz,  $^1J_{\text{PC}} = 70.9$  Hz,  $\text{PCH}_2\text{P}$ ). UV-VIS ( $\text{CH}_2\text{Cl}_2$ , r.t., nm): < 385, 256. PL (solid,  $\lambda_{\text{excitation}} = 350$  nm, nm): 499 (FWHM = 5400  $\text{cm}^{-1}$ ). PLE (solid,  $\lambda_{\text{emission}} = 560$  nm, nm): < 430.  $\tau$  (solid,  $\lambda_{\text{excitation}} = 373$  nm,  $\lambda_{\text{emission}} = 410$  nm, ns): 4.3.

### 3.5. Synthesis of Cu complexes

All the preparations were started with the dissolution of the proper copper(I) precursor in a suitable solvent, followed by the addition of the ligand. In particular, acetonitrile was used in combination with copper(I) halides, while  $[\text{Cu}(\text{NCCH}_3)_4][\text{BF}_4]$  was dissolved in dichloromethane. The reactions were performed at room temperature with vigorous stirring. The work-up procedure was based on the removal of the solvent under reduced pressure, followed by the addition of diethyl ether to precipitate the final products. All the syntheses were performed in glovebox under  $\text{N}_2$  inert atmosphere.

## Synthesis of [CuX(dppm<sup>NPh</sup>)] (X = Cl, Br, I)

In a typical preparation, the proper copper(I) halide (1.0 mmol; X = Cl, 0.099 g; X = Br, 0.143 g; X = I, 0.190 g) was dissolved in 25 mL of acetonitrile. dppm<sup>NPh</sup> (0.475 g, 1.0 mmol) was then added under vigorous stirring. After 4 hours the solvent was removed under reduced pressure and a white solid began to precipitate. To complete the precipitation diethyl ether was dropwise added. The pale green solid obtained was filtered, washed with diethyl ether and dried under vacuum. The complex showed greenish luminescence under Wood lamp irradiation. Yield = 73% (X = Cl), 85% (X = Br), 83% (X = I).

*Characterization of [CuCl(dppm<sup>NPh</sup>)].* M.p. 148 °C. IR (KBr, cm<sup>-1</sup>): 3073-3011 (ν<sub>CH</sub> aromatic), 2991-2849 (ν<sub>CH</sub> aliphatic), 1589-1437 (ν<sub>CC</sub> aromatic), 1284, 1265 (ν<sub>CN</sub>), 1112-1074 (ν<sub>PN+δCH</sub>). <sup>1</sup>H NMR (CDCl<sub>3</sub>, 300 K): δ 8.05-6.55 (m, 25H, Ph); 3.36 (s, br, 2H, PCH<sub>2</sub>P). <sup>31</sup>P{<sup>1</sup>H} NMR (CDCl<sub>3</sub>, 300 K): δ 23.9 (br), -31.9 (br). UV-VIS (CH<sub>2</sub>Cl<sub>2</sub>, r.t., nm): < 400, 296 sh, 260 sh. PL (solid, λ<sub>excitation</sub> = 280 nm, nm): 522 (FWHM = 4900 cm<sup>-1</sup>). PLE (solid, λ<sub>emission</sub> = 560 nm, nm): < 450. τ (solid, λ<sub>excitation</sub> = 373 nm, λ<sub>emission</sub> = 420 nm, ns): 12.9.

*Characterization of [CuBr(dppm<sup>NPh</sup>)].* M.p. 153 °C. IR (KBr, cm<sup>-1</sup>): 3072-3010 (ν<sub>CH</sub> aromatic), 2918-2850 (ν<sub>CH</sub> aliphatic), 1589-1437 (ν<sub>CC</sub> aromatic), 1283, 1265 (ν<sub>CN</sub>), 1112-1074 (ν<sub>PN+δCH</sub>). <sup>1</sup>H NMR (CDCl<sub>3</sub>, 300 K): δ 8.00-6.60 (m, 25H, Ph); 3.30 (s, br, 2H, PCH<sub>2</sub>P). <sup>31</sup>P{<sup>1</sup>H} NMR (CDCl<sub>3</sub>, 300 K): δ 22.9 (br), -33.0 (br). UV-VIS (CH<sub>2</sub>Cl<sub>2</sub>, r.t., nm): < 400, 288 sh, 253 sh. PL (solid, λ<sub>excitation</sub> = 280 nm, nm): 516 (FWHM = 5200 cm<sup>-1</sup>). PLE (solid, λ<sub>emission</sub> = 620 nm, nm): < 480, 407 max. τ (solid, λ<sub>excitation</sub> = 373 nm, λ<sub>emission</sub> = 550 nm, μs): 3.4. τ (soaked with ether, λ<sub>excitation</sub> = 373 nm, λ<sub>emission</sub> = 550 nm, μs): 0.9.

*Characterization of [CuI(dppm<sup>NPh</sup>)].* M.p. 119 °C. IR (KBr, cm<sup>-1</sup>): 3071-3022 (ν<sub>CH</sub> aromatic), 2966-2850 (ν<sub>CH</sub> aliphatic), 1590-1436 (ν<sub>CC</sub> aromatic), 1287-1265 (ν<sub>CN</sub>), 1111-1079 (ν<sub>PN+δCH</sub>). <sup>1</sup>H NMR (CDCl<sub>3</sub>, 300 K): δ 8.00-6.60 (m, 25H, Ph); 3.32 (s, br, 2H, PCH<sub>2</sub>P). <sup>31</sup>P{<sup>1</sup>H} NMR (CDCl<sub>3</sub>, 300 K): δ 23.7 (br), -34.9 (br). UV-VIS (CH<sub>2</sub>Cl<sub>2</sub>, r.t., nm): < 350, 276 sh. PL (solid, λ<sub>excitation</sub> = 360 nm, nm): 484 (FWHM = 4500 cm<sup>-1</sup>). PLE (solid, λ<sub>emission</sub> = 520 nm, nm): < 475, 372 max. τ (solid, λ<sub>excitation</sub> = 290 nm, λ<sub>emission</sub> = 480 nm, μs): 0.9. τ (soaked with ether, λ<sub>excitation</sub> = 290 nm, λ<sub>emission</sub> = 480 nm, μs): 0.7.

### Synthesis of $[\text{Cu}(\text{dppm}^{\text{NPh}})_2][\text{BF}_4]$

$[\text{Cu}(\text{NCCH}_3)_4][\text{BF}_4]$  (1.0 mmol, 0.315 g) was dissolved in 25 mL of dichloromethane. The ligand  $\text{dppm}^{\text{NPh}}$  (0.951 g, 2.0 mmol) was then added under vigorous stirring. After 5 hours the solvent was removed under reduced pressure. A white solid separated by addition of diethyl ether. The product was collected by filtration, washed with diethyl ether and dried under vacuum. The complex did not exhibit appreciable luminescence under Wood lamp irradiation. Yield = 90%.

*Characterization of  $[\text{Cu}(\text{dppm}^{\text{NPh}})_2][\text{BF}_4]$ .* M.p. 215 °C (dec).  $\Lambda_{\text{M}}$  (acetone, 298 K)  $123 \text{ ohm}^{-1} \text{ mol}^{-1} \text{ cm}^2$ . IR (KBr,  $\text{cm}^{-1}$ ): 3074-3024 ( $\nu_{\text{CH}}$  aromatic), 2913-2850 ( $\nu_{\text{CH}}$  aliphatic), 1592-1438 ( $\nu_{\text{CC}}$  aromatic), 1282, 1265 ( $\nu_{\text{CN}}$ ), 1140-940 ( $\nu_{\text{PN}+\delta_{\text{CH}}}$ ,  $\nu_{\text{BF}_4}$ ).  $^1\text{H}$  NMR ( $\text{CDCl}_3$ , 300 K):  $\delta$  7.80-6.80 (m, br, 20H, P-Ph); 7.26 (d, 2H,  $J_{\text{HH}} = 8.3 \text{ Hz}$ , N-Ph); 7.01 (dd, 2H,  $J_{\text{HH}} = 8.3 \text{ Hz}$ ,  $J_{\text{HH}} = 7.3 \text{ Hz}$ , N-Ph); 6.80 (t, 1H,  $J_{\text{HH}} = 7.3 \text{ Hz}$ , N-Ph); 3.38 (s, br, 2H,  $\text{PCH}_2\text{P}$ ).  $^{31}\text{P}\{^1\text{H}\}$  NMR ( $\text{CDCl}_3$ , 300 K):  $\delta$  24.0 (virtual t,  $J_{\text{PP}} = 34.0 \text{ Hz}$ ), -19.8 (s, br). UV-VIS ( $\text{CH}_2\text{Cl}_2$ , r.t., nm): < 400, 292 sh, 255. PL (solid,  $\lambda_{\text{excitation}} = 280 \text{ nm}$ , nm): 531 (FWHM =  $5100 \text{ cm}^{-1}$ ). PLE (solid,  $\lambda_{\text{emission}} = 560 \text{ nm}$ , nm): < 435, 362.  $\tau$  (solid,  $\lambda_{\text{excitation}} = 373 \text{ nm}$ ,  $\lambda_{\text{emission}} = 420 \text{ nm}$ , ns): 7.7.

### Synthesis of $[\text{Cu}(\text{dppe})_2][\text{BF}_4]$

$[\text{Cu}(\text{NCCH}_3)_4][\text{BF}_4]$  (1.0 mmol, 0.315 g) was dissolved in 25 mL of dichloromethane, then 1,2-bis(diphenylphosphino)ethane (dppe, 0.797 g, 2.0 mmol) was added under vigorous stirring. After 3 hours the solvent was removed under reduced pressure. A white solid separated by addition of diethyl ether. The product was collected by filtration, washed with diethyl ether and dried under vacuum. The complex shows greenish luminescence under Wood lamp irradiation. Yield = 87%.

*Characterization of  $[\text{Cu}(\text{dppe})_2][\text{BF}_4]$ .* M.p. 205°C (dec). IR (KBr,  $\text{cm}^{-1}$ ): 3074-3004 ( $\nu_{\text{CH}}$  aromatic), 2913-2850 ( $\nu_{\text{CH}}$  aliphatic), 1484-1435 ( $\nu_{\text{CC}}$  aromatic), 1099-995 ( $\delta_{\text{CH}}$ ,  $\nu_{\text{BF}_4}$ ).  $^1\text{H}$  NMR ( $\text{CDCl}_3$ , 300 K):  $\delta$  7.34 (t, 4H,  $J_{\text{HH}} = 7.0 \text{ Hz}$ , Ph); 7.26-7.14 (m, 16H, Ph); 2.49 (m, br, 4H,  $\text{CH}_2\text{CH}_2$ ).  $^{31}\text{P}\{^1\text{H}\}$  NMR ( $\text{CDCl}_3$ , 300 K):  $\delta$  7.5 (s, br). UV-VIS ( $\text{CH}_2\text{Cl}_2$ , r.t., nm): < 345, 265. PL (solid,  $\lambda_{\text{excitation}} = 300 \text{ nm}$ , nm): 513 (FWHM =  $6100 \text{ cm}^{-1}$ ). PLE (solid,  $\lambda_{\text{emission}} = 515 \text{ nm}$ , nm): < 465, 358 max.  $\tau$  (solid,  $\lambda_{\text{excitation}} = 373 \text{ nm}$ ,  $\lambda_{\text{emission}} = 420 \text{ nm}$ , ns): 3.2.  $\tau$  (solid,  $\lambda_{\text{excitation}} = 290 \text{ nm}$ ,  $\lambda_{\text{emission}} = 510 \text{ nm}$ ,  $\mu\text{s}$ ): 66.

### 3.6. Synthesis of Zn complexes

The syntheses were started with the preparation of a solution of the proper zinc(II) precursor in acetonitrile, followed by the addition of the ligand. The reactions were carried out at room temperature with vigorous stirring. Common steps of the work-up procedures are the removal of the solvent under reduced pressure and the addition of diethyl ether to precipitate the final products. All the syntheses were performed in glovebox under N<sub>2</sub> atmosphere.

#### Synthesis of [ZnX<sub>2</sub>(dppm<sup>NPh</sup>)] (X = Cl, Br, I)

In a typical preparation, the proper anhydrous zinc halide (1.0 mmol; X = Cl, 0.136 g; X = Br, 0.225 g; X = I, 0.319 g) was dissolved in 25 mL of acetonitrile. A stoichiometric quantity (1.0 mmol, 0.475 g) of dppm<sup>NPh</sup> was added under vigorous stirring. The products started to precipitate after a couple of hours. In the cases of X = Cl and X = Br, the solution was concentrated under reduced pressure after 6 hours and diethyl ether was added to complete the precipitation. The separation of the iodo-complex from the acetonitrile solution did not require any further work-up procedure. The white solids obtained were collected by filtration, washed with diethyl ether and dried under vacuum. The complexes exhibited scarcely appreciable luminescence under Wood lamp irradiation. Yield = 73% (X = Cl), 80% (X = Br), 80% (X = I).

*Characterization of [ZnCl<sub>2</sub>(dppm<sup>NPh</sup>)]* M.p. > 230 °C. IR (KBr, cm<sup>-1</sup>): 3078-3023 (ν<sub>CH</sub> aromatic), 2918-2850 (ν<sub>CH</sub> aliphatic), 1588-1438 (ν<sub>CC</sub> aromatic), 1250 (ν<sub>CN</sub>), 1116-1102 (ν<sub>PN+δCH</sub>). <sup>1</sup>H NMR (CDCl<sub>3</sub>, 300 K): δ 7.97-7.25 (m, 20H, P-Ph); 7.10 (d, 2H, J<sub>HH</sub> = 8.2 Hz, N-Ph); 6.99 (dd, 2H, J<sub>HH</sub> = 8.2 Hz, J<sub>HH</sub> = 7.3 Hz, N-Ph); 6.79 (t, 1H, J<sub>HH</sub> = 7.3 Hz, N-Ph); 3.37 (dd, 2H, J<sub>PH</sub> = 10.9 Hz, J<sub>PH</sub> = 5.7 Hz, PCH<sub>2</sub>P). <sup>31</sup>P{<sup>1</sup>H} NMR (CDCl<sub>3</sub>, 300 K): AB spin system, δ<sub>A</sub> = 25.5 ppm (PPh<sub>2</sub>=NPh), δ<sub>B</sub> = -36.3 ppm (PPh<sub>2</sub>), J<sub>AB</sub> = 12.0 Hz. UV-VIS (CH<sub>2</sub>Cl<sub>2</sub>, r.t., nm): < 365, 276 sh, 269 sh. PL (solid, λ<sub>excitation</sub> = 360 nm, nm): 515 (FWHM = 6500 cm<sup>-1</sup>). PLE (solid, λ<sub>emission</sub> = 510 nm, nm): < 400, 347. τ (solid, λ<sub>excitation</sub> = 373 nm, λ<sub>emission</sub> = 430 nm, ns): 12.9.

*Characterization of [ZnBr<sub>2</sub>(dppm<sup>NPh</sup>)<sub>2</sub>]* M.p. > 230 °C. IR (KBr, cm<sup>-1</sup>): 3078-3023 (ν<sub>CH</sub> aromatic), 2918-2850 (ν<sub>CH</sub> aliphatic), 1588-1438 (ν<sub>CC</sub> aromatic), 1249, 1239 (ν<sub>CN</sub>), 1116-1102 (ν<sub>PN+δCH</sub>). <sup>1</sup>H NMR (CDCl<sub>3</sub>, 300 K): δ 8.00-7.15 (m, 20H, P-Ph); 7.11 (d, 2H, J<sub>HH</sub> = 7.8 Hz, N-Ph); 6.98 (t, 2H, J<sub>HH</sub> = 7.6 Hz, N-Ph); 6.78 (t, 1H, J<sub>HH</sub> = 7.4 Hz, N-Ph); 3.41 (dd, 2H, J<sub>PH</sub> = 10.7 Hz, J<sub>PH</sub> = 5.7 Hz, PCH<sub>2</sub>P). <sup>31</sup>P{<sup>1</sup>H} NMR (CDCl<sub>3</sub>, 300 K): δ 26.5 (d, J<sub>PP</sub> = 12.0 Hz, PPh<sub>2</sub>=NPh); -38.0 (s, br, PPh<sub>2</sub>). UV-VIS (CH<sub>2</sub>Cl<sub>2</sub>, r.t., nm): < 365, 276 sh, 269 sh. PL (solid, λ<sub>excitation</sub> = 280 nm, nm): 459 (FWHM = 5700 cm<sup>-1</sup>). PLE (solid, λ<sub>emission</sub> = 510 nm, nm): < 385. τ (solid, λ<sub>excitation</sub> = 373 nm, λ<sub>emission</sub> = 430 nm, ns): 3.7.

*Characterization of [ZnI<sub>2</sub>(dppm<sup>NPh</sup>)<sub>2</sub>]*. M.p. > 230 °C. IR (KBr, cm<sup>-1</sup>): 3078-3023 (ν<sub>CH</sub> aromatic), 2918-2850 (ν<sub>CH</sub> aliphatic), 1588-1438 (ν<sub>CC</sub> aromatic), 1253 (ν<sub>CN</sub>), 1116-1110 (ν<sub>PN+δCH</sub>). UV-VIS (CH<sub>2</sub>Cl<sub>2</sub>, r.t., nm): < 350, 276 sh, 269 sh. PL (solid, λ<sub>excitation</sub> = 290 nm, nm): 515 sh, 597. PL (solid, λ<sub>excitation</sub> = 280 nm, nm): 340-700 (very weak).

#### Synthesis of [Zn(dppm<sup>NPh</sup>)<sub>2</sub>][BF<sub>4</sub>]

Zn<sub>(s)</sub> (1.0 mmol, 0.065 g) was suspended in 25 mL of acetonitrile, then 141 μl of HBF<sub>4</sub>·Et<sub>2</sub>O (1.0 mmol) were added. The progressive dissolution of metallic zinc was observed. Traces of unreacted Zn were removed after 30 minutes by decanting the solution. 0.960 g (2.0 mmol) of dppm<sup>NPh</sup> were added under vigorous stirring. After 1 hour the solvent was removed under reduced pressure. The residual solid was collected by filtration after addition of diethyl ether and dried under vacuum. The complex shows pale green luminescence under Wood lamp irradiation. Yield = 80%.

*Characterization of [Zn(dppm<sup>NPh</sup>)<sub>2</sub>][BF<sub>4</sub>]*. M.p. 65 °C (dec). Λ<sub>M</sub> (acetone, 298 K) 206 ohm<sup>-1</sup> mol<sup>-1</sup>cm<sup>2</sup>. IR (KBr, cm<sup>-1</sup>): 3078-3023 (ν<sub>CH</sub> aromatic), 2918-2850 (ν<sub>CH</sub> aliphatic), 1588-1438 (ν<sub>CC</sub> aromatic), 1253 (ν<sub>CN</sub>), 1170-970 (ν<sub>PN+δCH</sub>, ν<sub>BF<sub>4</sub></sub>). <sup>1</sup>H NMR (CDCl<sub>3</sub>, 300 K): δ 8.00-7.15 (m, 20H, P-Ph); 7.07 (t, 2H, J<sub>HH</sub> = 7.8 Hz, N-Ph); 6.91 (t, 1H, J<sub>HH</sub> = 7.6 Hz, N-Ph); 6.82 (d, 2H, J<sub>HH</sub> = 8.2 Hz, N-Ph); 3.84 (d, 2H, J<sub>PH</sub> = 16.1 Hz, PCH<sub>2</sub>P). <sup>31</sup>P{<sup>1</sup>H} NMR (CDCl<sub>3</sub>, 300 K): δ 34.2 (s, br, PPh<sub>2</sub>=NPh); -32.6 (d, J<sub>PP</sub> = 79.1 Hz, PPh<sub>2</sub>). UV-VIS (CH<sub>2</sub>Cl<sub>2</sub>, r.t., nm): < 350, 264 sh. PL (solid, λ<sub>excitation</sub> = 280 nm, nm): 503 (FWHM = 5600 cm<sup>-1</sup>). PLE

(solid,  $\lambda_{\text{emission}} = 515 \text{ nm}$ , nm): < 415, 354 max.  $\tau$  (solid,  $\lambda_{\text{excitation}} = 373 \text{ nm}$ ,  $\lambda_{\text{emission}} = 420 \text{ nm}$ , ns): 7.2.

## 4. Result and discussion

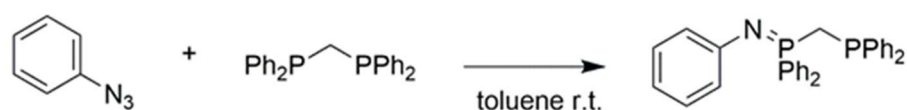
### 4.1 Staudinger reactions between diphosphines and organoazides

The approach followed during the thesis for the preparation of iminophosphorane-based [N,P]-ligands is the stoichiometric reaction between a bidentate phosphine and an organic azide, a method already explored in the past for the preparation of  $\text{Me}_3\text{SiN}=\text{PPh}_2\text{CH}_2\text{PPh}_2$  and of related intermediates to be oxidized to *N*-aryl-*P,P*-diphenyl-*P*-(diphenylphosphino)l)methyl- $\lambda^5$ -phosphazenes<sup>46,47</sup>. The phosphines considered during the thesis work are bis(diphenylphosphino)methane (dppm) and 1,2-bis(diphenylphosphino)ethane (dppe). Both aromatic and aliphatic organoazides were reacted with the diphosphines.

The preliminary screening revealed that the reactions with dppe did not afford the desired products, despite the fact that the syntheses were carried out under inert atmosphere and with anhydrous solvents. In particular, the 1:1 reaction between dppe and  $\text{PhN}_3$  allowed to isolate a solid dominated by a single, slightly broad  $^{31}\text{P}\{^1\text{H}\}$  NMR resonance at 7.2 ppm ( $\text{CDCl}_3$ , 300 K), suggesting chemical equivalence of the two phosphorus atoms on the NMR timescale. The  $^{31}\text{P}\{^1\text{H}\}$  NMR resonance of the reactant was not observable. Besides stoichiometry problems, the chemical shift value is not compatible with the formation of the symmetric compound related to the Staudinger reaction on both the phosphorus atoms<sup>63</sup>. An AB spin system ( $\delta_A = 31.1$  ppm,  $\delta_B = -12.6$  ppm,  $J_{AB} = 50.8$  Hz) was present only in traces. The  $^1\text{H}$  NMR spectrum shows resonances in the aromatic region attributable to both P- and N-bonded phenyl rings. Moreover, a broad resonance at 2.75 ppm is possibly related to an ethylene fragment bridging the phosphorus atoms. The same outcomes were obtained by carrying out the reaction in a NMR tube filled under  $\text{N}_2$ , in order to avoid possible decompositions in the work-up procedure (Figure S1, S2). The NMR data are not compatible with the formation of an asymmetric [N,P]-donor species and are also in contrast to the mechanism proposed for the dppe-based Staudinger/aza-Wittig synthesis of glycosyl amides<sup>64</sup>. The presence of unreacted  $\text{PhN}_3$  or the isolation of phosphazides was excluded by the IR spectra. The characterization data are not sufficient to propose a formulation for the apparently symmetric compound obtained. Single-crystal X-ray diffraction appears necessary to unambiguously understand the structure of the isolated species. Attempts to isolate single crystals suitable for X-ray diffraction are in progress.

The initial screening also revealed that benzylic azides do not lead to the formation of stable [N,P]-donor ligands. In particular, after several attempts the reaction between dppm and  $\text{CH}_3\text{C}_6\text{H}_4\text{CH}_2\text{N}_3$  at room temperature was followed by NMR spectroscopy. After few minutes the  $^{31}\text{P}\{^1\text{H}\}$  NMR spectrum showed the presence of an AB spin system ( $\delta_{\text{A}} = 10.8$  ppm,  $\delta_{\text{B}} = -29.0$  ppm,  $J_{\text{AB}} = 53.3$  Hz,  $\text{CDCl}_3$ , 300 K) compatible with the target product *N*-4-methylbenzyl-1-((diphenylphosphaneyl)methyl)-1,1-diphenyl-phosphanimine ( $\text{dppm}^{\text{NBz}}$ ). The solution contained a large quantity of unreacted dppm and the  $^1\text{H}$  NMR spectrum revealed the presence of free  $\text{CH}_3\text{C}_6\text{H}_4\text{CH}_2\text{N}_3$ . During time the progressive appearance of other products was observed in the  $^{31}\text{P}\{^1\text{H}\}$  NMR spectrum before the complete disappearance of dppm (Figure S3). It is concluded that the formation of  $\text{dppm}^{\text{NBz}}$  is followed by a faster reaction causing the progressive decomposition. The presence of unreacted dppm does not allow the use of the crude reaction mixture immediately obtained after mixing the reactants in coordination chemistry studies with  $d^{10}$  metal centres.

The ligand 1-((diphenylphosphaneyl)methyl)-*N*,1,1-triphenyl-phosphanimine ( $\text{dppm}^{\text{NPh}}$ ), obtained from the reaction between dppm and  $\text{PhN}_3$  at room temperature in toluene, revealed to be sufficiently stable to be used in coordination chemistry studies with suitable metal precursors. The  $^1\text{H}$  NMR spectrum ( $\text{CDCl}_3$ , 300 K) shows both N- and P-bonded phenyl resonances in the high-frequency region. The methylene bridge resonates at 3.27 ppm and couples with one of the two phosphorus atoms ( $J_{\text{PH}} = 12.9$  Hz), most likely the  $\text{P}=\text{NPh}$  one. The coupling was confirmed by  $^1\text{H}\{^{31}\text{P}\}$  NMR spectroscopy (Figure 26). The lack of coupling with the other phosphorus is not surprising, considering that the same coupling is not detectable also for free dppm under the same conditions. The corresponding  $^{13}\text{C}\{^1\text{H}\}$  NMR resonance was individuated at 29.7 ppm thanks to the *edited*-HSQC spectrum. The methylene carbon couples with both the phosphorus atoms, with  $^1J_{\text{PC}}$  coupling constants of 33.2 and 70.9 Hz. The  $^{31}\text{P}\{^1\text{H}\}$  NMR spectrum shows an AB spin system ( $\delta_{\text{A}} = 4.0$  ppm,  $\delta_{\text{B}} = -27.9$  ppm,  $J_{\text{AB}} = 53.8$  Hz,  $\text{CDCl}_3$ , 300 K), as observable in Figure 27.



**Scheme 1.** synthesis of  $\text{dppm}^{\text{NPh}}$ .

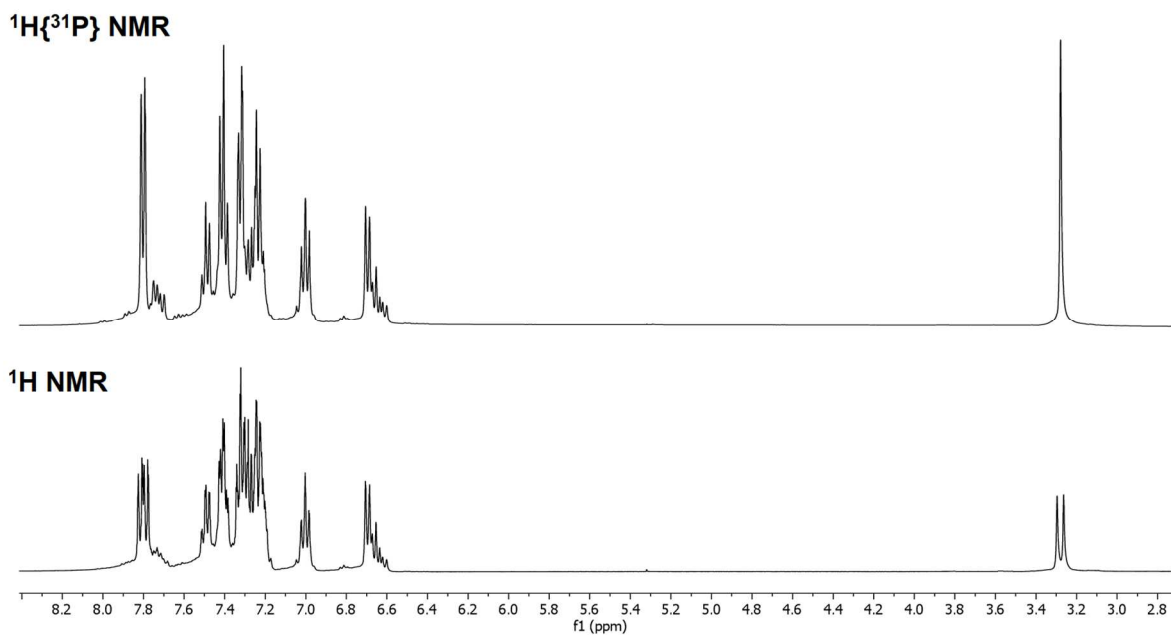


**Figure 26.**  $^1\text{H}$  NMR and  $^1\text{H}\{^{31}\text{P}\}$  NMR spectra of  $\text{dppm}^{\text{NPh}}$ .  $\text{CDCl}_3$ , 300 K.

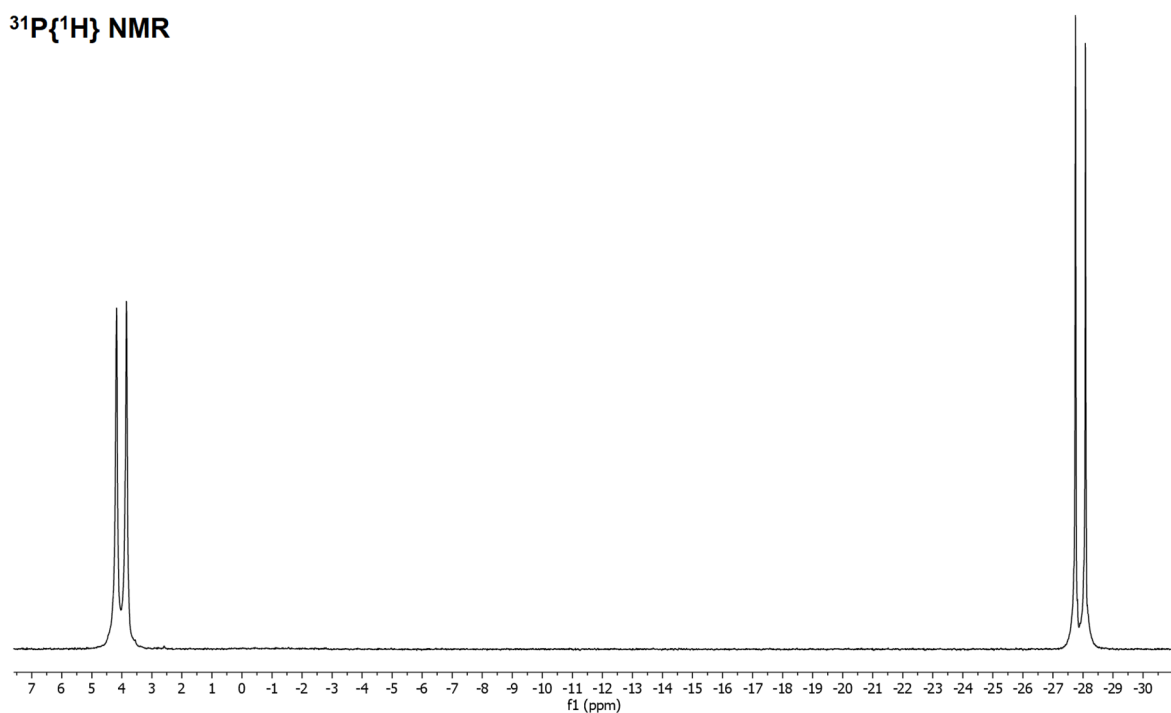


**Figure 27.**  $^{31}\text{P}\{^1\text{H}\}$  NMR spectrum of  $\text{dppm}^{\text{NPh}}$ .  $\text{CDCl}_3$ , 300 K.

The IR spectrum (Figure 28), recorded trying to avoid the interaction of  $\text{dppm}^{\text{NPh}}$  with water, shows the typical bands associated to the phenyl substituents and the C-N bond. The  $\nu_{\text{P=N}}$  stretching is tentatively assigned to a medium intensity band at  $1106\text{ cm}^{-1}$ , according to the literature<sup>65</sup>. The assignment was confirmed by the IR simulation carried

out on the DFT-optimized structure of  $\text{dppm}^{\text{NPh}}$ , shown in Figure 28. The  $\nu_{\text{P=N}}$  stretching results mixed with several  $\delta_{\text{CH}}$  bendings, involving in particular the N-bonded phenyl ring. The computed P=N distance, 1.597 Å, is longer than that experimentally found for the N-tyrimethylsilyl-substituted iminophosphorane  $\text{Me}_3\text{SiN}=\text{PPh}_2\text{CH}_2\text{PPh}_2$ , 1.529(3) Å<sup>47</sup>, probably because of partial delocalization of electron density on the N-bonded aromatic ring.

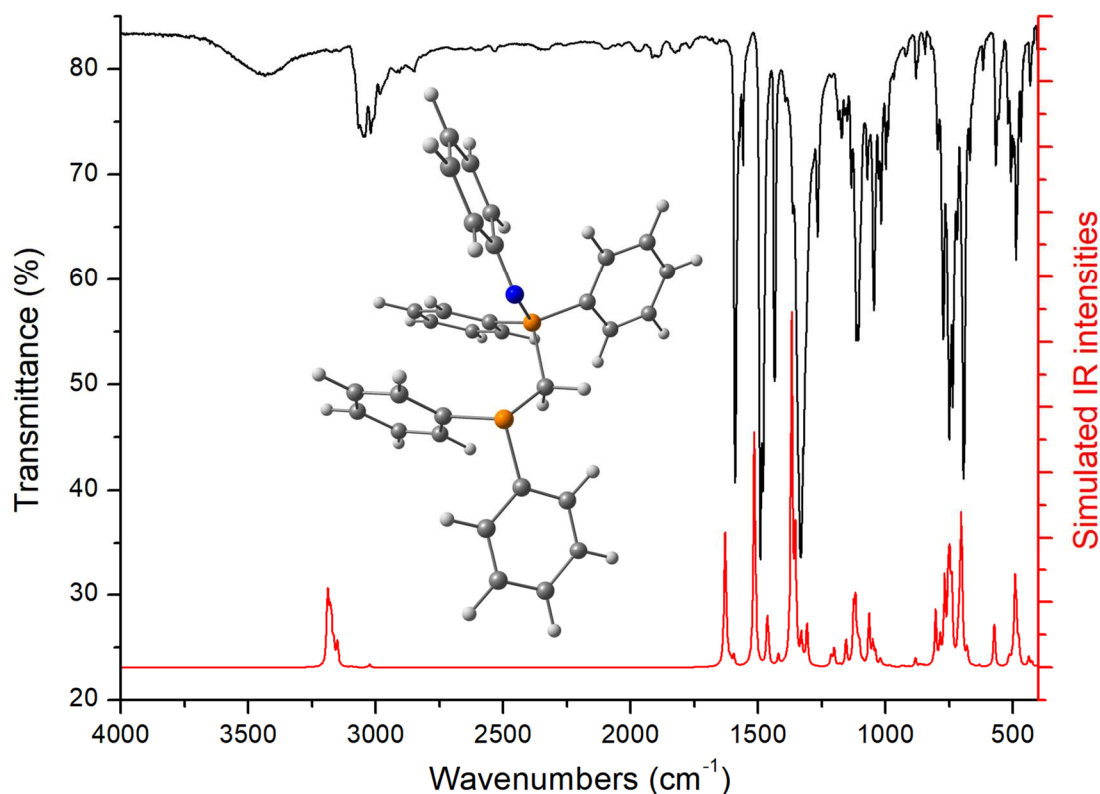


**Figure 28.** Experimental (black) and simulated (red, Lorentzian interpolation, FWHM = 8  $\text{cm}^{-1}$ ) IR spectra of  $\text{dppm}^{\text{NPh}}$  and DFT-optimized (r<sup>2</sup>SCAN-3c) structure (P, orange; N, blue; C, grey; H, white).

The ligand exhibited moderated thermal stability, decomposing at temperatures above 68 °C. The iminophosphorane moiety is rapidly hydrolysed in the presence of water traces, affording the related bis(diphenylphosphino)methane monoxide ( $\text{dppm}^{\text{O}}$ )<sup>46</sup>.

Cyclic voltammetry measurements in anhydrous acetonitrile showed a scarcely reversible oxidation peak with maximum around 0.45 V vs.  $\text{Fc}^+/\text{Fc}$ . The back-reduction process is however observable around 0.36 V vs.  $\text{Fc}^+/\text{Fc}$ , despite the low current intensity. The first oxidation is followed by further oxidation processes at higher potential. The cathodic region is dominated by a reduction process peaked at -1.77 V vs.  $\text{Fc}^+/\text{Fc}$ . Despite the fact

that a back-oxidation process is observable around -1.15 V, the reduction of  $\text{dppm}^{\text{NPh}}$  can be considered scarcely reversible (Figure 29). The quite low oxidation potential of  $\text{dppm}^{\text{NPh}}$  prompted to investigate the molecular regions most subjected to electron loss from a computational point of view. The HOMO of  $\text{dppm}^{\text{NPh}}$  is mostly localized on the  $\{\text{P}=\text{NPh}\}$  fragment, with the participation of the phenyl rings bonded to the iminophosphorane phosphorus (Figure 29). The involvement of the iminophosphorane moiety, the  $\{\text{NPh}\}$  fragment in particular, in the first oxidation process is confirmed by the spin density plot of the DFT-optimized radical cation  $[\text{dppm}^{\text{NPh}}]^+$ , observable in Figure 29.

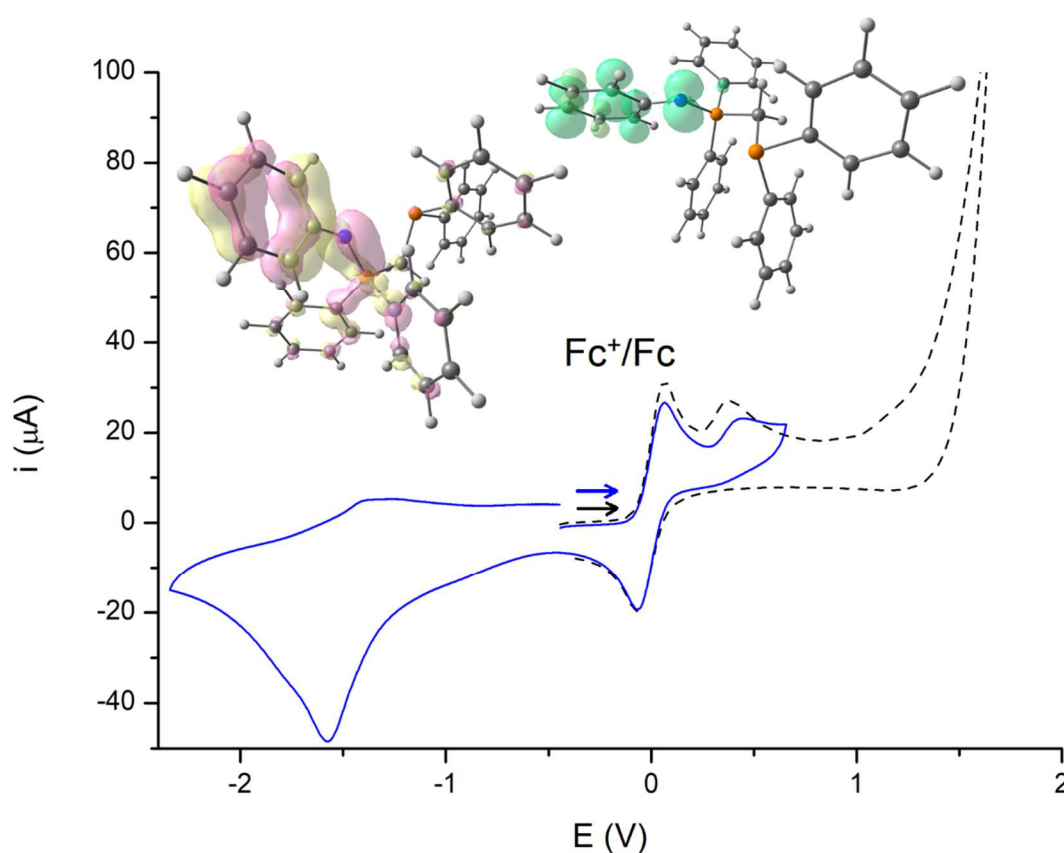


**Figure 29.** Cyclic voltammograms of  $\text{dppm}^{\text{NPh}}$  (Pt, acetonitrile/ $\text{LiClO}_4$ , scan speed =  $250 \text{ mV s}^{-1}$ , potentials referred to  $\text{Fc}^+/\text{Fc}$ ), HOMO of  $\text{dppm}^{\text{NPh}}$  (pink and yellow tones, isovalue = 0.03 a.u.) and spin density of  $[\text{dppm}^{\text{NPh}}]^+$  (green tones, isovalue = 0.005 a.u.). P, orange; N, blue; C, grey; H, white. C-PCM/ $r^2\text{SCAN-3c}$  calculations, acetonitrile as continuous medium.

Dichloromethane solutions of  $\text{dppm}^{\text{NPh}}$  absorb radiation in the UV range for wavelengths shorter than 385 nm (Figure 30). The compound exhibited weak emission at the solid state at room temperature upon excitation with UV light ( $\Phi$  around 3%). The wide PL band

(FWHM = 4800  $\text{cm}^{-1}$ ) is centred at 496 nm. The chromaticity coordinates are  $x = 0.276$  and  $y = 0.392$ , corresponding to a point in the green region of the CIE 1931 chromaticity diagram<sup>66</sup>. The PLE spectrum revealed that the emission occurs for excitation wavelengths shorter than 430 nm (Figure 30).

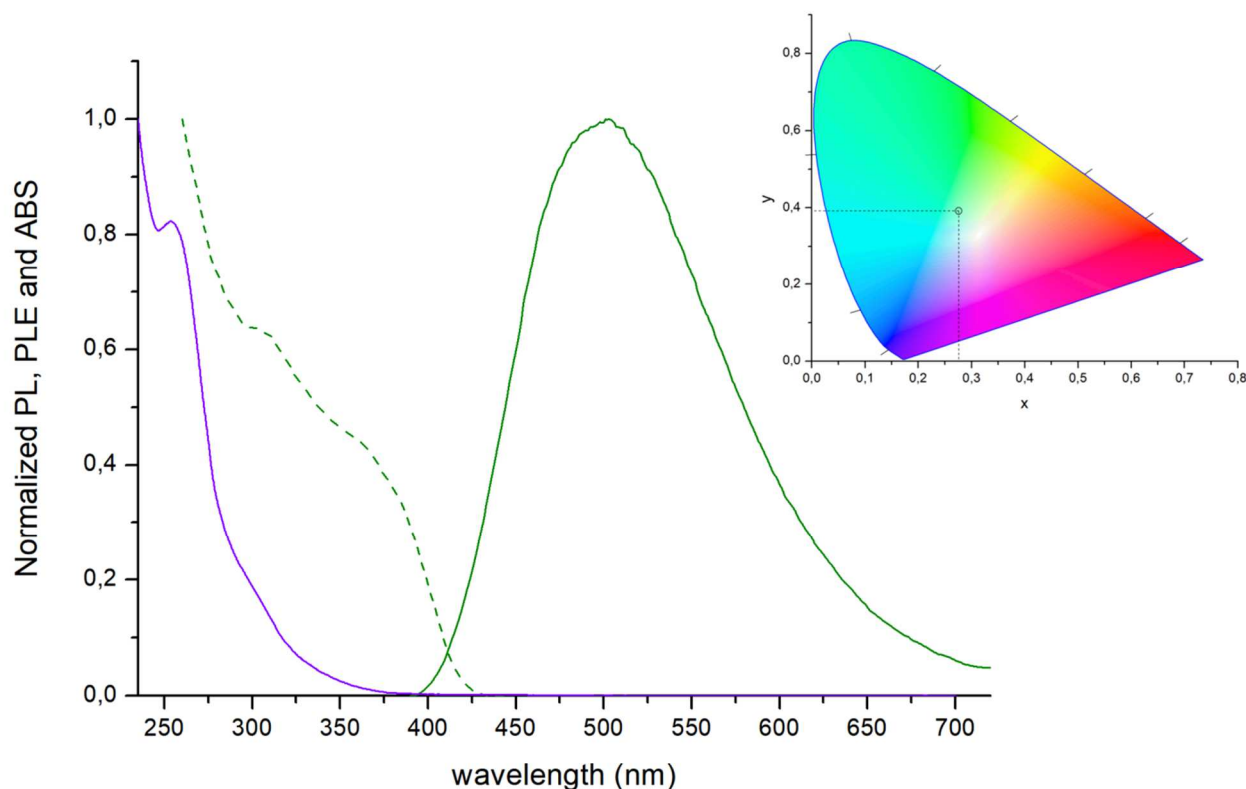


**Figure 30.** Normalized absorption (dichloromethane solution, r.t., violet line), emission and excitation (solid sample, r.t., continuous and dashed green lines,  $\lambda_{\text{excitation}} = 280$  nm,  $\lambda_{\text{emission}} = 560$  nm) spectra of  $\text{dppm}^{\text{NPh}}$ . CIE 1931 chromaticity diagram and chromaticity coordinates.

The lifetime derived from the PL decay curve is around 4 ns, thus the radiative emission of  $\text{dppm}^{\text{NPh}}$  can be considered as a fluorescence (Figure 31). The decay curve suggests the possible presence of a second, much longer component, but the weak intensity of the emission prevented its determination. The first singlet excited state is predicted by TD-DFT calculations with relative energy of 3.75 eV (330 nm) considering the ground-state optimized geometry, and the value is almost unaffected by the inclusion of spin-orbit coupling. The transition involves the frontier orbitals, *i.e.* the previously described HOMO and the LUMO, this last mainly localized on the  $\{\text{Ph}_2\text{PN}\}$  fragment. The fluorescent emission is most likely derived from the first singlet excited state after relaxation of the structure. On considering the orbitals involved, the emission appears best described as

derived from an intraligand charge transfer (ILCT), as also deducible from the hole-electron distribution<sup>67</sup> shown in Figure 31. The approximate value of quantum yield prevents a precise determination of the radiative ( $k_r$ ) and non-radiative ( $k_{nr}$ ) decay constants, that can be however estimated in the  $10^6 \text{ s}^{-1}$  and  $10^8 \text{ s}^{-1}$  ranges, respectively.

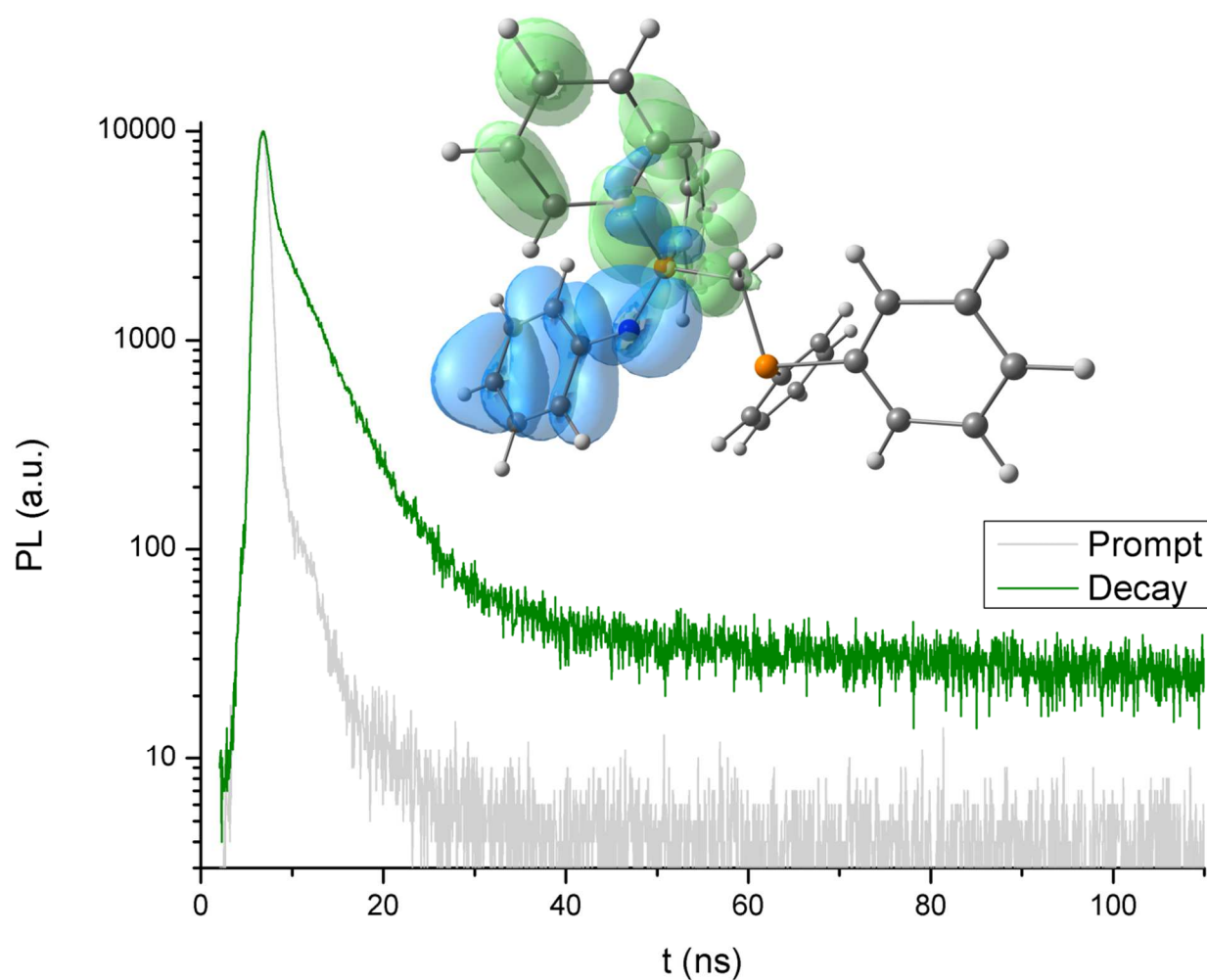
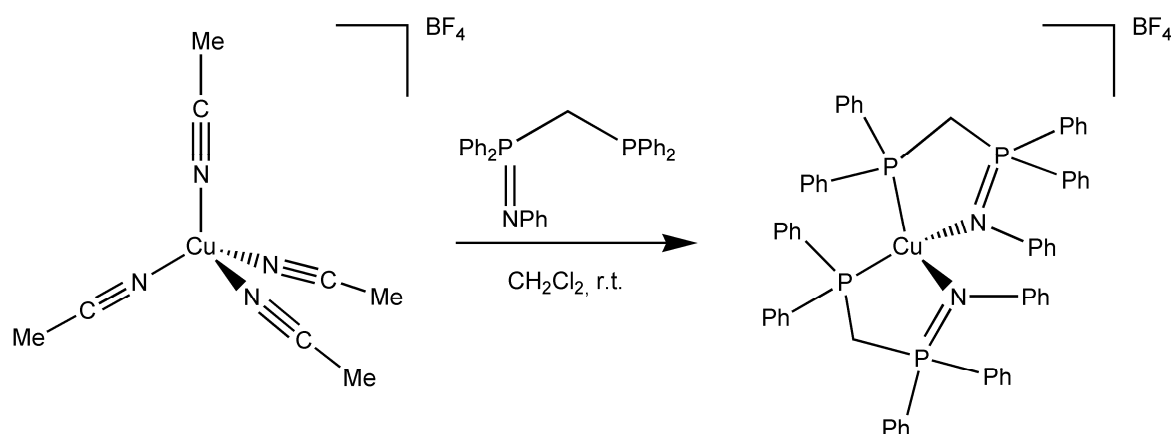


**Figure 31.** Photoluminescence decay curve of  $\text{dppm}^{\text{NPh}}$  (solid sample, r.t.,  $\lambda_{\text{excitation}} = 373 \text{ nm}$ ,  $\lambda_{\text{emission}} = 410 \text{ nm}$ ). Hole (blue) and electron (green) distributions for the  $S_1 \leftarrow S_0$  transition (isovalue = 0.001 a.u.). Emission is the reverse process. C-PCM/TPSS0/def2-TZVP calculations, dichloromethane as continuous medium. Cu, red; P, orange; C, grey; H, white.

## 4.2 Copper(I) complexes with $\text{dppm}^{\text{NPh}}$

The studies on coordination compounds started by reacting  $\text{dppm}^{\text{NPh}}$  with  $[\text{Cu}(\text{NCCH}_3)_4][\text{BF}_4]$  as metal precursor in 2:1 ratio, to obtain the homoleptic complex having formula  $[\text{Cu}(\text{dppm}^{\text{NPh}})_2][\text{BF}_4]$  (Scheme 2).



**Scheme 2.** Synthesis of  $[\text{Cu}(\text{dppm}^{\text{NPh}})_2][\text{BF}_4]$ .

The  $^1\text{H}$  and  $^{31}\text{P}\{^1\text{H}\}$  NMR spectra, reported in Figures 32-33, show resonances in line with those of the free ligand, broadened by the fluxional coordination behaviour. In particular, in the aromatic region of the  $^1\text{H}$  NMR spectrum a doublet at 7.26 ppm and two triplets at 7.01 and 6.80 ppm are attributable to the N-bonded phenyl rings, also thanks to the lack of couplings with  $^{31}\text{P}$ . On the other hand, the P-bonded phenyl resonances between 7.90 and 6.85 ppm are much broader, most likely because of the steric congestion caused by coordination. The methylene bridges correspond to a broad singlet centred at 3.38 ppm. The  $^{31}\text{P}\{^1\text{H}\}$  NMR spectrum shows two distinct signals, one broad at -19.8 ppm attributable to the phosphine moieties, and the other sharp ( $\delta = 24.0$  ppm) and associated to the iminophosphorane fragments. It is worth noting that this last  $^{31}\text{P}$  resonance is high-frequency shifted by about 20 ppm with respect to the free ligand, probably because the coordination makes the ylidic form of the  $\{\text{PNPh}\}$  moiety more relevant. The coupling among non-equivalent phosphorus nuclei furnishes a proof of the presence of two ligands in the coordination sphere of the same Cu(I) centre. The resonance at higher frequency is in fact a triplet because of a second-order effect known as virtual coupling<sup>68</sup>. The presence of a  $^2J_{\text{PP}}$  coupling between the two phosphine moieties, unobservable because

of the magnetic equivalency, causes the apparent coupling of the iminophosphorane groups with the  $^{31}\text{P}$  nuclei of both the phosphines present in the complex. The real  $J_{\text{PP}}$  phosphine-iminophosphorane coupling constant in  $[\text{Cu}(\text{dppm}^{\text{NPh}})_2][\text{BF}_4]$  is 34.0 Hz, while the  $^2J_{\text{PP}}$  constant between the phosphines is expected to be almost two times greater.

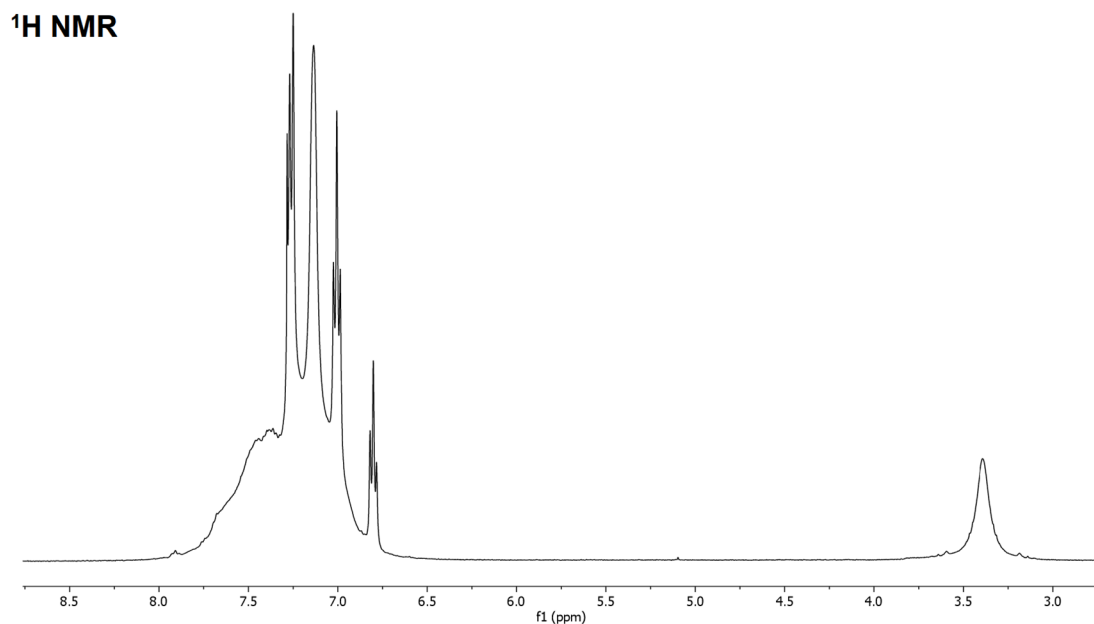


**Figure 32.**  $^1\text{H}$  NMR spectrum of  $[\text{Cu}(\text{dppm}^{\text{NPh}})_2][\text{BF}_4]$ .  $\text{CDCl}_3$ , 300 K.

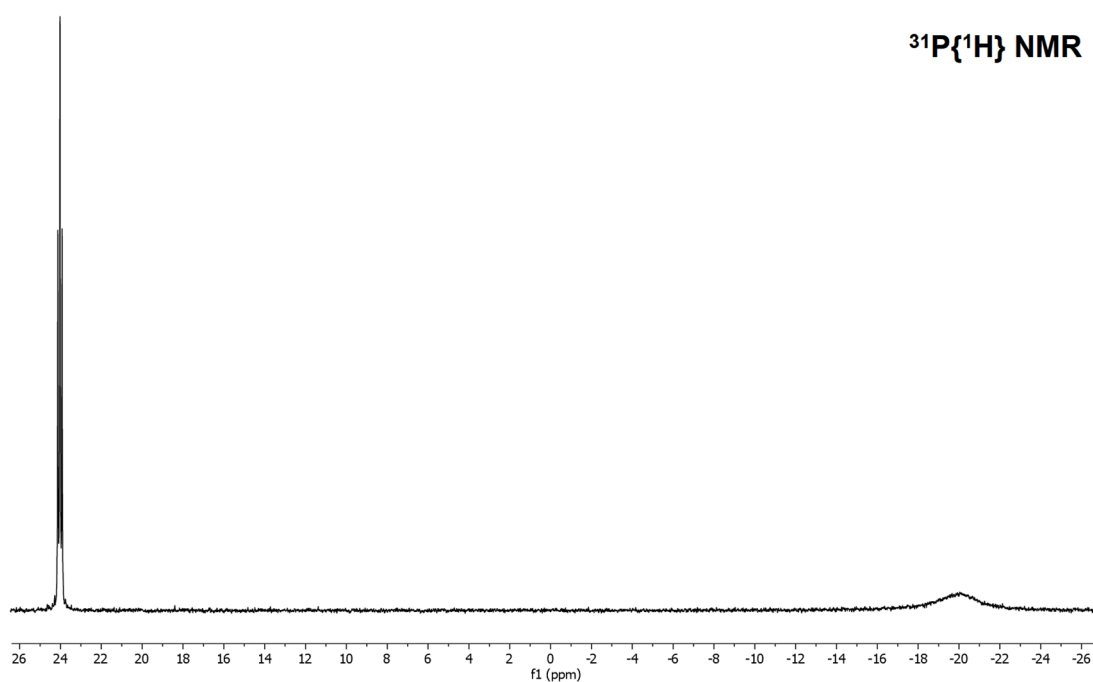


**Figure 33.**  $^{31}\text{P}\{^1\text{H}\}$  NMR spectrum of  $[\text{Cu}(\text{dppm}^{\text{NPh}})_2][\text{BF}_4]$ .  $\text{CDCl}_3$ , 300 K.

Melting point measurements revealed that the decomposition temperature of the complex is around 200 °C, much higher than that of free  $\text{dppm}^{\text{NPh}}$ . It is likely to suppose that the alteration of the iminophosphorane electronic structure caused by coordination, evidenced by the  $^{31}\text{P}\{^1\text{H}\}$  NMR spectrum, raises the activation energy of the decomposition pathways.

The IR spectrum is quite similar to that of the free ligand, with the obvious superposition of bands attributable to the tetrafluoroborate anion around  $1000\text{ cm}^{-1}$ . Unfortunately, the presence of  $\nu_{\text{BF}_4}$  stretchings make difficult the assignment of the  $\nu_{\text{PN}}$  bands. It is however worth noting that the coordination causes a noticeable shift at lower wavenumbers of the band present at  $1333\text{ cm}^{-1}$  in the spectrum of free  $\text{dppm}^{\text{NPh}}$ , attributed to the  $\nu_{\text{CN}}$  stretching. In the  $[\text{Cu}(\text{dppm}^{\text{NPh}})_2][\text{BF}_4]$  the signal is replaced by two bands at  $1282$  and  $1265\text{ cm}^{-1}$ , compatible with the presence of two ligands in the same molecule (Figure 34). The lower wavenumbers suggest that the  $\sigma$ -donation from the N-donor moieties weakens the N-Ph bonds.

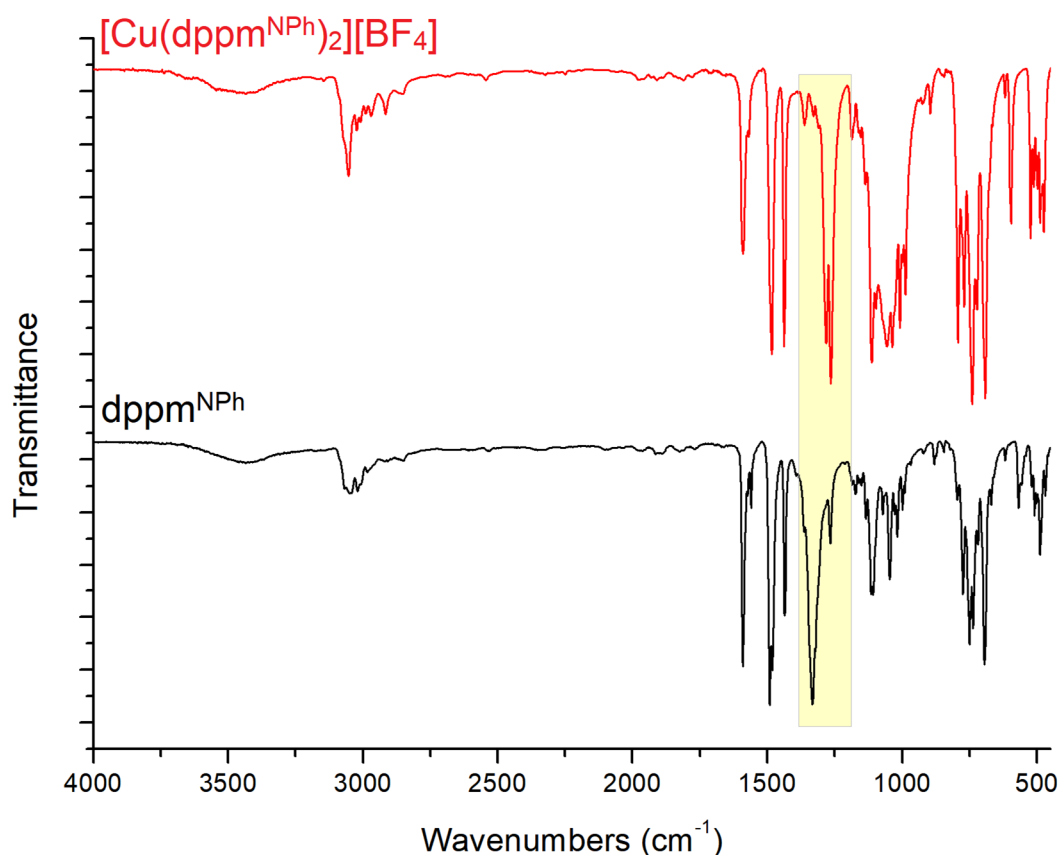


**Figure 34.** IR spectra of  $\text{dppm}^{\text{NPh}}$  and  $[\text{Cu}(\text{dppm}^{\text{NPh}})_2][\text{BF}_4]$ .

The reaction was extended to 1,2-bis(diphenylphosphino)ethane (dppe) for comparative purposes, given the formation of the same five-membered metallacycle expected for  $\text{dppm}^{\text{NPh}}$  and the coincidence of a coordinating moiety. The displacement of acetonitrile from the Cu(I) coordination sphere was achieved in all the cases at room temperature, using dichloromethane as solvent. As for  $[\text{Cu}(\text{dppm}^{\text{NPh}})_2][\text{BF}_4]$ , the complex  $[\text{Cu}(\text{dppe})_2][\text{BF}_4]$  revealed fluxional behaviour in solution evidenced by NMR spectroscopy. The  $[\text{Cu}(\text{dppe})_2]^+$  cation is already known in the literature<sup>69</sup>, but  $[\text{Cu}(\text{dppe})_2][\text{BF}_4]$  was not crystallographically investigated and during the thesis it was possible to obtain crystals suitable to study the structure by single-crystal X-ray diffraction (Figure 35).  $[\text{Cu}(\text{dppe})_2][\text{BF}_4]$  crystallizes in the monoclinic  $P2_1/c$  space group and the asymmetric unit contains two  $[\text{Cu}(\text{dppe})_2]^+$  cations and two  $[\text{BF}_4]^-$  anions. The coordination sphere surrounding the Cu(I) centre is quite distorted with respect to the ideal tetrahedral geometry, the  $\tau_4$ <sup>70</sup> parameter being 0.78. The complex is better described as trigonal pyramidal, with average Cu-P distance equal to 2.28 Å.

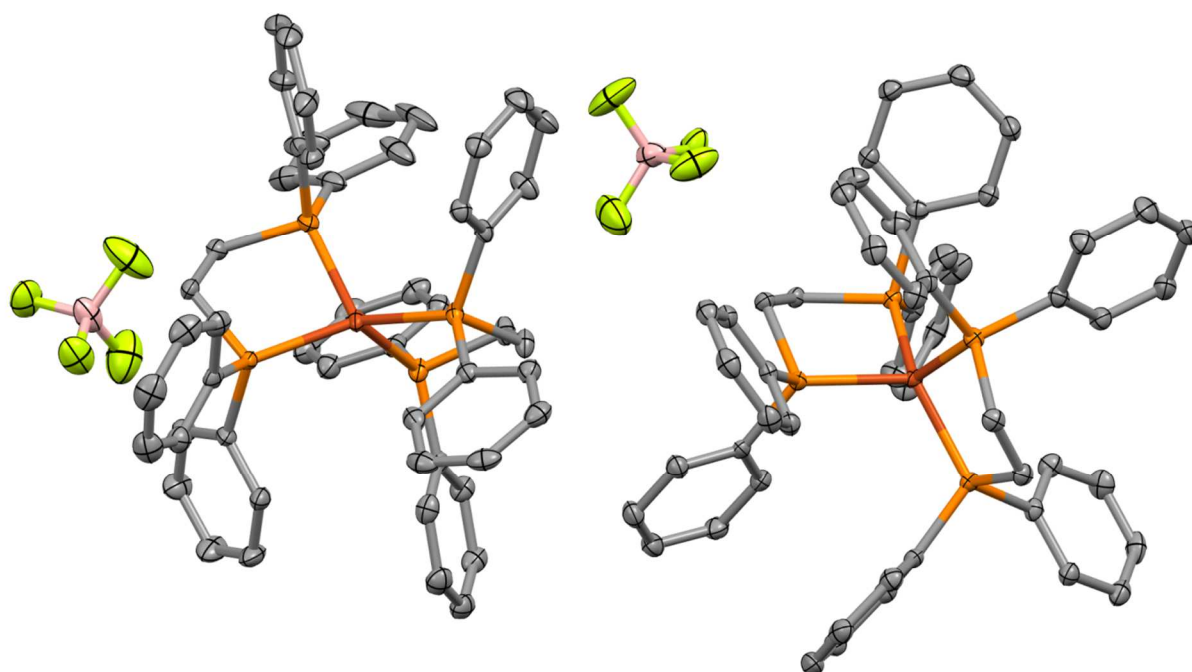


**Figure 35.** Single-crystal X-ray structure of  $[\text{Cu}(\text{dppe})_2][\text{BF}_4]$ . Ellipsoids drawn at 50% probability. Cu, red; P, orange; F, yellowish green; C, grey; B, pink. Hydrogen atoms omitted for clarity.

Both the compounds behave as 1:1 electrolytes in solution. Electrochemical measurements in acetone/LiClO<sub>4</sub> solution were carried out using a Pt microelectrode and ferrocene as internal standard. The comparison of the cyclic voltammograms with those of the free ligands allowed to determine the potentials associated to the Cu(I) oxidation (Figure 36). The previously described oxidation of dppm<sup>NPh</sup> is present at about the same potential in the cyclic voltammogram of [Cu(dppm<sup>NPh</sup>)]<sup>+</sup>, but the process becomes almost reversible, with a back-reduction peak at 0.30 V vs. Fc<sup>+</sup>/Fc. The E<sub>1/2</sub> value is 0.35 V. It is likely to suppose that the coordination prevents the decomposition of dppm<sup>Ph</sup> after its oxidation. The oxidation of the ligand is followed by the oxidation of Cu(I), centred at about 0.71 V vs. Fc<sup>+</sup>/Fc. Also in this case the back-reduction process can be observed, around 0.58 V vs. Fc<sup>+</sup>/Fc (E<sub>1/2</sub> = 0.64 V vs. Fc<sup>+</sup>/Fc). Quite surprisingly, it must be concluded that the Cu(I) oxidation in [Cu(dppm<sup>NPh</sup>)]<sup>+</sup> is almost in part reversible<sup>71</sup>. For comparison (Figure 36), the oxidation process of Cu(I) in [Cu(dppe)<sub>2</sub>][BF<sub>4</sub>] is centred at slightly higher potential, 0.80 V vs. Fc<sup>+</sup>/Fc, followed by the oxidation of the ligand around 1.01 V vs. Fc<sup>+</sup>/Fc, about 50 mV higher than what observed for free dppe. Both the processes are irreversible, and the peak associated to the back-reduction process of the metal centre is present around -0.59 V vs. Fc<sup>+</sup>/Fc. For what concerns the cathodic scans, [Cu(dppm<sup>NPh</sup>)]<sup>+</sup> shows an irreversible reduction peak around -1.87 V vs. Fc<sup>+</sup>/Fc, a potential about 0.10 V lower than that of free dppm<sup>NPh</sup>. As for the free ligand, peaks related to the back-oxidation are observable at much higher potential.

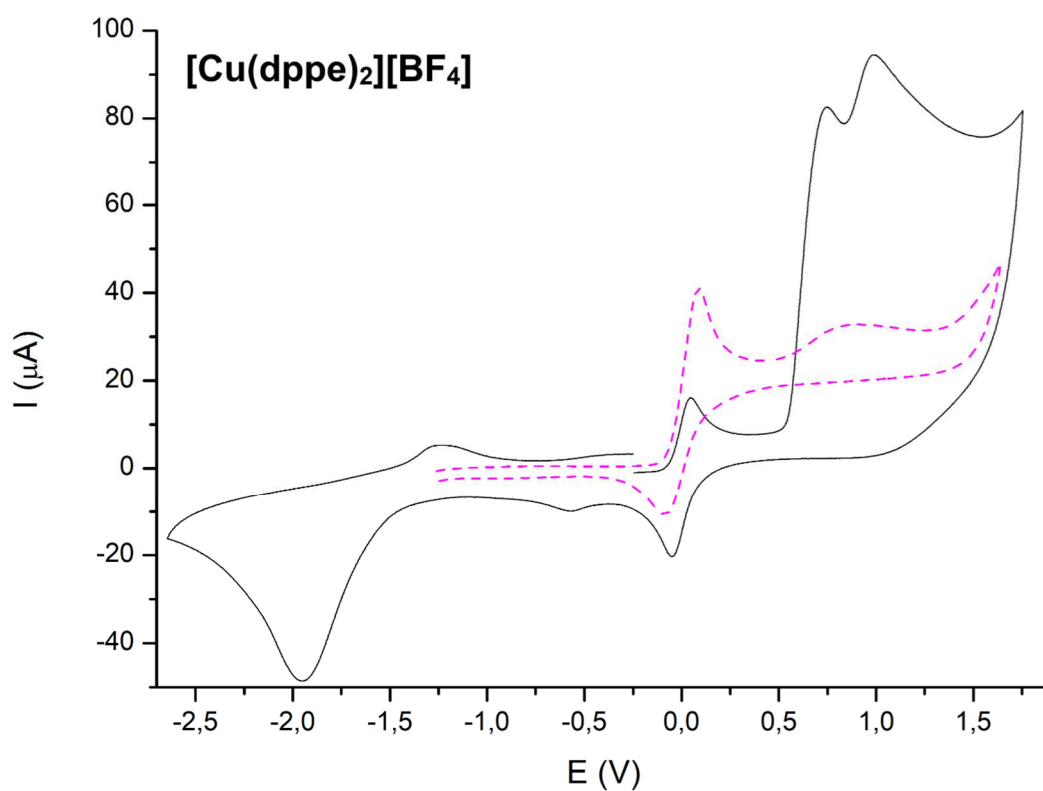
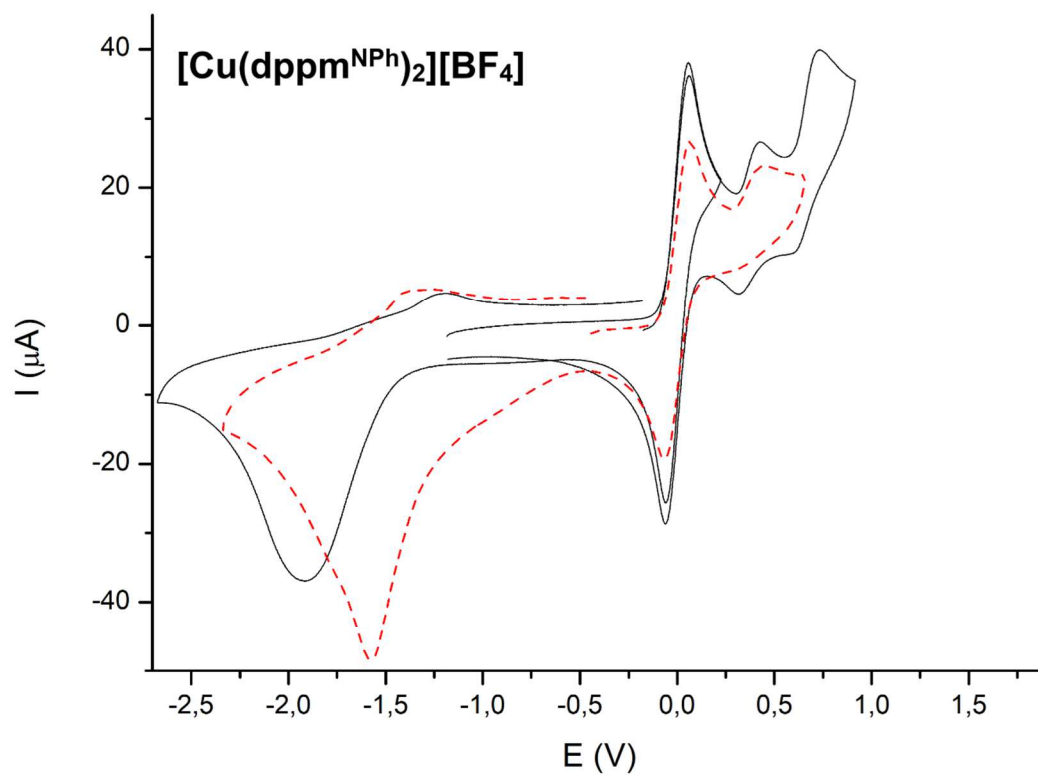


**Figure 36** Cyclic voltammeteries: below of  $[\text{Cu}(\text{dppe})_2][\text{BF}_4]$  (black line),  $\text{dppe}$  (dash purple line), above of  $[\text{Cu}(\text{dppm}^{\text{NPh}})_2][\text{BF}_4]$  (black line),  $\text{dppm}^{\text{NPh}}$  (dash red line), (Pt, acetonitrile/ $\text{LiClO}_4$ , scan speed =  $250 \text{ mV s}^{-1}$ , potentials referred to  $\text{Fc}^+/\text{Fc}$ ).

Attempts to crystallize  $[\text{Cu}(\text{dppm}^{\text{NPh}})_2][\text{BF}_4]$  are in progress. The possible structure of the compound was modelled by means of DFT calculations (Figure 37). The average computed Cu-P and Cu-N distances are 2.27 Å and 2.10 Å, respectively. The degree of distortion from the ideal tetrahedral geometry is lower than that of  $[\text{Cu}(\text{dppe})_2][\text{BF}_4]$ , the  $\tau_4$  parameter being 0.83. The HOMO of the complex maintains part of the localization of the HOMO on the {NPh} fragments, but also the other aromatic rings and *d*-type orbitals of the Cu(I) centre are involved. The LUMO is mainly localized on the P-bonded phenyl rings, those belonging to the {Ph<sub>2</sub>PN} fragments in particular, as previously described for the free ligand.

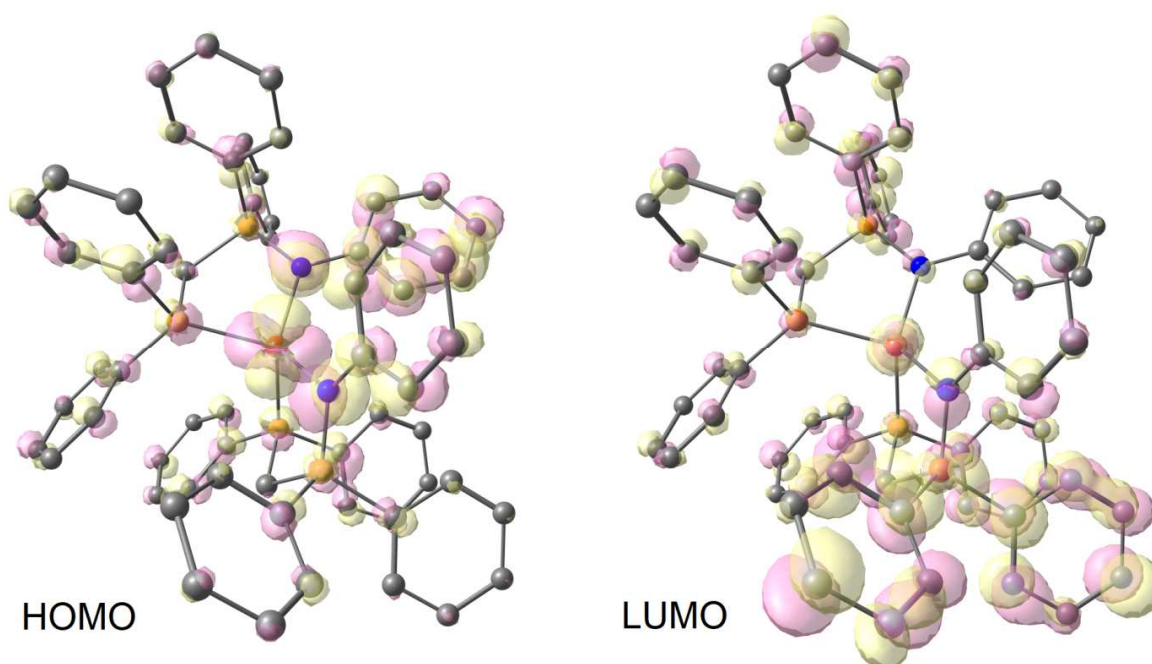


**Figure 37.** DFT-optimized ( $r^2\text{SCAN-3c}$ ) structure of  $[\text{Cu}(\text{dppm}^{\text{NPh}})_2]^+$ , plots of the HOMO and LUMO (pink and yellow tones, isovalue = 0.03 a.u.). Cu, red; P, orange; C, grey. Hydrogen atoms omitted for clarity.

Despite the differences concerning the HOMO, the absorptions of dichloromethane solutions of  $[\text{Cu}(\text{dppm}^{\text{NPh}})_2][\text{BF}_4]$  remain limited to the UV range, as for the free ligand (Figure 38). At the solid state the complex exhibits quite weak luminescence at room temperature upon excitation with UV light ( $\Phi$  around 8 %). The emission spectrum is composed by a single, wide band (FWHM = 5600  $\text{cm}^{-1}$ ) centred at 531 nm, as observable

in Figure 14. For comparison, the maximum of the weak emission band of  $[\text{Cu}(\text{dppe})_2][\text{BF}_4]$  falls at 513 nm. The PLE spectrum confirms that the excitation interval essentially falls in the UV region (Figure 38). The chromaticity coordinates are  $x = 0.345$  and  $y = 0.461$ , thus the emitted colour falls in the yellowish green region of the CIE 1931 diagram (Figure 38). Despite the fact that the emission band is wider and red-shifted with respect to the free ligand, the photoluminescence decay curve (Figure 39) indicates a lifetime value of the excited state in the nanoseconds range, without longer components.

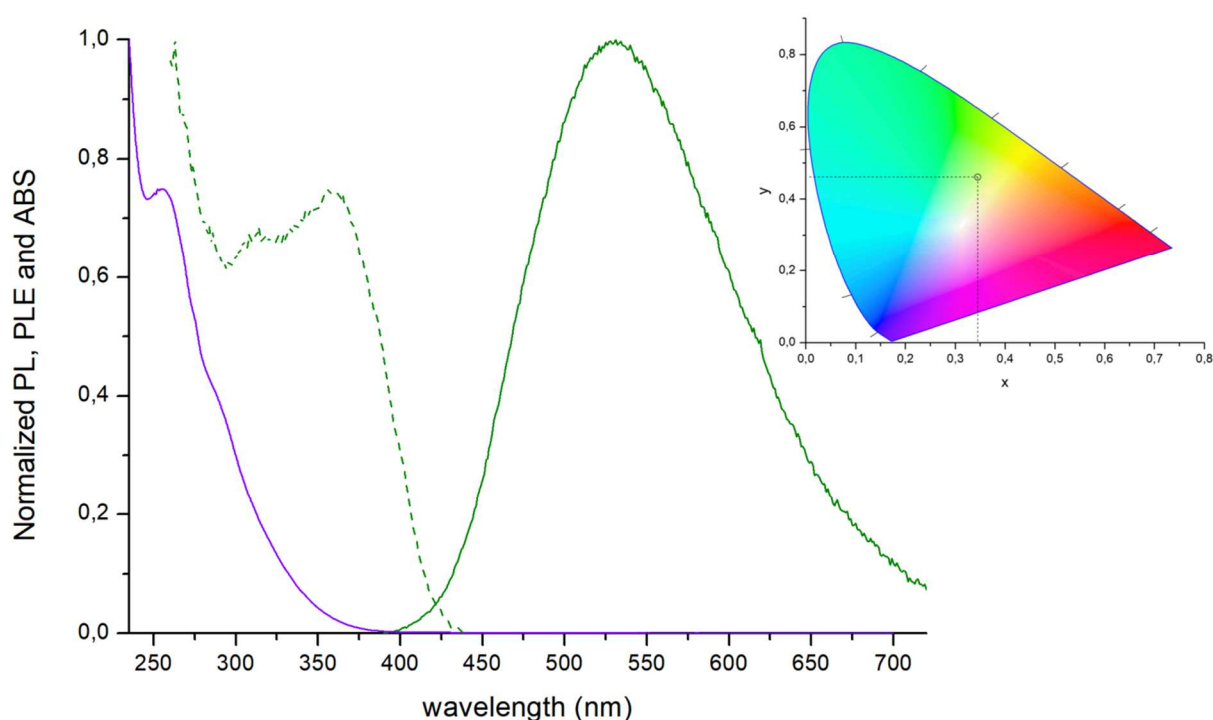


**Figure 38.** Normalized absorption (dichloromethane solution, r.t., violet line), emission and excitation (solid sample, r.t., continuous and dashed green lines,  $\lambda_{\text{excitation}} = 280$  nm,  $\lambda_{\text{emission}} = 560$  nm) spectra of  $[\text{Cu}(\text{dpmp}^{\text{NPh}})_2][\text{BF}_4]$ . CIE 1931 chromaticity diagram and chromaticity coordinates.

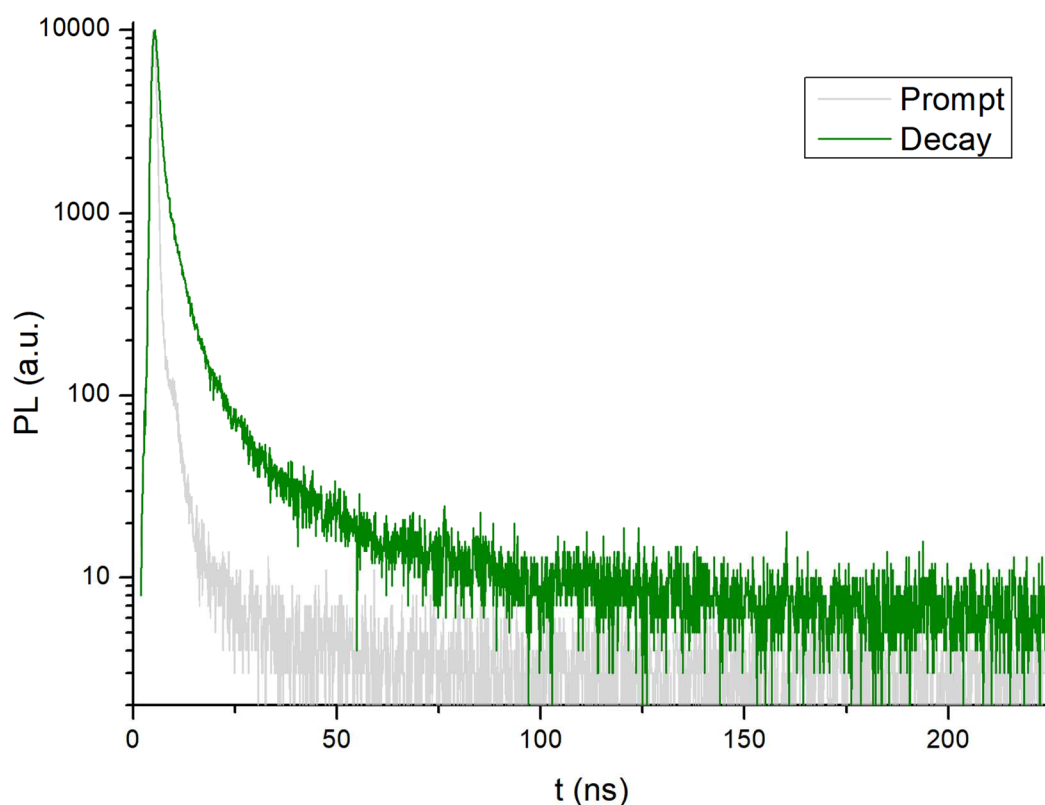
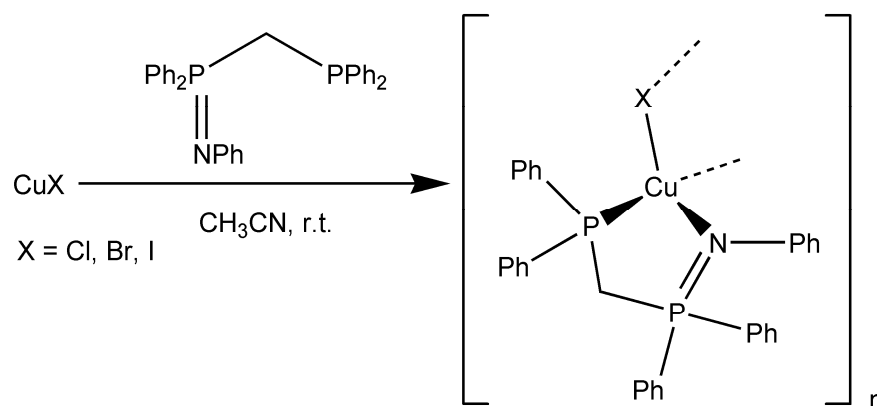


**Figure 39.** Semi-log plot of the luminescence decay curve of  $[\text{Cu}(\text{dppm}^{\text{NPh}})_2][\text{BF}_4]$  (solid, r.t.,  $\lambda_{\text{excitation}} = 373$  nm,  $\lambda_{\text{emission}} = 420$  nm).

Further attempts to obtain Cu(I) complexes with  $\text{dppm}^{\text{NPh}}$  in the coordination sphere were carried out by reacting the ligand with the precursor  $[\text{Cu}(\kappa^2\text{-BH}_4)(\text{PPh}_3)_2]$  in the presence of an acid to decompose the coordinated borohydride. Mixtures of products were isolated and the optimization of the experimental conditions is in progress.

The study on the coordinating behaviour of  $\text{dppm}^{\text{NPh}}$  towards Cu(I) was prosecuted by reacting the ligand with anhydrous Cu(I) halides ( $\text{CuX}$ , X = Cl, Br, I) in 1:1 ratio, to obtain compounds whose proposed general formula is  $[\text{CuX}(\text{dppm}^{\text{NPh}})]_n$ , with probable formation of polynuclear compounds with halides as bridging ligands (Scheme 3).



**Scheme 3.** Synthesis of  $[\text{CuX}(\text{dppm}^{\text{NPh}})]_n$ .

Different solvents were considered, but in all the cases the products separated as poorly soluble species, the iodo-complex in particular. The best reaction conditions were achieved using acetonitrile as solvent, working at room temperature under strictly inert atmosphere. The scarce solubility made the characterizations in solution and the attempts to crystallize the complexes difficult. Coordinating solvents such as DMSO caused the immediate decomposition of the species. The IR spectra of the three species are superimposable, and the P=N stretching is tentatively attributed to a quite intense band at  $1110 \text{ cm}^{-1}$  (Figure 40).

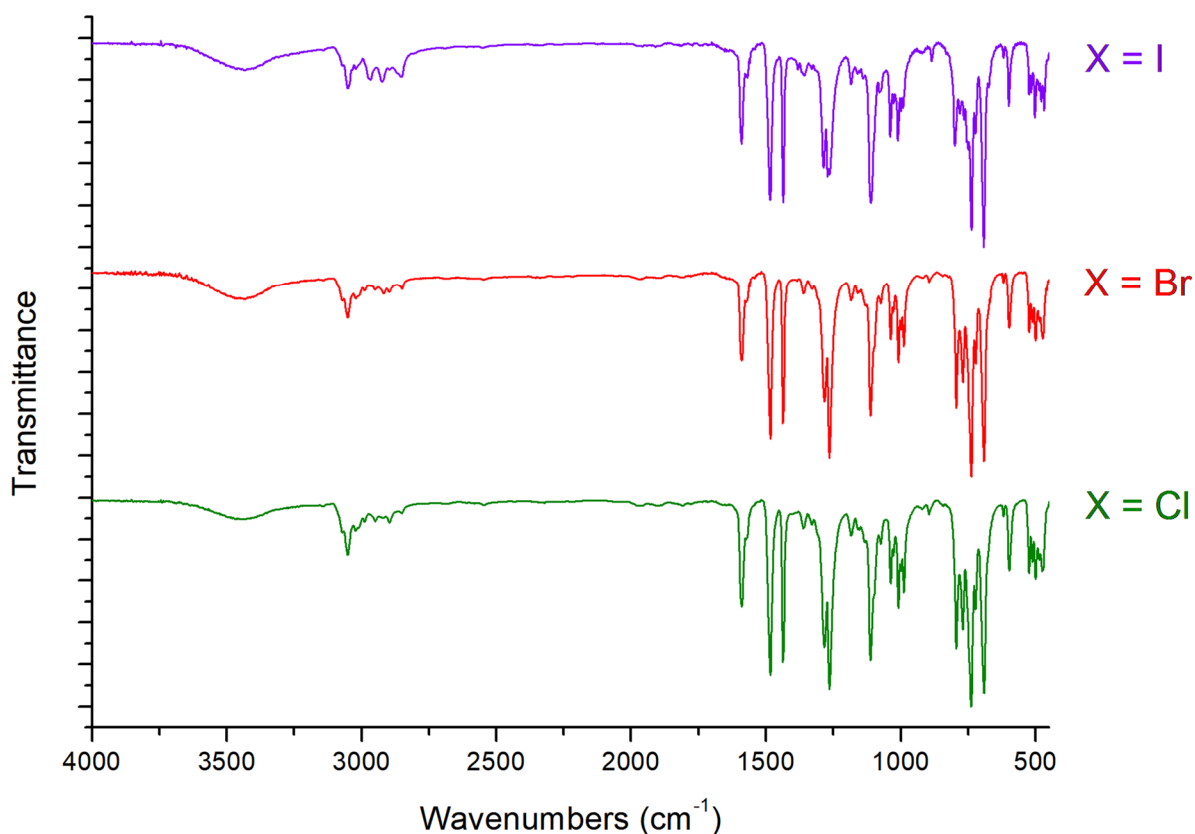


**Figure 40.** IR spectra of  $[\text{CuX}(\text{dppm}^{\text{NPh}})]_n$  ( $X = \text{Cl}, \text{Br}, \text{I}$ ).

The NMR spectra in  $\text{CDCl}_3$  at 300 K indicates fluxional behaviour. The  $^1\text{H}$  NMR resonance of the methylene bridge appears in all the compounds as a broad singlet around 3.3 ppm. The two signals in the  $^{31}\text{P}\{^1\text{H}\}$  NMR spectra for the non-equivalent phosphorus atoms are too broad to allow the measurement of the  $J_{\text{PP}}$  coupling constant. As previously described for  $[\text{Cu}(\text{dppm}^{\text{NPh}})_2][\text{BF}_4]$ , the  $^{31}\text{P}\{^1\text{H}\}$  NMR signals of the iminophosphorane groups are noticeably high-frequency shifted with respect to the free ligand. The spectra of  $[\text{CuI}(\text{ddpm}^{\text{NPh}})]_n$  are shown as examples in Figure 41. XRF measurements were carried out on  $[\text{CuI}(\text{ddpm}^{\text{NPh}})]_n$  to verify the correctness of the minimal formula (Figure 42). The percentages of Cu and I derived from the integrals of the bands confirm the composition of the complex.

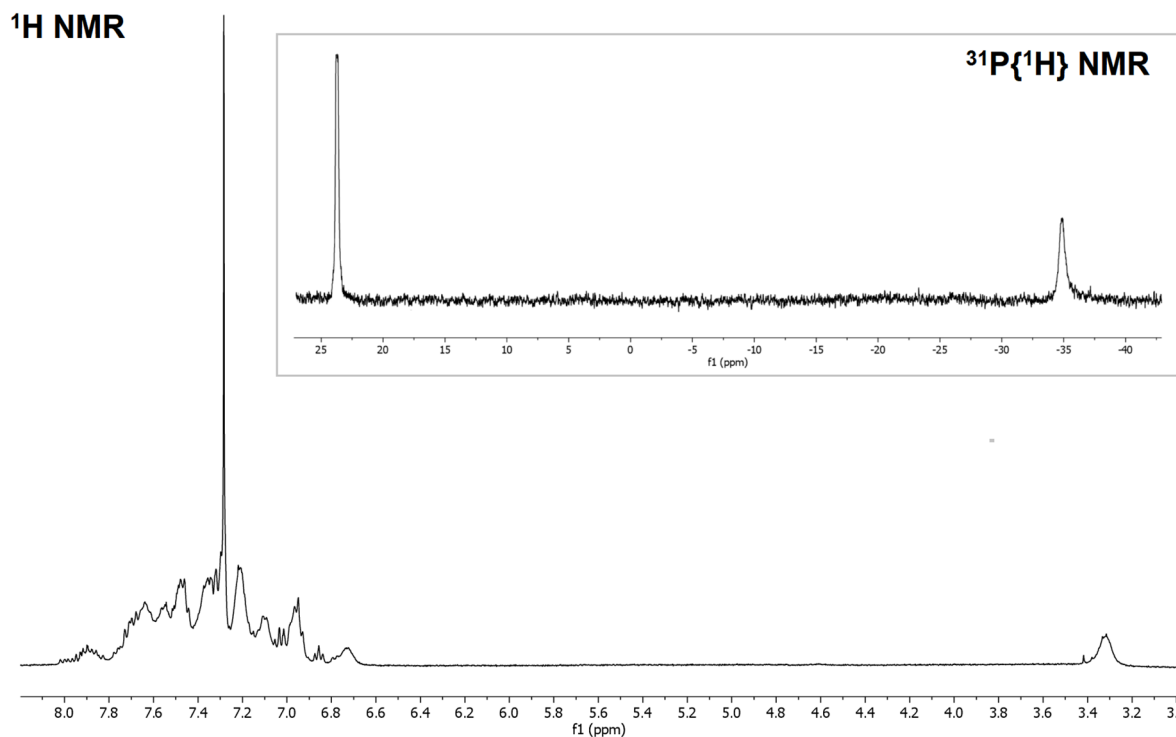


**Figure 41.**  $^1\text{H}$  NMR and  $^{31}\text{P}\{^1\text{H}\}$  NMR spectra of  $[\text{CuI}(\text{dppm}^{\text{NPh}})]_n$ .  $\text{CDCl}_3$ , 300 K.

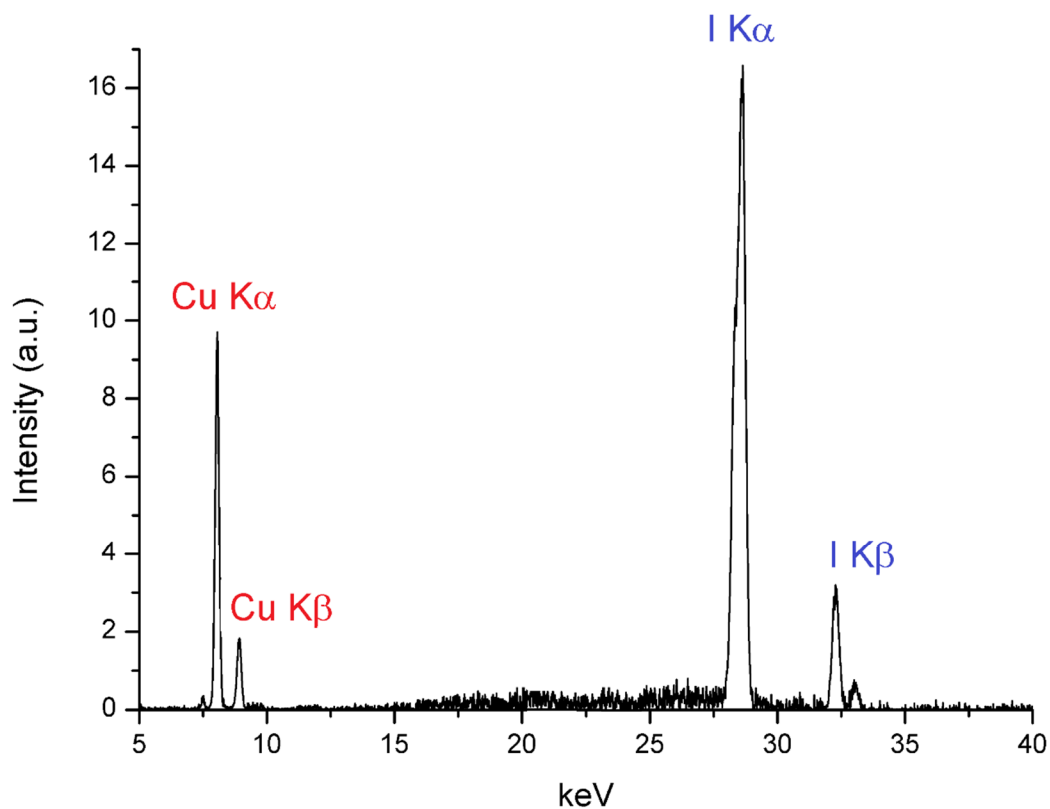


**Figure 42.** XRF spectra of  $[\text{CuI}(\text{dppm}^{\text{NPh}})]_n$

The relative Gibbs energy values of the mononuclear three-coordinated form of the bromo-complex and of the related tetracoordinated  $[\text{Cu}_2(\mu\text{-Br})_2(\text{dppm}^{\text{NPh}})_2]$  species were compared by means of DFT calculations (Figure 43). The Gibbs energy variation for the reaction  $2 [\text{CuBr}(\text{dppm}^{\text{NPh}})] \rightarrow [\text{Cu}_2(\mu\text{-Br})_2(\text{dppm}^{\text{NPh}})_2]$  is meaningfully negative, around  $-30.7 \text{ kcal mol}^{-1}$ . The formation of halide-bridged species is therefore highly supported by the computational studies.

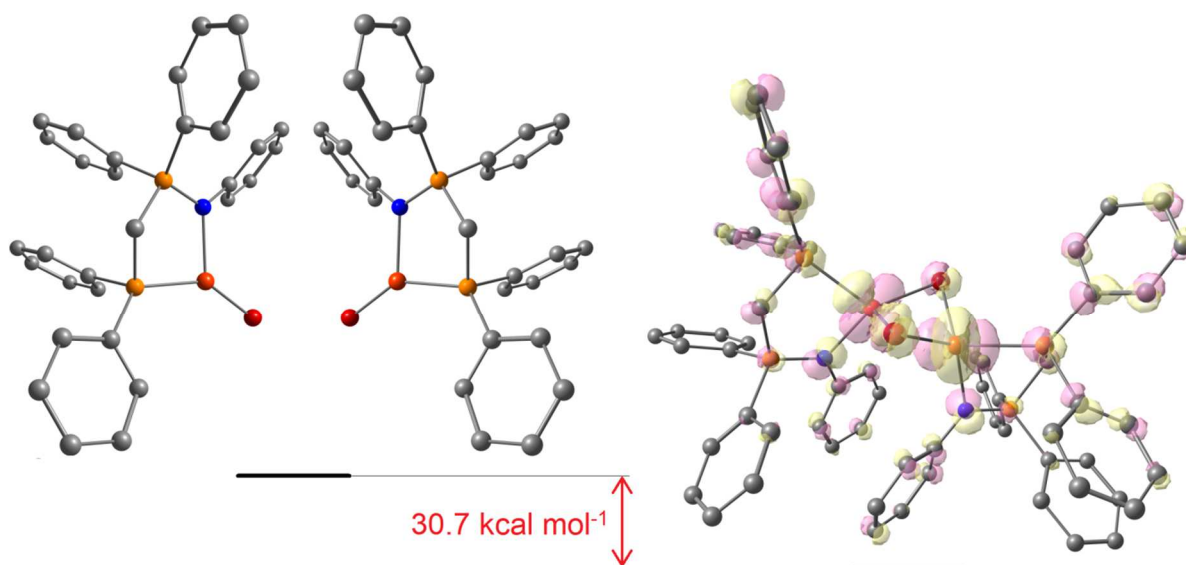


**Figure 43.** DFT-optimized (PBEh-3c) structures of  $[\text{CuBr}(\text{dppm}^{\text{NPh}})]_n$  ( $n = 1, 2$ ) with Gibbs energy variation and plot of the HOMO of  $[\text{CuBr}(\text{dppm}^{\text{NPh}})]_2$  (pink and yellow tones, isovalue = 0.03 a.u.). Cu, red; Br, dark red; P, orange; C, grey. Hydrogen atoms omitted for clarity.

The absorption spectra of diluted dichloromethane solutions showed only absorptions in the UV range (Figure 44). The absorption bands of  $[\text{CuCl}(\text{dppm}^{\text{NPh}})]_n$  and  $[\text{CuBr}(\text{dppm}^{\text{NPh}})]_n$  are roughly superimposable, while the spectrum of  $[\text{CuI}(\text{dppm}^{\text{NPh}})]_n$  starts at lower wavelengths, possibly because  $(\text{M}+\text{X})\text{LCT}$  transitions require more energy when  $\text{X} = \text{I}$  <sup>21,24</sup>.

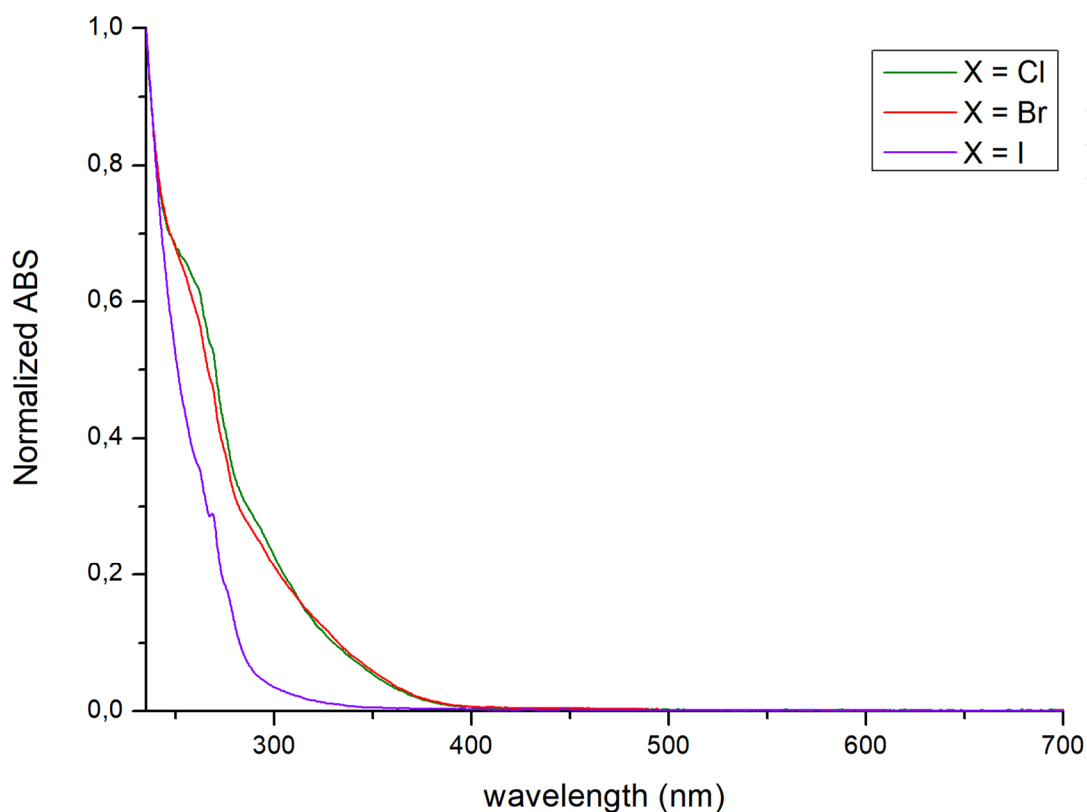


**Figure 44.** Normalized absorption spectra (dichloromethane solution, r.t.) of  $[\text{CuX}(\text{dppm}^{\text{NPh}})]_n$  ( $X = \text{Cl}, \text{Br}, \text{I}$ ).

Excitation of solid samples with UV light afforded emissions in the yellowish green and blueish green regions (chromaticity coordinates:  $X = \text{Cl}$ ,  $x = 0.330$ ,  $y = 0.472$ ;  $X = \text{Br}$ ,  $x = 0.324$ ,  $y = 0.461$ ;  $X = \text{I}$ ,  $x = 0.247$ ,  $y = 0.370$ ), with maxima comprised between 484 and 522 nm, depending upon the choice of the coordinated halide (Figure 45). In particular, the PL band of the iodo-complex is blue-shifted by about 38 nm with respect to the other species, while the chloro- and the bromo-complexes have strictly similar emission features. Such a result appears coherent with the previously described absorption spectra and can be ascribed to the higher stabilization of the Cu(I) oxidation state in the presence of iodide as ligand. The superposition of metal and halide orbitals in the HOMO can be observed in the plot reported in Figure 43. FWHM values above  $4000 \text{ cm}^{-1}$  indicate strong participation of the coordinated [N,P]-ligand in the emission. The superposition of emission and excitation spectra (Figure 45) reveals quite scarce Stokes shifts.

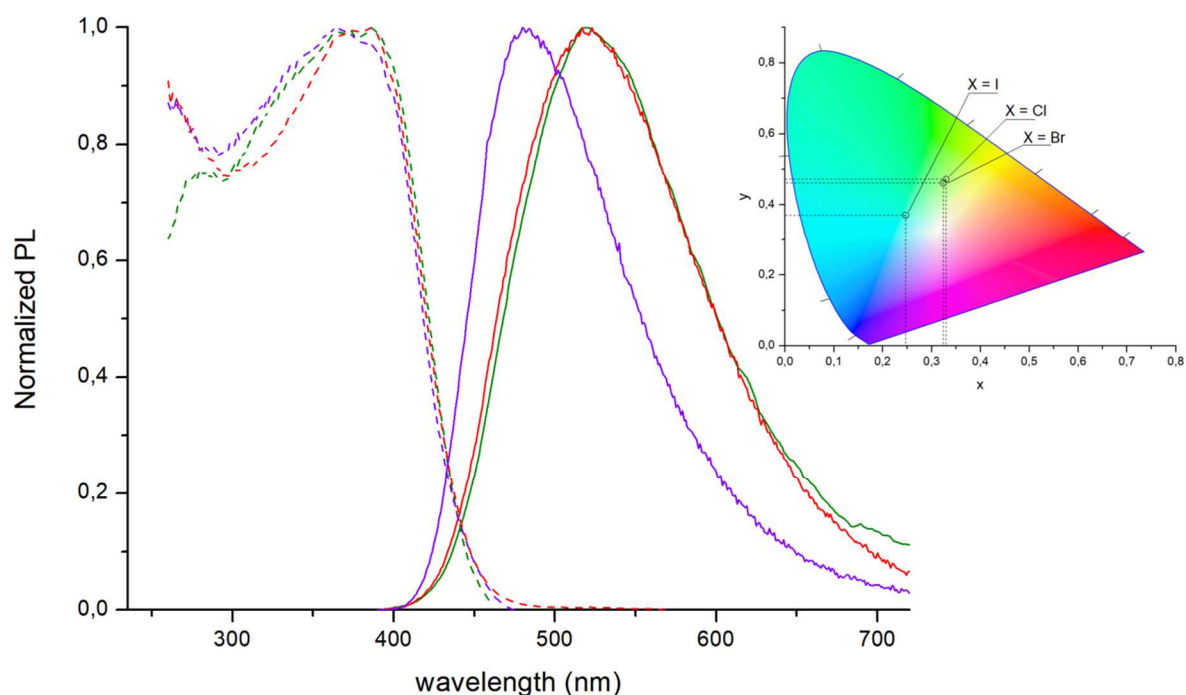


**Figure 45.** Normalized emission and excitation (solid sample, r.t., continuous and dashed lines,  $\lambda_{\text{excitation}} = 280 \text{ nm}$ ,  $\lambda_{\text{emission}} = 560 \text{ nm}$ ) spectra of  $[\text{CuX}(\text{dppm}^{\text{NPh}})]_n$  (X = Cl, green; X = Br, red; X = I, violet). CIE 1931 chromaticity diagram and chromaticity coordinates.

The average observed lifetime at room temperature is around 13 ns for the chloro-species, while values slightly lower than 1  $\mu\text{s}$  were obtained for the bromo- and iodo-derivatives. It is therefore likely to suppose that excited states with triplet multiplicity participate to the luminescence of the complexes having heavier halides in the coordination sphere. Unfortunately, the quantum yields were all estimated below 5%.

An interesting feature is the change of intensity of the emission of solid samples of  $[\text{CuBr}(\text{dppm}^{\text{NPh}})]_n$  in the presence of traces of solvent, clearly appreciable with the naked eye. Such a point was investigated by carrying out luminescence measurements on solids soaked with diethyl ether. The shapes of the emission and excitation bands are not meaningfully altered by the addition of the solvent, while the average observed lifetime lowers to about one third of the original. A possible explanation of the experimental outcomes is that the interaction of the compound with the solvent does not influence the non-radiative decay routes, but the change of polarity of the surrounding medium makes faster the radiative decay, with consequent increase of the observed luminescence.

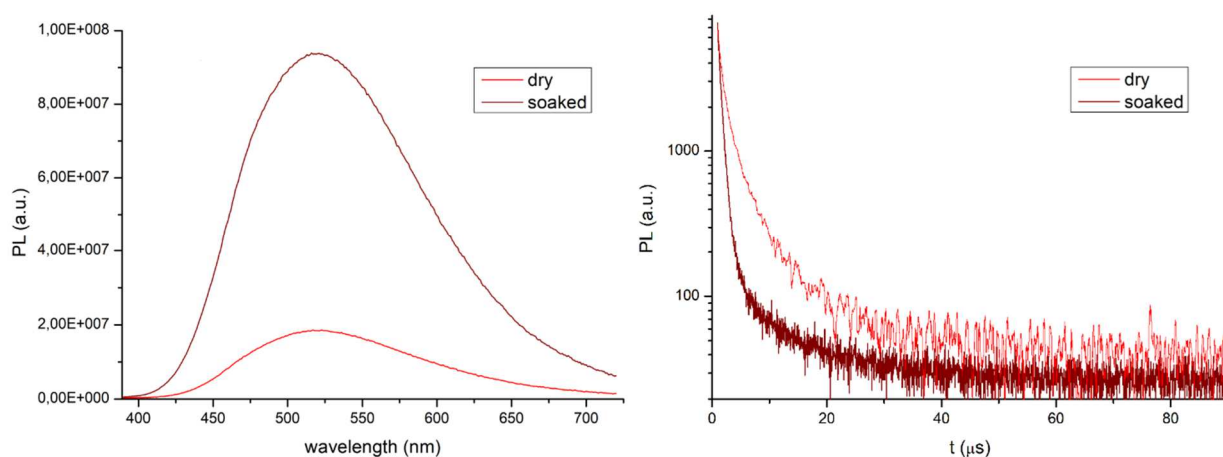


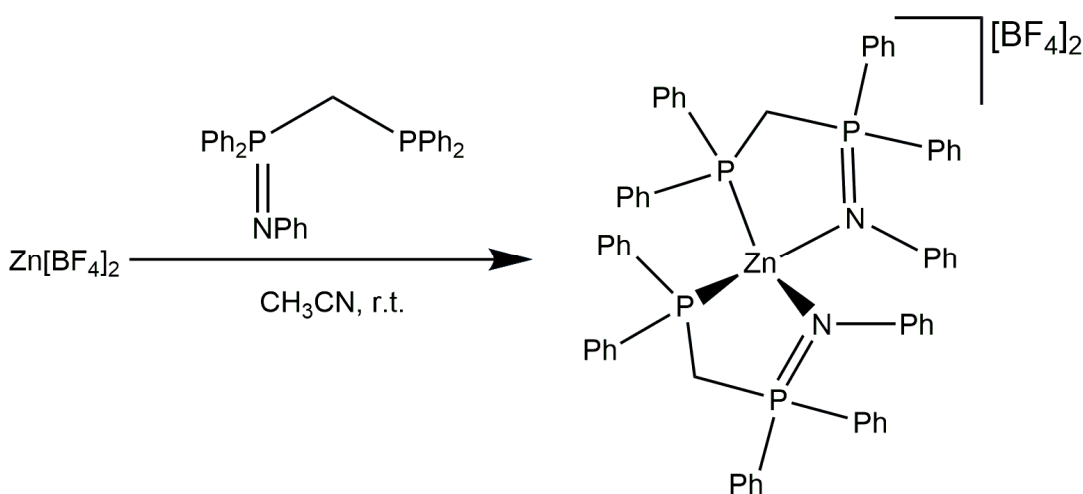
**Figure 46.** Left: emission (solid, r.t.,  $\lambda_{\text{excitation}} = 373 \text{ nm}$ ,  $\lambda_{\text{emission}} = 550 \text{ nm}$ ) spectra of  $[\text{CuBr}(\text{dppm}^{\text{NPh}})]_n$ . Right: semi-log plots of the luminescence decay curves of  $[\text{CuBr}(\text{dppm}^{\text{NPh}})]_n$  (solid, r.t.,  $\lambda_{\text{excitation}} = 373 \text{ nm}$ ,  $\lambda_{\text{emission}} = 550 \text{ nm}$ ). Red line dry sample, wine line sample soaked with diethyl ether.

### 4.3 Zinc(II) complexes with $\text{dppm}^{\text{NPh}}$

The second  $d^{10}$  metal centre investigated during the internship is Zn(II). The first metal precursor considered is  $\text{Zn}(\text{ClO}_4)_2 \cdot 6\text{H}_2\text{O}$ , that was reacted with two equivalents of  $\text{dppm}^{\text{NPh}}$  in acetonitrile at room temperature. The  $^1\text{H}$  NMR spectrum (Figure S4) of the isolated product ( $\text{CDCl}_3$ , 300 K) shows between 8.15 and 7.20 ppm the resonances related to the P-bonded phenyl rings, while the N-bonded aromatic substituent falls between 7.15 and 6.80 ppm. The methylene bridge corresponds to a doublet at 3.96 ppm ( $J_{\text{PH}} = 16.3 \text{ Hz}$ ), slightly high-frequency shifted with respect to  $\text{dppm}^{\text{NPh}}$ . The  $^{31}\text{P}\{^1\text{H}\}$  NMR spectrum (Figure S5) is composed by a sharp AB spin system ( $\delta_{\text{A}} = 35.5 \text{ ppm}$ ,  $\delta_{\text{B}} = -32.6 \text{ ppm}$ ,  $J_{\text{PP}} = 79.8 \text{ Hz}$ ). The absence of broad signals in the NMR spectra is in contrast with what previously described for the homoleptic complex  $[\text{Cu}(\text{dppm}^{\text{NPh}})_2][\text{BF}_4]$ . Moreover, the IR spectrum shows a band around  $3250 \text{ cm}^{-1}$  that can be assigned to  $\nu_{\text{NH}}$  stretchings. Another wide band centred at  $3480 \text{ cm}^{-1}$  appears related to  $\nu_{\text{OH}}$  stretchings. The presence of perchlorate is indicated by a strong band around  $1100 \text{ cm}^{-1}$ . On considering the presence of water molecules introduced with the precursor, it is unlikely that the characterization data correspond to a homoleptic Zn(II) complex with  $\text{dppm}^{\text{NPh}}$  in the coordination sphere. Among the various possibilities, the formation of the N-protonated conjugate acid of  $\text{dppm}^{\text{NPh}}$ ,  $[\text{Hdppm}^{\text{NPh}}]\text{ClO}_4$ , cannot be ruled out. XRF measurements revealed the presence of zinc in the isolated samples, but this result can be due to the

co-precipitation of zinc derivatives such as  $\text{Zn}(\text{OH})_2$ . Given the lack of appreciable luminescence in solution and at the solid state, different synthetic approaches were considered.

Characterization data more in agreement with the formation of a  $\text{dppm}^{\text{NPh}}$   $\text{Zn}(\text{II})$  complex having formula  $[\text{Zn}(\text{dppm}^{\text{NPh}})_2][\text{BF}_4]_2$  were obtained by reacting the ligand in 2:1 ratio with an acetonitrile solution of anhydrous  $\text{Zn}(\text{II})$  tetrafluoroborate, prepared *in situ* from  $\text{Zn}$  powder and  $\text{HBF}_4 \cdot \text{Et}_2\text{O}$ . The reaction afforded a white solid characterized by appreciable green luminescence upon irradiation with UV light. Unfortunately, the presence of strong bands in the  $1170 - 970 \text{ cm}^{-1}$  range in the IR spectrum associated to the presence of the tetrafluoroborate anion makes the assignment of the  $\nu_{\text{P}=\text{N}}$  stretching difficult. The  $^1\text{H}$  NMR spectrum (Figure 47) is composed by a set of resonances in the aromatic region related to the P- and N-bonded phenyl rings. Moreover, a doublet at 3.84 ppm is attributable to the methylene bridge of the ligand ( $J_{\text{PH}} = 16.1 \text{ Hz}$ ). The  $^{31}\text{P}\{^1\text{H}\}$  NMR spectrum shows two signals respectively centred at 34.4 and -36.2 ppm. The first one, probably related to the  $\{\text{PNPh}\}$  moieties, is broad, while the second is a resolved doublet with  $J_{\text{PP}}$  coupling constant of 79.1 Hz (Figure 48). The opposite situation regarding the broadness of the  $^{31}\text{P}$  resonances was previously described for  $[\text{Cu}(\text{dppm}^{\text{NPh}})_2][\text{BF}_4]$ , possibly because of the different hardness of the two metal centres and the consequent different affinities towards N- and P-donor moieties.



**Scheme 4** Synthesis of  $[\text{Zn}(\text{dppm}^{\text{NPh}})_2][\text{BF}_4]_2$ .

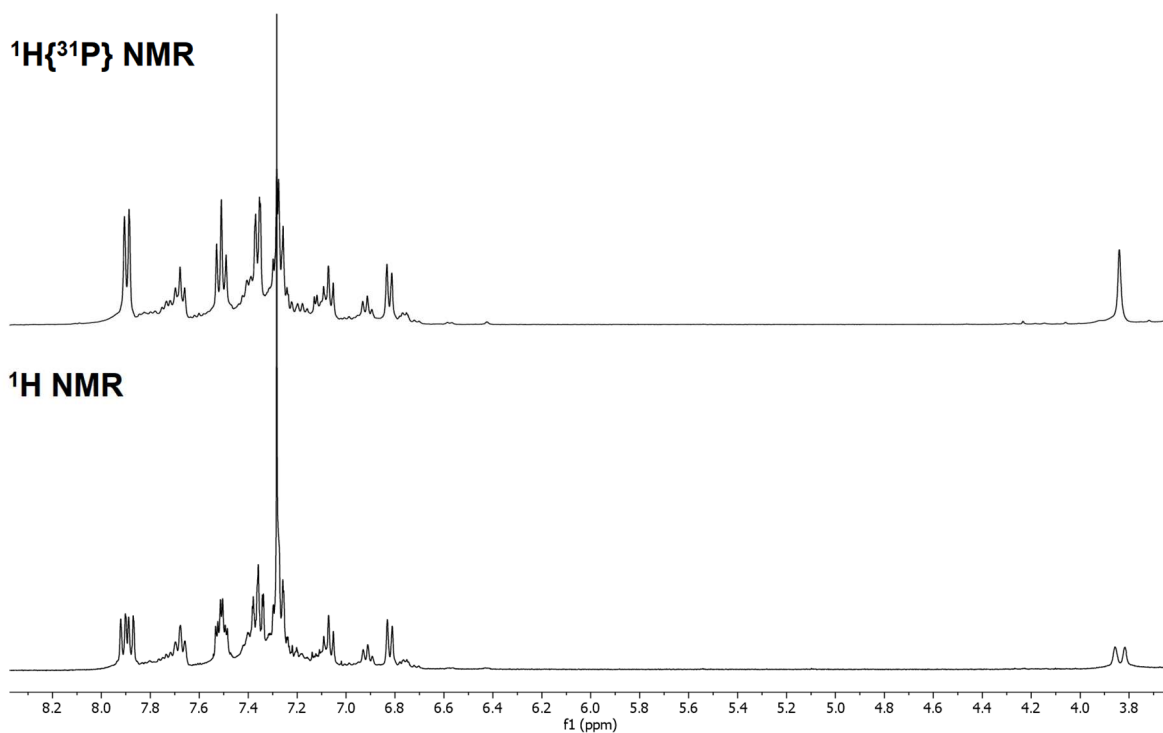


**Figure 47.**  $^1\text{H}$  NMR and  $^1\text{H}\{^{31}\text{P}\}$  NMR spectra of  $[\text{Zn}(\text{dppm}^{\text{NPh}})_2][\text{BF}_4]_2$ .  $\text{CDCl}_3$ , 300 K.

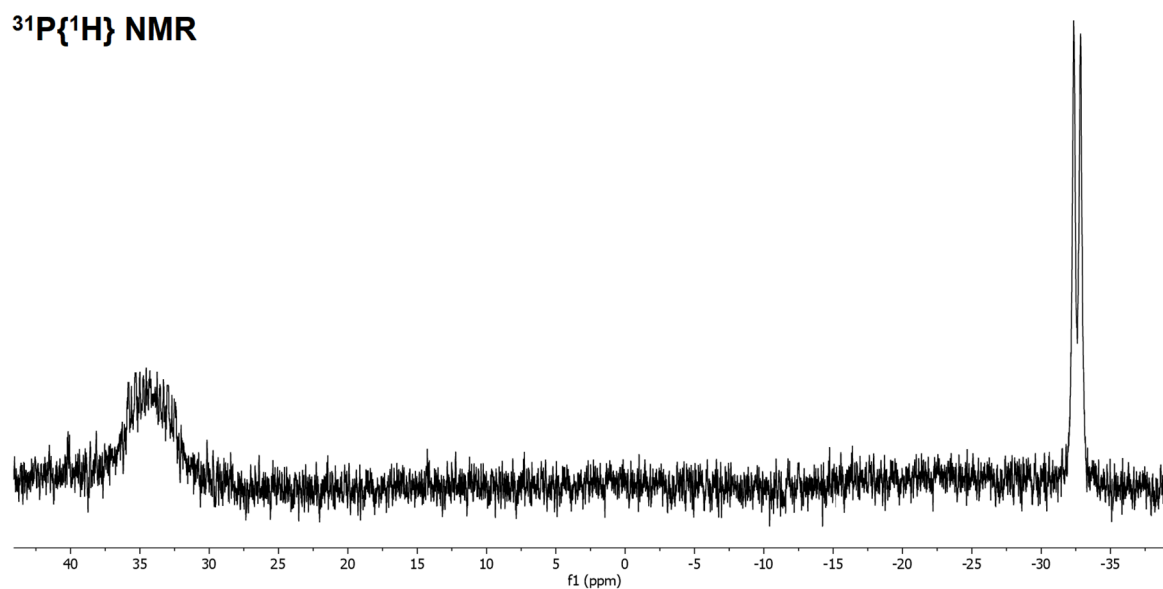


**Figure 48.**  $^{31}\text{P}\{^1\text{H}\}$  NMR spectrum of  $[\text{Zn}(\text{dppm}^{\text{NPh}})_2][\text{BF}_4]_2$ .  $\text{CDCl}_3$ , 300 K.

The absorptions of  $\text{CH}_2\text{Cl}_2$  solutions of the complex are limited to wavelengths in the UV range shorter than 350 nm (Figure 49). The emission spectra collected for solid samples

of  $[\text{Zn}(\text{dppm}^{\text{NPh}})_2][\text{BF}_4]_2$  are composed by a single, wide band ( $\text{FWHM} = 5600 \text{ cm}^{-1}$ ) centred at 503 nm, close to the emission recorded for the free ligand (maximum at 496 nm). The chromaticity coordinates of the emission are  $x = 0.281$  and  $y = 0.391$ , falling in the green region of the CIE 1931 chromaticity diagram (Figure 49). The excitation range at the solid state is meaningfully red-shifted compared to the absorption spectrum in solution, with a wide band centred around 350 nm (Figure 49). The photoluminescence quantum yield is estimated around 9%.

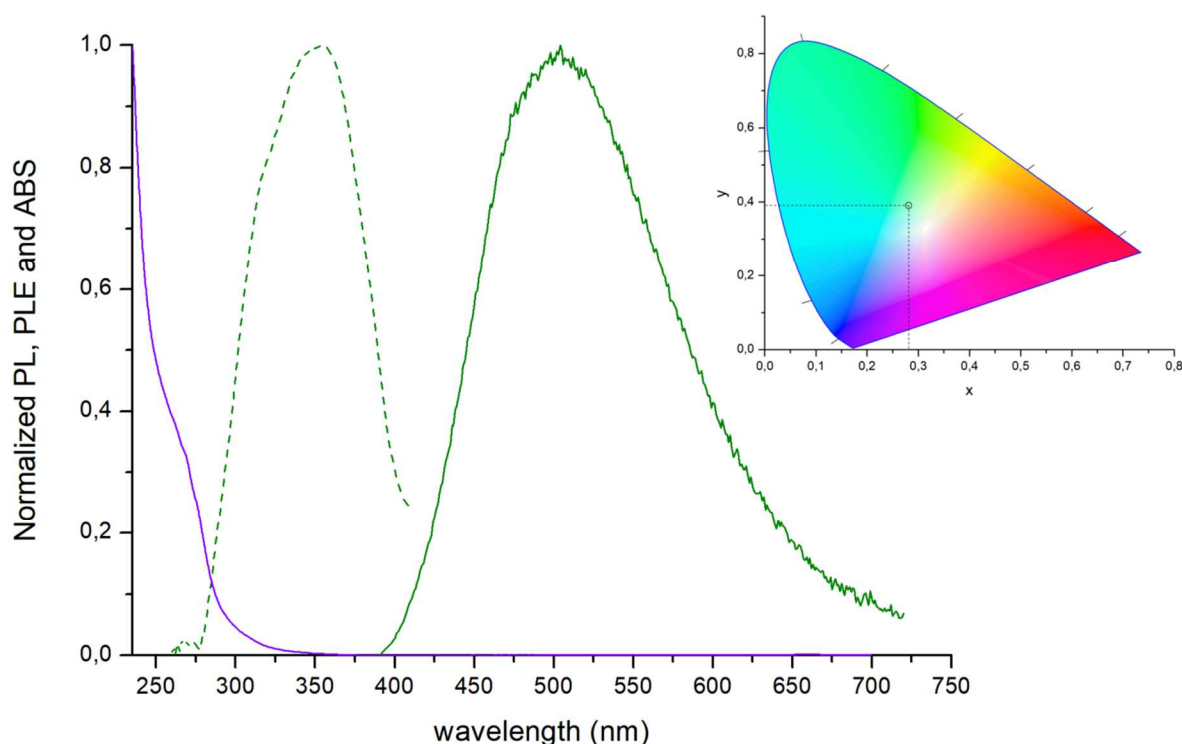


**Figure 49.** Normalized absorption (dichloromethane solution, r.t., violet line), emission and excitation (solid sample, r.t., continuous and dashed green lines,  $\lambda_{\text{excitation}} = 280 \text{ nm}$ ,  $\lambda_{\text{emission}} = 515 \text{ nm}$ ) spectra of  $[\text{Zn}(\text{dppm}^{\text{NPh}})_2][\text{BF}_4]_2$ . CIE 1931 chromaticity diagram and chromaticity coordinates.

The shift between emission and excitation maxima is quite limited, around  $8500 \text{ cm}^{-1}$ . This result and the lifetime of the excited state in the nanoseconds range (see Figure 50 for the luminescence decay curve) indicate that the emission of  $[\text{Zn}(\text{dppm}^{\text{NPh}})_2][\text{BF}_4]_2$  can be classified as a fluorescence. The study of the frontier molecular orbitals obtained after computational geometry optimization however reveals that both the HOMO and the LUMO of the complex are not exclusively localized on the coordinated ligands, the {NPh}

fragments in the case of the HOMO, since a contribution from d-type metal orbitals can be observed (Figure 51). From a structural point of view, the atoms composing the first coordination sphere of Zn(II) describe a distorted tetrahedral geometry ( $\tau_4 = 0.80$ ), as previously described for the analogous Cu(I) complex. The computed average Zn-P and Zn-N distances are 2.43 Å and 2.00 Å, respectively. It is worth noting that the M-P bond length is meaningfully longer than that calculated for the Cu(I) derivative, while the M-N bonds are shorter. This outcome could explain the previously described different fluxional behaviour of  $[\text{Zn}(\text{dppm}^{\text{NPh}})_2][\text{BF}_4]_2$  compared to  $[\text{Cu}(\text{dppm}^{\text{NPh}})_2][\text{BF}_4]$ , deduced from the  $^{31}\text{P}\{^1\text{H}\}$  NMR spectra.

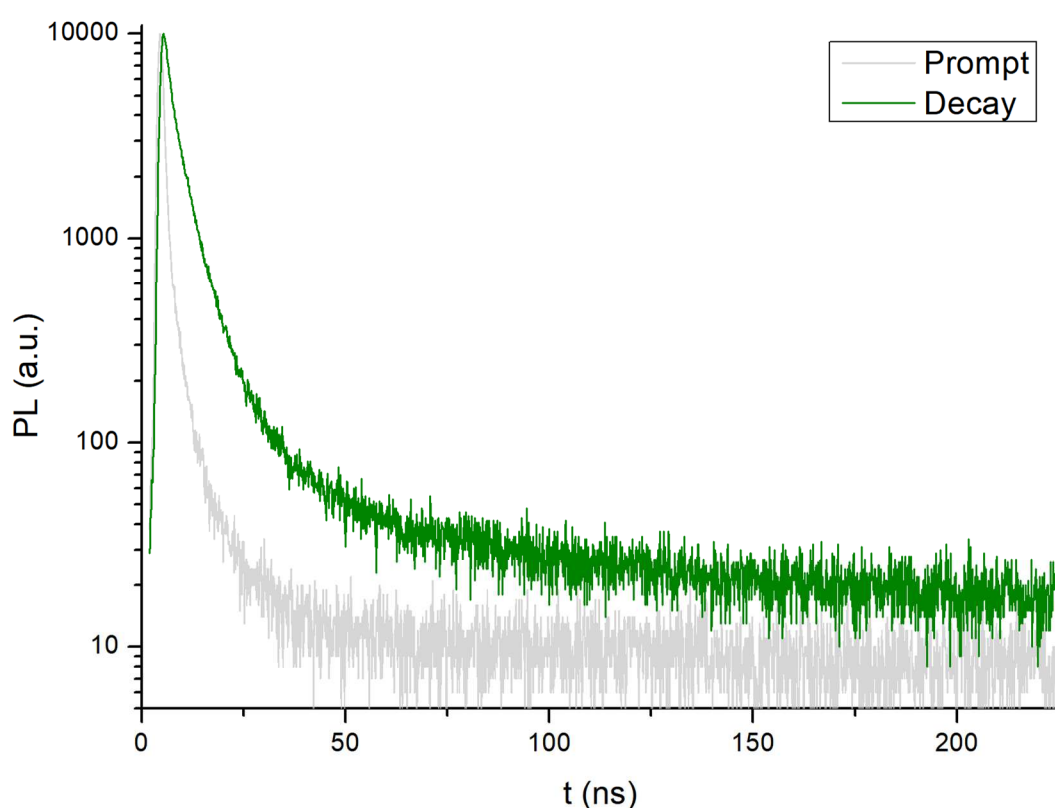


**Figure 50.** Semi-log plot of the luminescence decay curve of  $[\text{Zn}(\text{dppm}^{\text{NPh}})_2][\text{BF}_4]_2$  (solid, r.t.,  $\lambda_{\text{excitation}} = 373$  nm,  $\lambda_{\text{emission}} = 420$  nm).

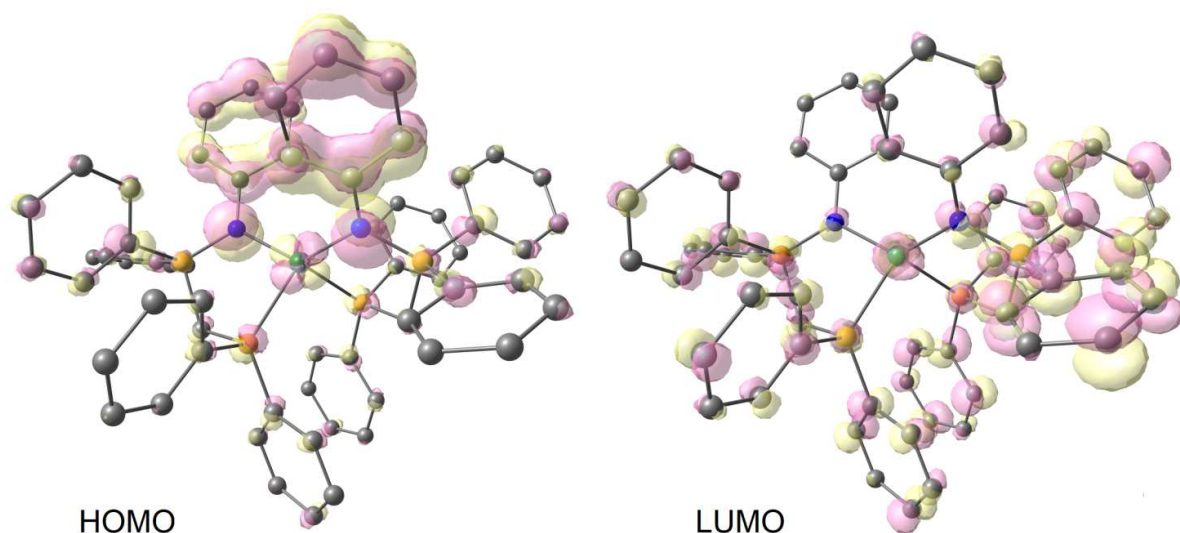
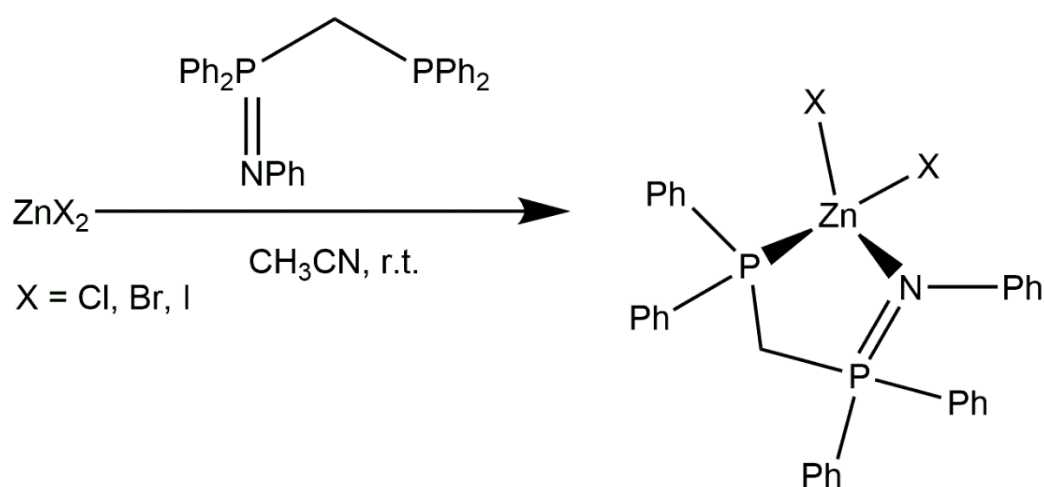


**Figure 51.** DFT-optimized (PBEh-3c) structure of  $[\text{Zn}(\text{dppm}^{\text{NPh}})_2]^{2+}$ , plots of the HOMO and LUMO (pink and yellow tones, isovalue = 0.03 a.u.). Zn, green; P, orange; C, grey. Hydrogen atoms omitted for clarity.

Further metal precursors for the preparation of Zn(II) complexes were  $\text{ZnX}_2$  anhydrous halides ( $\text{X} = \text{Cl}, \text{Br}, \text{I}$ ). The reaction with a stoichiometric amount of  $\text{dppm}^{\text{NPh}}$  in acetonitrile caused in all the cases the separation of a white solid. Characterization data support the formation of complexes having general formula  $[\text{ZnX}_2(\text{dppm}^{\text{NPh}})]$  ( $\text{X} = \text{Cl}, \text{Br}, \text{I}$ ). The IR spectra of the three compounds are almost identical, and the  $\nu_{\text{P}=\text{N}}$  stretching is tentatively assigned around  $1100 \text{ cm}^{-1}$  (Figure 52).



**Scheme 5** Synthesis of  $[\text{Zn}(\text{dppm}^{\text{NPh}})\text{X}_2]$ .

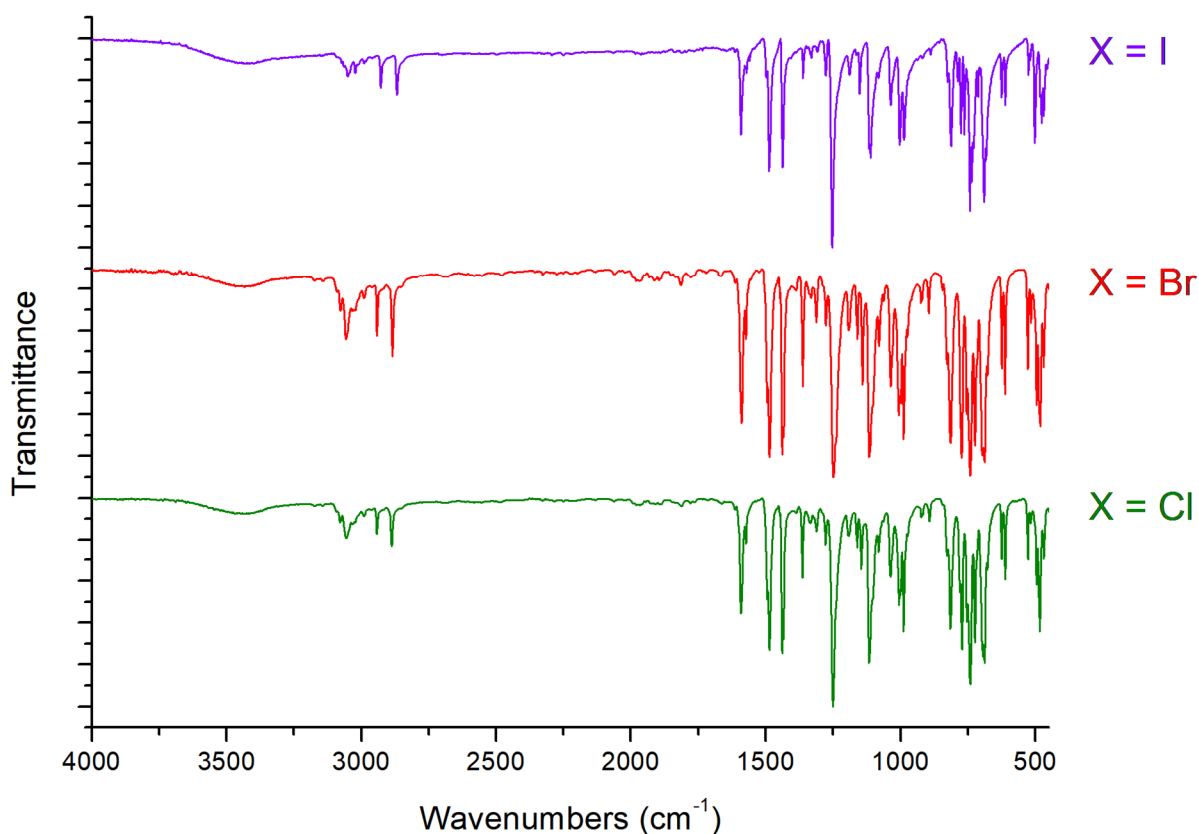


**Figure 52.** IR spectra of  $[\text{ZnX}_2(\text{dppm}^{\text{NPh}})]$  ( $\text{X} = \text{Cl}, \text{Br}, \text{I}$ ).

The NMR characterizations, limited to the chloro- and the bromo-complexes for solubility issues of the iodo-derivative, confirmed the coordination of  $\text{dppm}^{\text{NPh}}$ . In particular, in the aromatic regions of the  $^1\text{H}$  NMR spectra ( $\text{CDCl}_3$ , 300 K) both the P- and N-bonded phenyl rings can be detected. The coordination alters the multiplicity of the signal related to the methylene bridge, that resonates around 3.4 ppm as doublet of doublets. The first  $J_{\text{PH}}$  coupling constant is about 11 Hz, slightly lower than the free ligand. Differently from the homoleptic complex, also the coupling with the other phosphorus atom becomes observable, with  $J_{\text{PH}}$  around 6 Hz (Figure 53). The  $^{31}\text{P}\{^1\text{H}\}$  NMR spectra are composed by AB spin systems with  $J_{\text{PP}}$  coupling constants around 12 Hz, more broadened in the case of  $\text{X} = \text{Br}$ . As already described for the Cu(I) derivatives, the coordination causes a noticeable high-frequency shift of the  $^{31}\text{P}$  resonance of the iminophosphorane moiety (Figure 54).

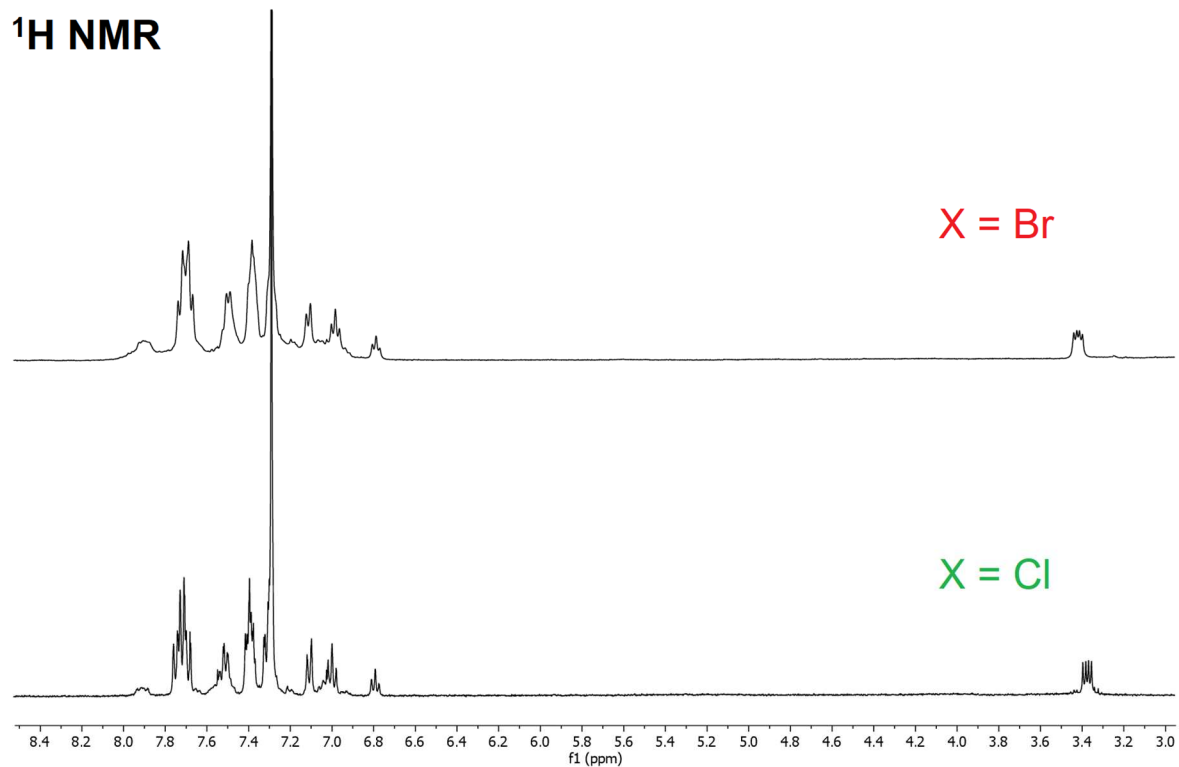


**Figure 53.**  $^1\text{H}$  NMR spectra of  $[\text{ZnX}_2(\text{dppm}^{\text{NPh}})]$  ( $\text{X} = \text{Cl}, \text{Br}$ ).  $\text{CDCl}_3$ , 300 K.

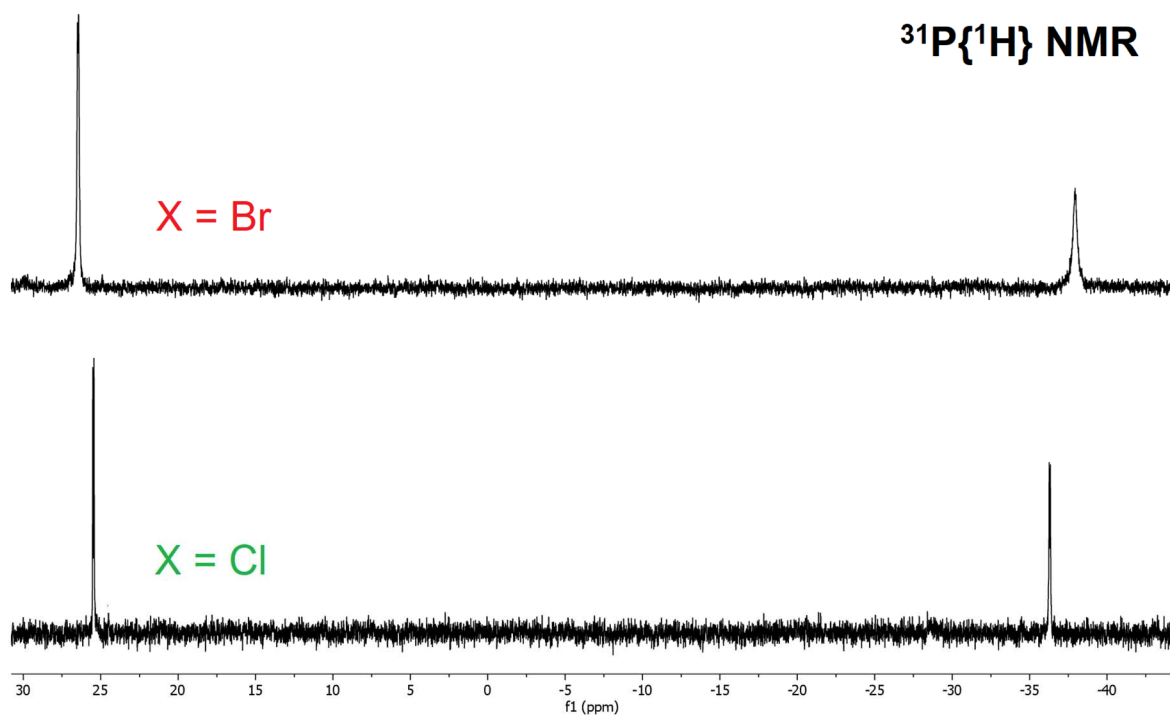


**Figure 54.**  $^{31}\text{P}\{^1\text{H}\}$  NMR spectra of  $[\text{ZnX}_2(\text{dppm}^{\text{NPh}})]$  ( $\text{X} = \text{Cl}, \text{Br}$ ).  $\text{CDCl}_3$ , 300 K.

The absorption spectra confirm that the absorption range is limited to the UV region below 350 nm, as already observed for the homoleptic complex. The compounds are not appreciably luminescent under UV irradiation, this preventing the determination of the photoluminescence quantum yields with the available instrument. Photoluminescence measurements carried out on solid samples however revealed weak broad emission bands centred around 515 nm for the chloro-derivative and at about 459 nm for the bromo-complex upon excitation with UV light. Selected emission and excitation spectra are shown in Figure 55.

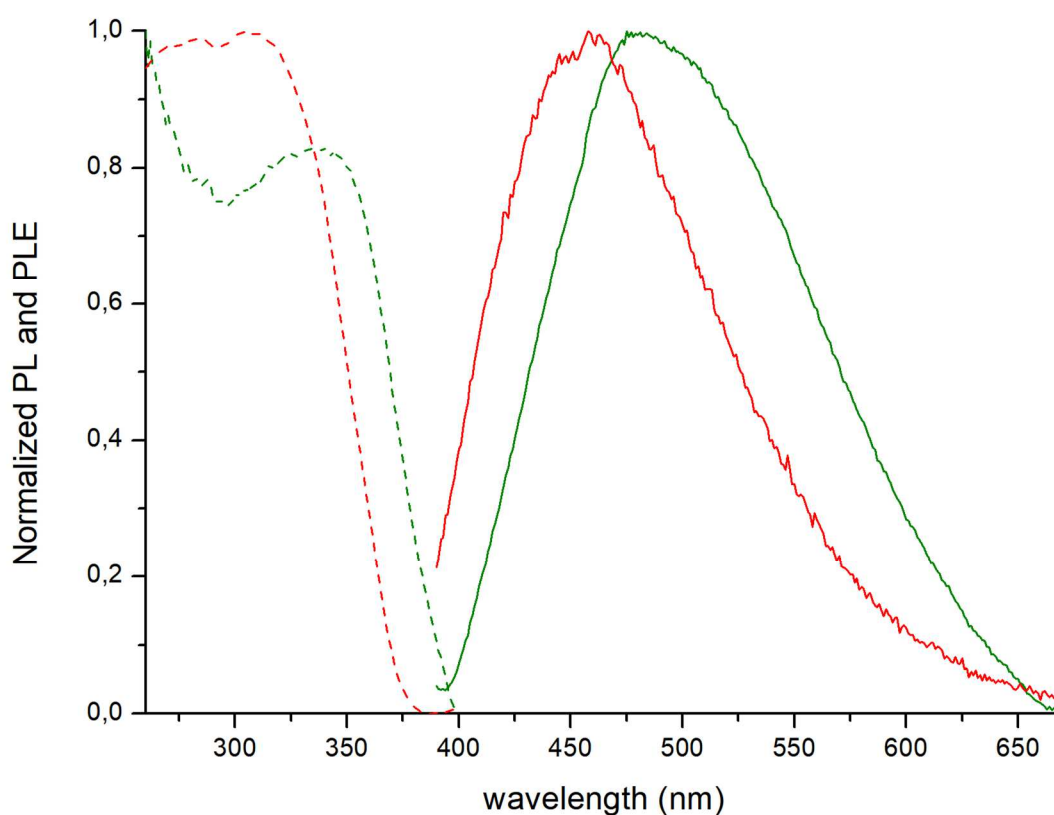


**Figure 55.** Normalized emission and excitation (solid sample, r.t., continuous and dashed lines,  $\lambda_{\text{excitation}} = 300\text{-}360$  nm,  $\lambda_{\text{emission}} = 515$  nm) spectra of  $[\text{ZnX}_2(\text{dppm}^{\text{NPh}})]$  (X = Cl, green; X = Br, red).

Lifetime measurements on the chloro- and bromo-complexes at room temperature clearly indicate that the emission is a fluorescence from the coordinated ligands (Figure 56), with lifetimes of the excited states in the nanoseconds range. The luminescence of  $[\text{ZnI}_2(\text{dppm}^{\text{NPh}})]$  resulted too low to allow the lifetime measurement. It is likely to suppose that the presence of iodide in the coordination sphere favours the intersystem crossing to

excited triplet states, followed by non-radiative decay. The noticeable shift of the emission maximum moving from X = Cl to X = Br and the luminescence quenching observed for X = I prompted to investigate the frontier molecular orbitals of  $[\text{ZnBr}_2(\text{dppm}^{\text{NPh}})]$ , taken as example. As observable in Figure 57, the  $\pi$ -delocalized orbitals of the ligands superimpose with Zn- and Br-centred functions in both the HOMO and the LUMO, this almost in part justifying the influence of the choice of the halide on the luminescent features.

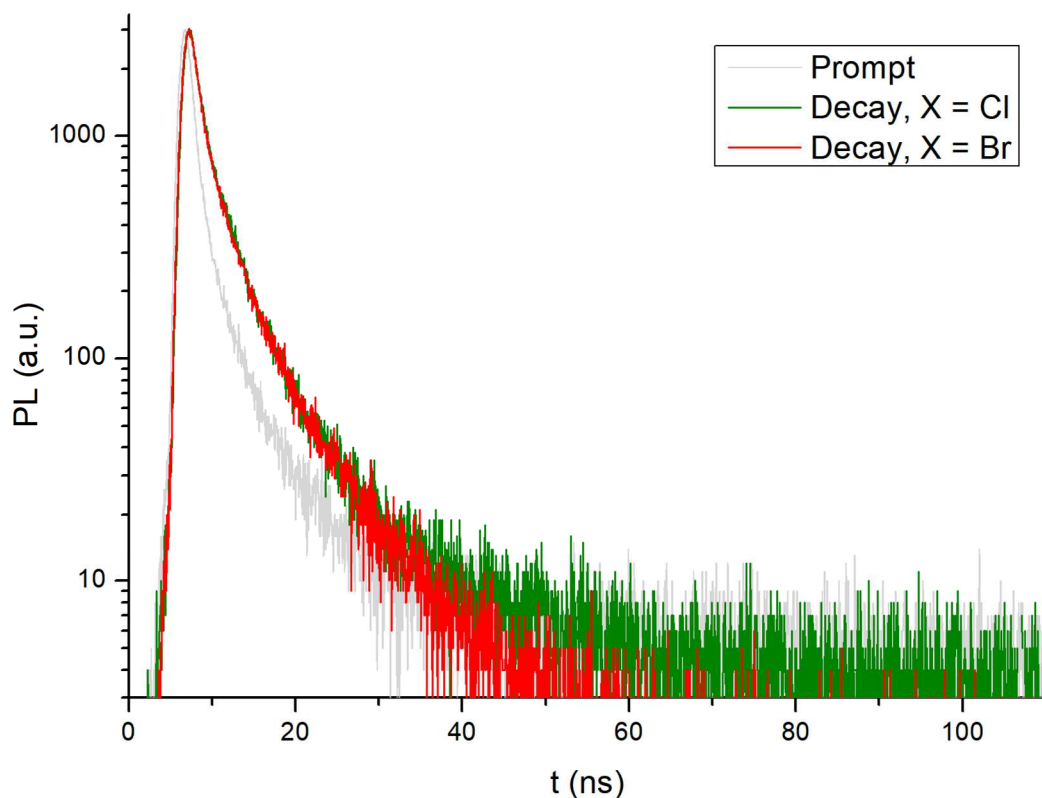


**Figure 56.** Semi-log plots of the luminescence decay curves of  $[\text{ZnX}_2(\text{dppm}^{\text{NPh}})]$  (solid, r.t.,  $\lambda_{\text{excitation}} = 373$  nm,  $\lambda_{\text{emission}} = 430$  nm).

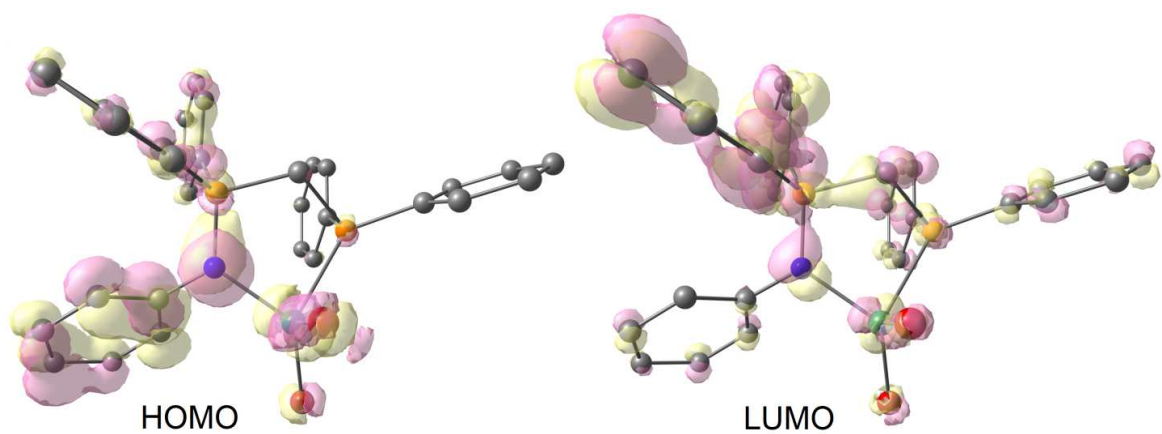


**Figure 57.** DFT-optimized ( $r^2$ SCAN-3c) structure of [ZnBr<sub>2</sub>(dppm<sup>NPh</sup>)], plots of the HOMO and LUMO (pink and yellow tones, isovalue = 0.03 a.u.). Zn, green; P, orange; C, grey. Hydrogen atoms omitted for clarity.

## 5. Conclusions

The study concerning the preparation and application in coordination chemistry of [N,P]-donor ligands containing the iminophosphorane moiety revealed that the evolution of the Staudinger reaction between bidentate phosphines and organoazides depends upon the nature of the N-bonded substituent and upon the bridge connecting the phosphorus atoms. The synthetic approach allowed to isolate the ligand 1-((diphenylphosphaneyl)methyl)-*N*,1,1-triphenyl-phosphanimine,  $\text{dppm}^{\text{NPh}}$ , that revealed to be sufficiently stable to be used for the preparation of new complexes. The ligand itself showed some noticeable features, such as photoluminescence in the green region related to intraligand charge transfer and quite low oxidation potential thanks to the presence of the {P=NPh} fragment.

Homoleptic complexes with  $d^{10}$  metal centres belonging to the first row of the d-block were isolated and characterized. Both the Cu(I) and Zn(II) derivatives showed photoluminescence upon irradiation with UV light, characterized as fluorescence on the basis of the luminescence decay curves. Despite the apparently similar behaviour respect to the free ligand, DFT calculations highlighted the non-negligible role of metal-centred functions in the frontier molecular orbitals. A noticeable result concerns the electrochemical behaviour of the  $[\text{Cu}(\text{dppm}^{\text{NPh}})_2]^+$  cation, that exhibited uncommon reversible metal-centred oxidation after the reversible oxidation of the {Ph<sub>2</sub>P=NPh} moiety of the ligand.

Halide-complexes were obtained by reacting the ligand with anhydrous metal precursors. In the case of Cu(I) derivatives the formation of polynuclear species is highly probable, as suggested by DFT calculations. The luminescence features depend upon the nature of the metal centre and by the choice of the halide. The emissions of the Cu(I) derivatives resulted more appreciable compared to the Zn(II) complexes. The presence of heavier halides in the coordination sphere favours intersystem crossing processes, as revealed by the observed lifetimes. Preliminary measurements indicated that the luminescence of  $[\text{CuBr}(\text{dppm}^{\text{NPh}})]_n$  grows if the complex interacts with compounds such as diethyl ether, possibly because of an increase of the radiative decay rate. Such a feature is of potential interest in the field of luminescence-based sensors, but the possible application appears limited by the low emission of the complex.

Given the possibility of preparing new  $d^{10}$  luminescent metal complexes with [N,P]-donors based on the iminophosphorane fragment, possible future extensions of the investigation could be focused on the introduction of substituents in the skeleton of the ligand, with the aim of improving the photoluminescence of the corresponding complexes. Among the possible approaches, the use of functionalized aromatic azides in the Staudinger reaction appears of interest, given the role of paramount importance exhibited by the {P=NAr} fragment in the current study.

## 6. Appendix

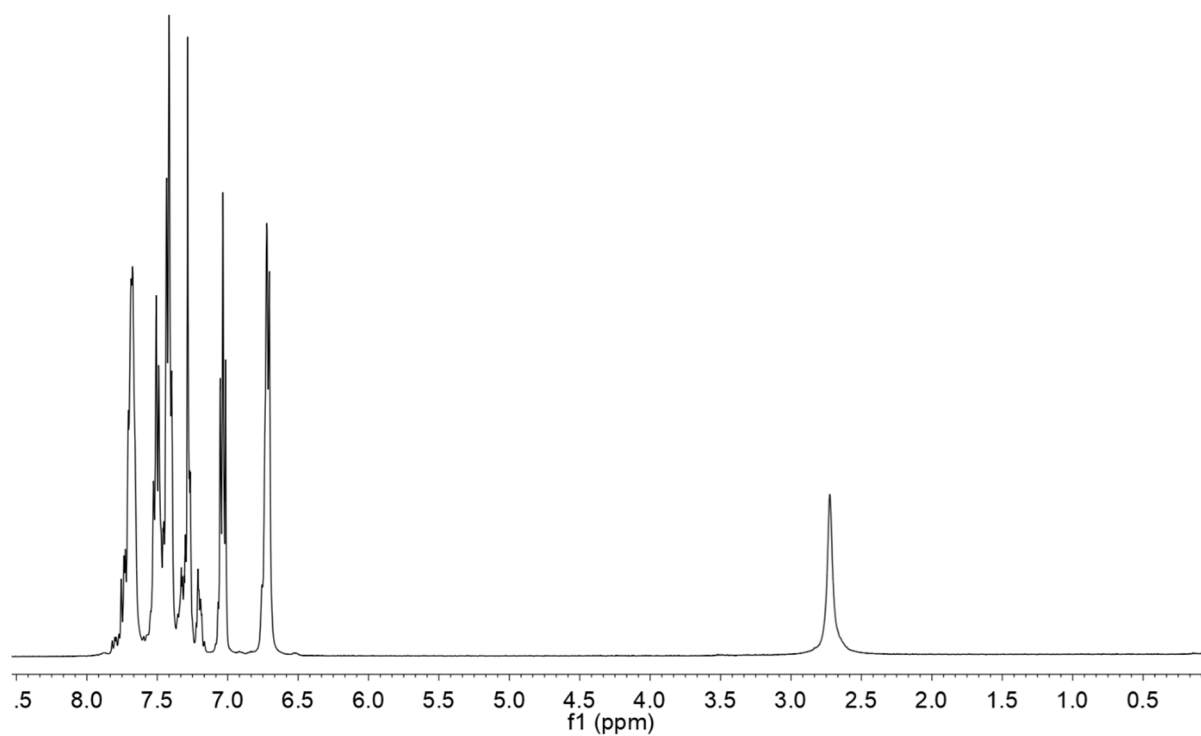


**Figure S 1.** dppe +  $\text{PhN}_3$   $^1\text{H}$  NMR spectrum.  $\text{CDCl}_3$ , 300 K.

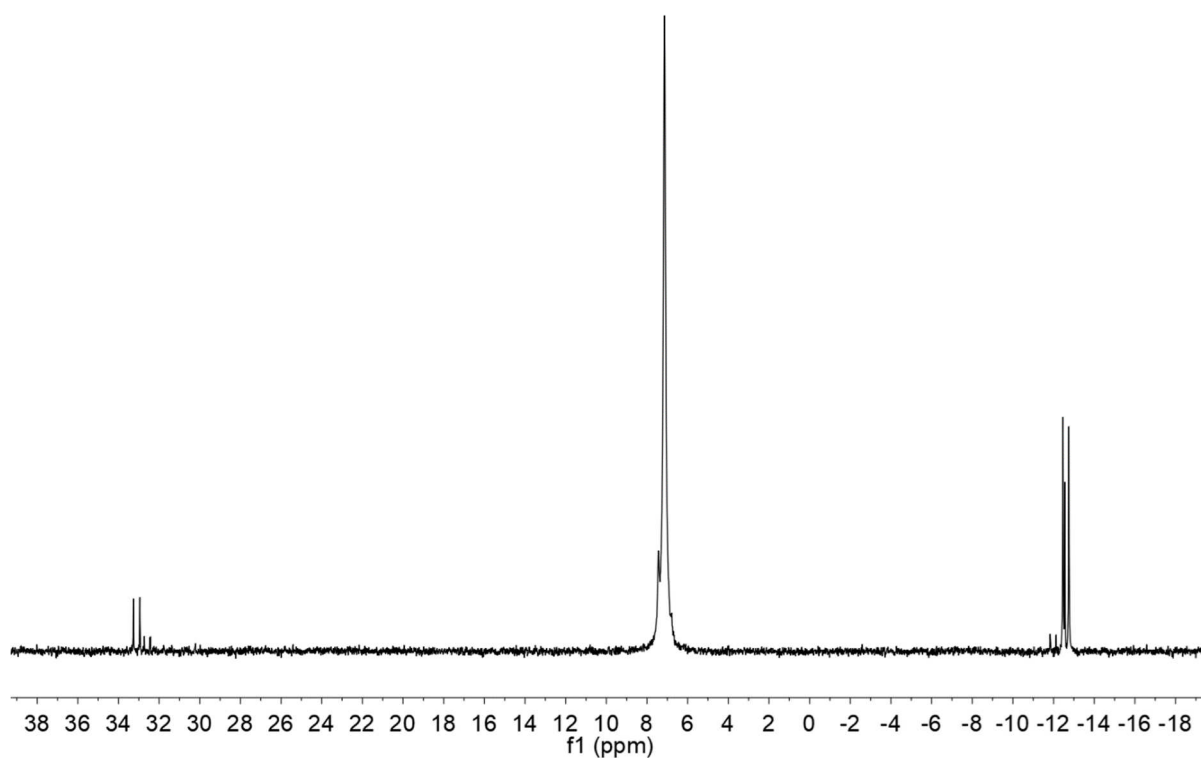


**Figure S 2.** dppe +  $\text{PhN}_3$   $^{31}\text{P}\{^1\text{H}\}$  NMR spectrum.  $\text{CDCl}_3$ , 300 K.

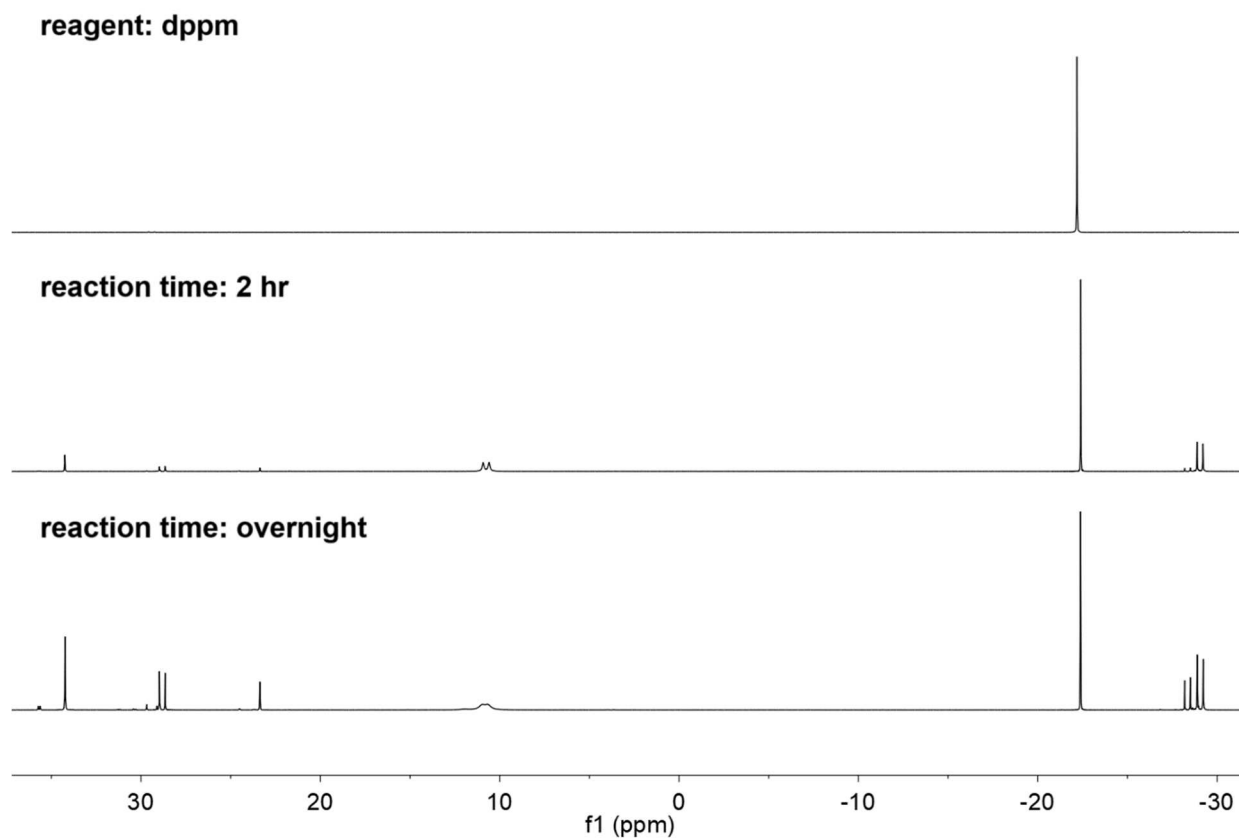


**Figure S 3.** dppm +  $\text{CH}_3\text{C}_6\text{H}_4\text{CH}_2\text{N}_3$ ,  $^{31}\text{P}\{^1\text{H}\}$  NMR spectra at different time.  $\text{CDCl}_3$ , 300 K.

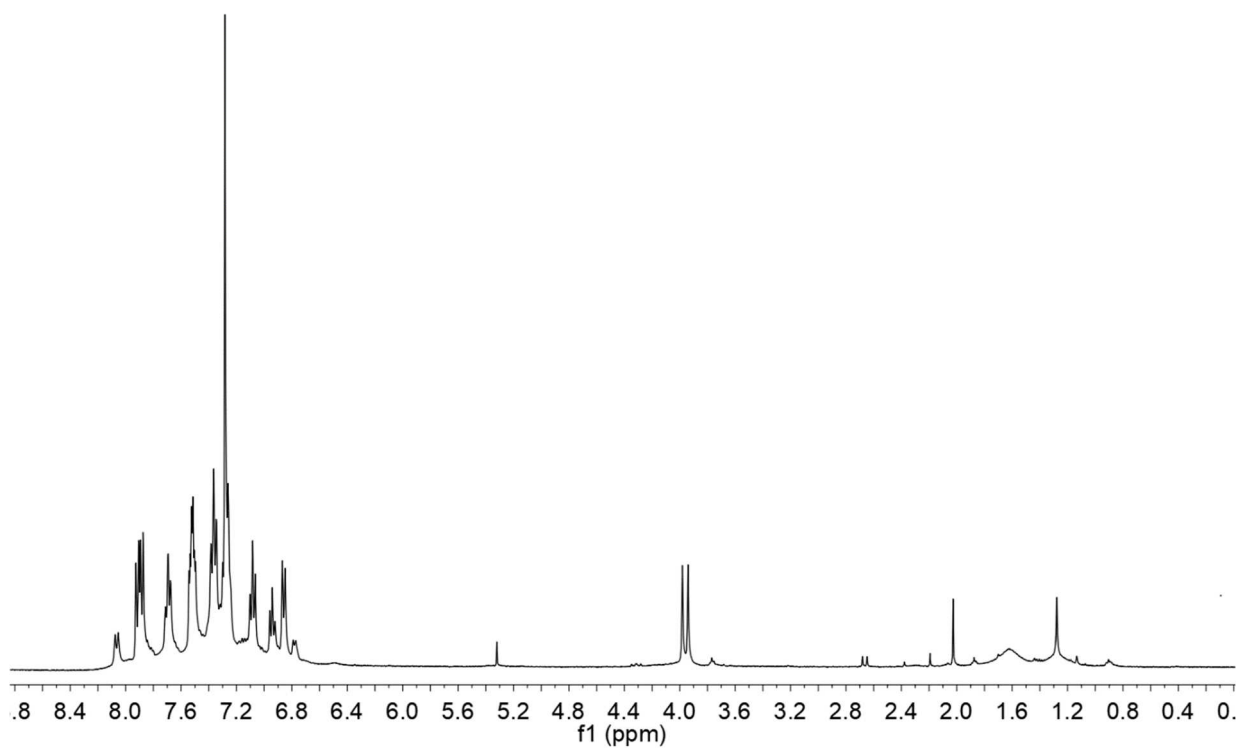


**Figure S 4** dppm<sup>NPh</sup> + Zn(ClO<sub>4</sub>)<sub>2</sub>·6H<sub>2</sub>O <sup>1</sup>H NMR. CDCl<sub>3</sub>, 300 K.

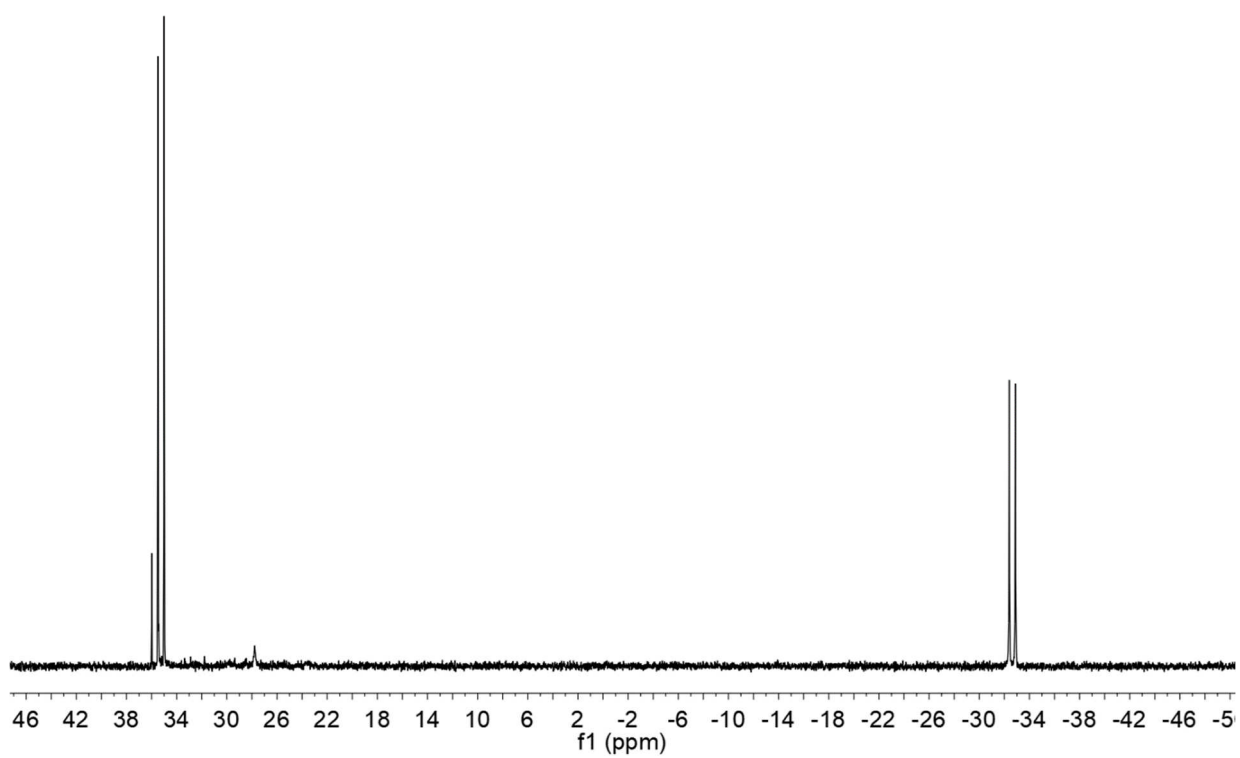


**Figure S 5** dppm<sup>NPh</sup> + Zn(ClO<sub>4</sub>)<sub>2</sub>·6H<sub>2</sub>O <sup>31</sup>P{<sup>1</sup>H} NMR. CDCl<sub>3</sub>, 300 K.

## 7. Bibliography

1. Balzani, V., Ceroni, P., Juris, A. *Photochemistry and Photophysics*, Wiley-VCH, Weinheim, 2014.
2. Browne, A. J., Krajewska, A., Gibbs, A. S. (2021). *J Mater Chem C*, 9(35), 11640-11654.
3. Yersin, H. *Highly Efficient OLEDs: Materials Based on Thermally Activated Delayed Fluorescence*, Wiley-VCH, Weinheim, 2018.
4. Mathur, N., Mukherjee, A., Gao, X., Luo, J., McCullian, B. A., Li, T., Fuchs, G. D. (2022). *Nat Commun*, 13(1), 3233.
5. (a) Wang, Y., Bao, P., Wang, J., Jia, R., Bai, F. Q., Zhang, H. X. (2018). *Inorg Chem*, 57(11), 6561-6570. (b) Lüdtke, N., Föllner, J., Marian, C. M. (2020). *Phys Chem Chem Phys*, 22(41), 23530-23544. (c) Yang, Z. H., Li, Y., Ullrich, C. A. (2012). *J Chem Phys*, 137(1). (d) González, L., Escudero, D., Serrano-Andrés, L. (2012). *ChemPhysChem*, 13(1), 28-51.
6. Housecroft, C. E., Sharpe, A. G. *Inorganic Chemistry*, 4th edition, Pearson, Harlow, 2012.
7. Montaldi, M., Credi, A., Prodi, L., Gandolfi, M. T. *Handbook of Photochemistry*, 3rd edition, Chapter 2, CRC Press, Boca Raton, 2006.
8. Bünzli, J. C. G. (2010). *Chem Rev*, 110(5), 2729-2755.
9. (a) Yue, Y., Grusenmeyer, T., Ma, Z., Zhang, P., Schmehl, R. H., Beratan, D. N., Rubtsov, I. V. (2014). *J Phys Chem A*, 118(45), 10407-10415. (b) Yam, V. W. W., Lo, K. K. W. (1999). *Chem Soc Rev*, 28(5), 323-334. (c) Yam, V. W. W., Chan, A. K. W., Hong, E. Y. H. (2020). *Nat Rev Chem*, 4(10), 528-541.
10. Pashaei, B., Karimi, S., Shahroosvand, H., Abbasi, P., Pilkington, M., Bartolotta, A., Bonaccorso, F. (2019). *Chem Soc Rev*, 48(19), 5033-5139.
11. Bizzarri, C., Spuling, E., Knoll, D. M., Volz, D., Bräse, S. (2018). *Coord Chem Rev*, 373, 49-82.
12. (a) Sinha, N., Jiménez, J.-R., Pfund, B., Prescimone, A., Piguet, C., Wenger, O. S. (2021). *Angew Chem Int Ed*, 60, 23722-23728. (b) Beaudelot, J., Oger, S., Perusko, S., Phan, T. A., Teunens, T., Moucheron, C., Evano, G. (2022). *Chem Rev*, 122(22), 16365-16609. (c) Wenger, O.S. (2018). *J Am Chem Soc*, 140(42), 13522-13533. (d) Wegeberg, C., Wenger, O. S. (2021). *Jacs Au*, 1(11), 1860-1876.
13. Bortoluzzi, M. *Chimica degli elementi di transizione e della serie dei lantanidi*. Libreria Progetto. Padova 2021.

14. Greenwood, N. N., Earnshaw, A. *Chemistry of the elements*, 2nd ed., Butterworth-Heinemann, Oxford, 1997.
15. Liu, Y., Yiu, S. C., Ho, C. L., Wong, W. Y. (2018). *Coord Chem Rev*, *375*, 514-557.
16. Ruthkosky, M., Kelly, C. A., Castellano, F. N., Meyer, G. J. (1998). *Coord Chem Rev* *171*, 309-322.
17. (a) Kuang, S. M., Cuttell, D. G., McMillin, D. R., Fanwick, P. E., Walton, R. A. (2002). *Inorg Chem*, *41*(12), 3313-3322. (b) Zhang, Q., Zhou, Q., Cheng, Y., Wang, L., Ma, D., Jing, X., Wang, F. (2004) *Adv Mater*, *16*(5), 432-436. (c) McCormick, T., Jia, W. L., Wang, S. (2006) *Inorg Chem*, *45*(1), 147-155. (d) Che, G., Su, Z., Li, W., Chu, B., Li, M., Hu, Z., Zhang, Z. (2006). *Chem Appl Phys Lett*, *89*(10), 103511. (e) Zhang, Q., Ding, J., Cheng, Y., Wang, L., Xie, Z., Jing, X., Wang, F. (2007) *Adv Funct Mater*, *17*(15), 2983-2990. (f) Si, Z., Li, J., Li, B., Liu, S., Li, W. (2009). *J Lumin*, *129*(3), 181-186. (g) Min, J., Zhang, Q., Sun, W., Cheng, Y., Wang, L. (2011). *Dalton T*, *40*(3), 686-693. (h) Femoni, C., Muzzioli, S., Palazzi, A., Stagni, S., Zacchini, S., Monti, F., Marcaccio, M. (2013). *Dalton T*, *42*(4), 997-1010. (i) Bergmann, L., Braun, C., Nieger, M., Bräse, S. (2018). *Dalton T*, *47*(2), 608-621.
18. (a) Parmeggiani, F., Sacchetti, A. (2012). *J Chem Educ*, *89*(7), 946-949. (b) Artem'ev, A. V., Davydova, M. P., Berezin, A. S., Samsonenko, D. G., Bagryanskaya, I. Y., Brel, V. K., Li, J. (2022). *Acs Appl Mater Inter*, *14*(27), 31000-31009. (c) Watanabe, Y., Washer, B. M., Zeller, M., Savikhin, S., Slipchenko, L. V., Wei, A. (2022). *J Am Chem Soc*, *144*(23), 10186-10192. (d) Cariati, E., Lucenti, E., Botta, C., Giovanella, U., Marinotto, D., Righetto, S. (2016). *Coord Chem Rev*, *306*, 566-614.
19. Kondo, S., Yoshimura, N., Yoshida, M., Kobayashi, A., Kato, M. (2020). *Dalton T*, *49*(46), 16946-16953.
20. (a) Bai, Y., He, G. J., Zhao, Y. G., Duan, C. Y., Dang, D. B., Meng, Q. J. (2006). *Chem Commun*, (14), 1530-1532. (b) Allendorf, M. D., Bauer, C. A., Bhakta, R. K., Houk, R. J. T. (2009). *Chem Soc Rev*, *38*(5), 1330-1352.
21. (a) Artem'ev, A. V., Baranov, A. Y., Rakhmanova, M. I., Malysheva, S. F., Samsonenko, D. G. (2020). *New J Chem*, *44*(17), 6916-6922. (b) Artem'ev, A. V., Baranov, A. Y., Berezin, A. S., Stass, D. V., Hettstedt, C., Kuzmina, U. Y. A., Bagryanskaya, I. Y. (2023). *Int J Mol Sci*, *24*(6), 5145.

22. (a) Tao, Y., Yuan, K., Chen, T., Xu, P., Li, H., Chen, R., Huang, W. (2014). *Adv Mater*, *26*(47), 7931-7958. (b) Li, G., Zhu, Z. Q., Chen, Q., Li, J. (2019). *Org Electron*, *69*, 135-152. (c) Hofbeck, T., Monkowius, U., Yersin, H. (2015). *J Am Chem Soc*, *137*(1), 399-404.
23. (a) Leitzl, M. J., Kuchle, F. R., Mayer, H. A., Wesemann, L., Yersin, H. (2013). *J Phys Chem A*, *117*(46), 11823-11836. (b) Czerwieniec, R., Yu, J., Yersin, H. (2011). *Inorg Chem*, *50*(17), 8293-8301. (c) Li, K., Chen, Y., Wang, J., Yang, C. (2021). *Coord Chem Rev*, *433*, 213755.
24. (a) Bergmann, L., Hedley, G. J., Baumann, T., Bräse, S., Samuel, I. D. (2016). *Sci Adv*, *2*(1), e1500889. (b) Chen, X. L., Yu, R., Zhang, Q. K., Zhou, L. J., Wu, X. Y., Zhang, Q., Lu, C. Z. (2013). *Chem Mater*, *25*(19), 3910-3920. (c) Leitzl, M. J., Krylova, V. A., Djurovich, P. I., Thompson, M. E., & Yersin, H. (2014). *J Am Chem Soc*, *136*(45), 16032-16038. (d) Kobayashi, A., Hasegawa, T., Yoshida, M., Kato, M. (2016). *Inorg Chem*, *55*(5), 1978-1985. (e) Baranov, A. Y., Berezin, A. S., Samsonenko, D. G., Mazur, A. S., Tolstoy, P. M., Plyusnin, V. F., Artem'Ev, A. V. (2020). *Dalton T*, *49*(10), 3155-3163.
25. Hong, G., Gan, X., Leonhardt, C., Zhang, Z., Seibert, J., Busch, J. M., Bräse, S. (2021). *Adv Mater*, *33*(9), 2005630.
26. Jüstel, T., Möller, S., Winkler, H., Adam, W. *Luminescent Materials*, Ullman's Encyclopedia of Industrial Chemistry, Wiley-VCH, Weinheim, 2012.
27. (a) Kaim, W., Schwederski, B., Klein, A. *Bioinorganic Chemistry: Inorganic Elements in the Chemistry of Life*, Wiley, Chichester, 2013. (b) Wilkinson, G., *Comprehensive Coordination Chemistry*, Vol. 5, Pergamon Press, Oxford, 1987.
28. Dumur, F. (2014). *Synthetic Met*, *195*, 241-251.
29. Cepeda, J., San Sebastian, E., Padro, D., Rodríguez-Diéguez, A., García, J. A., Ugalde, J. M., Seco, J. M. (2016). *Chem Commun*, *52*(56), 8671-8674.
30. Tabone, R., Feser, D., Lemma, E. D., Schepers, U., Bizzarri, C. (2021). *Front Chem*, *9*, 754420.
31. Sakai, Y., Sagara, Y., Nomura, H., Nakamura, N., Suzuki, Y., Miyazaki, H., Adachi, C. (2015). *Chem Commun*, *51*(15), 3181-3184.
32. (a) Liu, Q. D., Wang, R., Wang, S. (2004). *Dalton T*, (14), 2073-2079. (b) Wei, J. H., Ou, W. T., Luo, J. B., Kuang, D. B. (2022). *Angew Chem Int Edit*, *61*(33), e202207985. (c) Ferraro, V., Baggio, F., Castro, J., Bortoluzzi, M. (2022). *Eur J Inorg Chem*, *2022*(16), e202200119.

33. Wang, J. Q., Mu, Y., Han, S. D., Pan, J., Li, J. H., Wang, G. M. (2019). *Inorg Chem*, *58*(14), 9476-9481.
34. (a) Kosky, C. A., Gayda, J. P., Gibson, J. F., Jones, S. F., Williams, D. J. (1982). *Inorg Chem*, *21*(8), 3173-3179. (b) Rose, J. P., Lalancette, R. A., Potenza, J. A., Schugar, H. J. (1980). *Acta Crystall B-Stru*, *36*(10), 2409-2411. (c) Liu, X., Wang, G., Dang, Y., Zhang, S., Tian, H., Ren, Y., Tao, X. (2016). *CrystEngComm*, *18*(10), 1818-1824. (d) Batesky, D. C., Goldfogel, M. J., Weix, D. J. (2017). *J Org Chem*, *82*(19), 9931-9936.
35. Sano, T., Nishio, Y., Hamada, Y., Takahashi, H., Usuki, T., Shibata, K. (2000). *J Mater Chem*, *10*(1), 157-161.
36. Gusev, A. N., Kiskin, M. A., Braga, E. V., Chapran, M., Wiosna-Salyga, G., Baryshnikov, G. V., Linert, W. (2019). *J Phys Chem C*, *123*(18), 11850-11859.
37. Staudinger, H., & Meyer, J. (1919). *Helv Chim Acta*, *2*(1), 635-646.
38. (a) Formica, M., Rozsar, D., Su, G., Farley, A. J., Dixon, D. J. (2020). *Accounts Chem Res*, *53*(10), 2235-2247. (b) Fresneda, P. M., Molina, P. (2004). *Synlett*, *2004*(01), 1-17. (c) Takeda, T., Terada, M. (2013). *J Am Chem Soc*, *135*(41), 15306-15309.
39. Fukui, M., Itoh, K., & Ishii, Y. (1975). *B Chem Soc Jpn*, *48*(7), 2044-2046.
40. Garcia-Alvarez, J., Garcia-Garrido, S. E., Cadierno, V. (2014). *J Organomet Chem*, *751*, 792-808.
41. Frik, M., Jiménez, J., Vasilevski, V., Carreira, M., De Almeida, A., Gascón, E., Contel, M. (2014). *Inorg Chem Front*, *1*(3), 231-241.
42. (a) García-Álvarez, J., Diez, J., Gimeno, J., Suarez, F. J., Vincent, C. (2012). *Eur J Inorg Chem*, *2012*(35), 5854-5863. (b) Venderbosch, B., Oudsen, J. P. H., van der Vlugt, J. I., Korstanje, T. J., Tromp, M. (2020). *Organometallics*, *39*(19), 3480-3489.
43. (a) Hill, M. S., Hitchcock, P. B. (2004). *J Organomet Chem*, *689*(20), 3163-3167. (b) Evans, D. J., Hill, M. S., Hitchcock, P. B. (2003). *Dalton T*, (4), 570-574. (c) Hill, M. S., Hitchcock, P. B. (2002). *J Chem Soc, Dalton T*, (24), 4694-4702. (d) Bayram, M., Gondzik, S., Bläser, D., Wölper, C., Schulz, S. (2016). *Z Anorg Allg Chem*, *642*(15), 847-852. (e) Wheaton, C. A., Ireland, B. J., Hayes, P. G. (2011). *Z Anorg Allg Chem*, *637*(14-15), 2111-2119.
44. Al-Benna, S., Sarsfield, M. J., Thornton-Pett, M., Ormsby, D. L., Maddox, P. J., Brès, P., Bochmann, M. (2000). *J Chem Soc, Dalton T*, (23), 4247-4257.

45. Jain, A., Karmakar, H., Roesky, P. W., Panda, T. K. (2023). *Chem Rev*, *123*(23), 13323-13373.
46. Alajarin, M., López-Leonardo, C., Llamas-Lorente, P., Bautista, D. (2000). *Synthesis*, *2000*(14), 2085-2091.
47. Schmidbaur, H., Bowmaker, G. A., Kumberger, O., Müller, G., Wolfsberger, W. (1990). *Z Naturforsch B*, *45*(4), 476-482.
48. Armarego, W. L. F., Chai, C. L. L. *Purification of Laboratory Chemicals*, 5th edition, ButterworthHeinemann, London, 2003.
49. Keller, R. N., Wrcoff, H. D., Marchi, L. E. (1946). *Inorg Syn*, *2*, 1-4.
50. Bianchini, C., Ghilardi, C. A., Meli, A., Midollini, S., & Orlandini, A. (1985). *Inorg Chem*, *24*(6), 924-931.
51. Kubas, G. J., Monzyk, B., Crumblis, A. L., *Inorganic Syntheses: Reagents for Transition Metal Complex and Organometallic Syntheses*, *28*, 68-70. John Wiley & Sons, Inc., Hoboken, 1990.
52. (a) Lindsay, R. O. (1942). *CFH Allen, Org Synth*, *22*, 96. (b) Islam, R. U., Taher, A., Choudhary, M., Witcomb, M. J., Mallick, K. (2015). *Dalton T*, *44*(3), 1341-1349.
53. Geary, W. J. (1971). *Coord Chem Rev*, *7*(1), 81-122.
54. Cramer, C. J. *Essentials of Computational Chemistry*, Wiley, Chichester, 2004
55. Grimme, S., Brandenburg, J. G., Bannwarth, C., Hansen, A. (2015). *J Chem Phys*, *143*(5).
56. Grimme, S., Hansen, A., Ehlert, S., Mewes, J. M. (2021). *J Chem Phys*, *154*(6).
57. Ullrich, C. A. *Time-Dependent Density-Functional Theory*, Oxford University Press, Oxford, 2012.
58. (a) Tao, J., Perdew, J. P., Staroverov, V. N., Scuseria, G. E. (2003). *Phys Rev Lett*, *91*(14), 146401. (b) Staroverov, V. N., Scuseria, G. E., Tao, J., Perdew, J. P. (2003). *J Chem Phys*, *119*(23), 12129-12137.
59. Weigend, F., Ahlrichs, R. (2005). *Phys Chem Chem Phys*, *7*(18), 3297-3305.
60. Cossi, M., Rega, N., Scalmani, G., Barone, V. (2003). *J Comput Chem*, *24*(6), 669-681.
61. (a) Neese, F. (2012). *Wires Comput Mol Sci*, *2*(1), 73-78 (b) Neese, F. (2022). *Wires Comput Mol Sci*, *12*(1), e1606
62. Lu, T., Chen, F. (2012). *J Comput Chem*, *33*(5), 580-592.
63. Aguiar, A. M., Beisler, J. (1964). *J Org Chem*, *29*(6), 1660-1662.

64. Temelkoff, D. P., Smith, C. R., Kibler, D. A., McKee, S., Duncan, S. J., Zeller, M., Norris, P. (2006). *Carbohydr Res*, 341(10), 1645-1656.
65. El-Sayed, N. F., El-Hussieny, M., Ewies, E. F., Fouad, M. A., Boulos, L. S. (2020). *Bioorg Chem*, 95, 103499.
66. Schubert, E. F. *Light-emitting diodes. second ed*, Cambridge University Press, Cambridge, 2006.
67. Liu, Z., Lu, T., Chen, Q. (2020). *Carbon*, 165, 461-467.
68. Jacobsen, N. E. *NMR Spectroscopy Explained*, John Wiley & Sons, Inc., Hoboken, 2007
69. Berners-Price, S. J., Johnson, R. K., Mirabelli, C. K., Faucette, L. F., McCabe, F. L., Sadler, P. J. (1987). *Inorg Chem*, 26(20), 3383-3387.
70. Yang, L., Powell, D. R., Houser, R. P. (2007). *Dalton T*, (9), 955-964.
71. Elgrishi, N., Rountree, K. J., McCarthy, B. D., Rountree, E. S., Eisenhart, T. T., Dempsey, J. L. (2018). *J Chem Educ*, 95(2), 197-206.